

ABSTRACT

Title of Thesis: NUTRIENTS, CHLOROPHYLL AND EMERGENT HARMFUL ALGAL BLOOM SPECIES OF CONCERN IN COASTAL WATERS OF ASSATEAGUE ISLAND NATIONAL SEASHORE

Morgan O'Hara Ross, Master of Science, 2021

Thesis Directed By: Associate Research Professor, Dr. Judith M. O'Neil, Marine, Estuarine, and Environmental Science

The Atlantic Ocean coastal zone of Maryland is important both ecologically and economically. Due to water quality issues, the coastal lagoons of Maryland have received considerable research attention, but little corresponding research in the coastal waters that exchange with the coastal lagoons. To better understand the linkages between the coastal ocean and the potential impacts of human activity on Maryland's coastal zone, 5 research cruises (2018-2019) were completed to investigate concentrations of nutrients and emergent harmful algal bloom (HAB) species of concern (*Dinophysis*, *Karenia*, *Pseudo-nitzschia*). Nutrient and HAB species had high intra-annual variability, as well as geographic variability with relation to the inlets, coastal lagoons, and offshore discharge sites. The most significant determinants across all sampling locations, depths, and times were nitrate

and ammonium. Continued eutrophication and climate change, as well as the impact of connected waterways, presents challenges for managing regional water quality issues in the coastal ocean.

NUTRIENTS, CHLOROPHYLL AND EMERGENT HARMFUL ALGAL
BLOOM SPECIES IN COASTAL WATERS OF ASSATEAGUE ISLAND
NATIONAL SEASHORE

by

Morgan O'Hara Ross

Thesis submitted to the Faculty of the Graduate School of the
University of Maryland, College Park, in partial fulfillment
of the requirements for the degree of
Master of Marine, Estuarine,
and Environmental Science
2021

Advisory Committee:
Dr. Judith M. O'Neil, Chair
Dr. William C. Dennison
Dr. James Pierson

© Copyright by
Morgan O'Hara Ross
2021

Acknowledgements

This thesis would not have been possible without the support, patience and guidance of my advisor, Dr. Judith M. O’Neil. I am so grateful for her flexibility and resilience as we navigated through rough waters (literally and figuratively) of research during natural disasters and a global pandemic. I would also like to thank my committee members; Dr. William C. Dennison, who provided unparalleled attention to detail, as well as science communication and visualization expertise, and Dr. James Pierson who is so committed to the success of his students, he offered to teach an entire course on Zooplankton Ecology at my request. I am honored to have had the opportunity to work with each of these brilliant scientists.

Huge thanks to the University of Maryland Center for Environmental Science (UMCES) *R.V. Rachel Carson* crew, Captain Michael Hulme and Chief Mate Rob Nilsen, as well as the University of Delaware *R.V. Joanne Daiber*, Captain Kevin Beam. Additionally, this project is largely the product of hard work from our collaborators at the Maryland Department of Natural Resources; Cathy Wazniak, Jen Wolny, Amy Hamilton, Carol Cain and Deb McKay. Many laborious hours were spent on the boat and in the lab for this project, and I am thankful for their hard work. Dylan Taillie and Heath Kelsey at the UMCES Integration and Application Network (IAN) were integral to the success of this project. If not for Dylan’s acquired expertise with a CTD, with help from Tom Wazniak (YSI/Xylem), Dr. Jeremy Testa and Dr. Ryan Woodland (both of UMCES Chesapeake Biological Lab), we would have been unable to collect data in the first place. We also received enormous

amounts of help from Roman Jesien, who organized the Maryland Coastal Bays Program field volunteers including Kat Phillips, Amanda Poskaitis, Carly Toulan and Ariana Russo. More invaluable field and lab help came from Ben Lee, Brendan Campbell, Max Hermanson, and Horn Point Lab REU students Norberto Latorre-Arzola, Ben Lane and Olivia Saliger. Special thanks to our National Park Service (NPS) partners at Assateague Island National Seashore (ASIS), Bill Hulslander (Chief of Resource Management), Brian Sturgis (NPS Ecologist), Carol Caine (Ranger) and field volunteer Sierra Hildebrant.

Special thanks go to Dr. Jacob Cram and Dr. Klaus Huebert for going way above and beyond to teach statistics and R software techniques on their own time. Thanks to Dr. Sairah Malkin and Dr. Greg Silsbe for facilitating essential field and lab equipment use. I am forever in debt to Diane Stoecker, whose generosity in letting me use her microscope lab made it possible to complete the lab analyses. The Horn Point Laboratory Analytical Service Lab was instrumental in the lab analyses for this thesis; thanks go to Erika Kiss for running all the nutrient analyses, and Meg Maddox for teaching me how to use the fluorometer.

My lovely officemates, MaryAnn Manley, Juli Brush, Carin Starr, and Linda Starling always kept a smile on my face. I would be remiss not to mention the friendship, field and lab help of my roommate, Anna Windle, and my dear friend, Lisa Ziegler. I don't think I would've survived a single semester without their reassuring words and monthly "international dinners". And of course, I would like to thank my family for supporting me throughout my academic career. Shout-out to my dad for listening to every presentation I gave for three straight years, to my mom for

keeping me focused on the end goal, and to my partner, Cody, for putting up with the late-night study sessions.

My thesis would not have been possible without funding from the HPL Education Committee, which provided a HPL Fellowship, HPL Travel Grants, a Teaching Assistantship for MEES 621 – Biological Oceanography, Bridge Funds, and UMCES COVID relief funds. Additional funding came from a University of Maryland, College Park, College of Computer, Mathematical and Natural Sciences Dean’s Fellowship and the UMCES – IAN for a Teaching Assistantship for MEES 620 – Environment and Society. The primary research grant, P17AC01540, which made this research possible was awarded by the NPS- Chesapeake Watershed Cooperative Ecosystem Studies Unit (CESU).

Table of Contents

Acknowledgements.....	ii
Table of Contents	v
List of Tables	vi
List of Figures	viii
INTRODUCTION:	1
Coastal Delmarva region.....	1
Anthropogenic influences	3
Impervious surfaces and runoff	10
Project aims and objectives.....	17
METHODS	20
Study Locations and Sampling Period	20
Field Sample Collection.....	20
Nutrient Analysis	24
Chlorophyll Extraction.....	24
Phytoplankton Community Analysis and Cell Counts	25
Synthesis of Nutrients, HABs, Environmental Factors	25
Principal Component Analysis	26
RESULTS	31
Nutrients and Physical Characteristics.....	31
Nutrients and Harmful Algal Bloom Species	32
Dissolved nutrient variations	36
Nutrient and Harmful Algal Bloom species variations at the surface	40
Nutrient and Harmful Algal Bloom species variations at the chlorophyll max ..	41
Nutrient, chlorophyll and Harmful Algal Bloom species threshold comparisons	48
Bioassay Experiments.....	66
Chlorophyll <i>a</i>	66
Harmful Algal Bloom species.....	67
DISCUSSION.....	70
Physical factors	70
Spatial Comparison.....	75
Nutrient limitation.....	77
<i>Karenia</i> spp.	79
<i>Dinophysis</i> spp.....	80
<i>Pseudo-nitzschia</i> spp.....	81
Management Implications.....	82
FUTURE RESEARCH	86
References.....	87

List of Tables

Table 1: MCB thresholds values for chl *a*, TN, TP, *Dinophysis* spp., *Karenia* spp., *Pseudo-nitzschia* spp.

Table 2: List of research cruise dates and research vessels.

Table 3: Statistical significance of the differences between HAB concentrations and nutrients/ physical parameters. Statistical significance of linear regression model is defined by p-value<0.05 for t-test (Integration and Application Network - ian.umces.edu/media-library).

Table 4: Statistical significance of the differences between sampling depth of HAB concentrations (surface, chl *a* max, bottom). Statistical significance of linear regression model is defined by p-value<0.05.

Table 5: List of nutrient bioassay dates and treatments.

Table 6: The 1st and 4th quartile concentration values of the average transect concentrations of combined nutrients (TN, TP, NH₄⁺, NO_x, PO₄³⁻) and combined HAB species (*Dinophysis* spp., *Karenia* spp., *Pseudo-nitzschia* spp.) for each sampling month (June, July, October 2018; May, July 2019). (A) Surface, (B) Chl *a* max sampling depths.

Table 7: List of MCB threshold exceedances of TN and TP, sampling location, depth and sampling time.

Table 8: List of MCB threshold exceedances of HAB species, sampling location, depth and sampling time.

Table 9: Average (+ standard deviation) concentrations from each sampling period of nutrient and environmental variables: DO, temperature, salinity, chl *a*, TN, TP, NH₄⁺, NO_x, PO₄³⁻ from all sampling depths and locations.

List of Figures

Figure 1: Land use land cover map of study region with areas of agricultural land, developed land, and barren land (Integration and Application Network - ian.umces.edu/media-library).

Figure 2: Map of the study area with data collection sites, transects, sewage outflow locations, and MCB inlet locations (Integration and Application Network - ian.umces.edu/media-library).

Figure 3: Aerial photograph of Ocean City with views of the Ocean City Inlet and Assateague Island. Photo by Jane Thomas-UMCES-IAN (CC BY-SA 4.0).

Figure 4: Photomicrograph of *Karenia* spp. samples collected during research cruises in the MD coastal ocean. (A) *Karenia mikimotoi*, (B) *Karenia papilionacea*, (C) *Karenia brevis*. Photomicrographs taken by Jen Wolny-MD DNR (used with permission).

Figure 5: Photomicrograph of *Dinophysis* spp. samples collected during research cruises in the MD coastal ocean. (A) *Dinophysis norvegica*, (B) *Dinophysis acuta*, (C) *Dinophysis acuminata*. Photomicrographs taken by Jen Wolny-MD DNR (used with permission).

Figure 6: Photomicrograph of a *Pseudo-nitzschia* sp. sample collected during research cruises in the MD coastal ocean. Photomicrographs taken by Jen Wolny-MD DNR (used with permission).

Figure 7: Photograph of Rosette with CTD and 8, 10 L Niskin bottles deployed at each sample site to measure *in-situ* physical parameters and collect discrete water

samples at the surface, chl *a* max and bottom depths. Photo by Max Hermanson-UMCES-IAN (used with permission).

Figure 8: Taylor Floats holding bioassay cubitainers used for incubating samples at ambient light and temperature in the Horn Point Laboratory Harbor. Photo by J.M. O'Neil- UMCES HPL (used with permission).

Figure 9: PCA bi-plots categorized by depth to include physical variables (temperature, salinity, DO), N:P ratios (dissolved and total), chl *a* and nutrient concentrations (TN, TP, NH_4^+ , NO_x , PO_4^{3-}). (A) Combined data from all sampling times (June, July, October 2018; May, July 2019), (B) data from May 2019, (C) data from June 2018, (D) data from July 2018, (E) data from July 2019, (F) data from October 2018.

Figure 10: PCA bi-plots categorized by depth (surface, chl *a* max, bottom) to include physical variables (temperature, salinity, DO), N:P ratios (dissolved and total), HAB species concentrations (*Dinophysis* spp., *Karenia* spp., and *Pseudo-nitzschia* spp.), chl *a* and nutrient concentrations (TN, TP, NH_4^+ , NO_x , PO_4^{3-}). (A) Combined data from all sampling times with the presence of *Dinophysis* spp., (B) combined data from all sampling times with the presence of *Karenia* spp., (C) combined data from all sampling times with the presence of *Pseudo-nitzschia* spp.

Figure 11: Average dissolved nutrient concentrations (NH_4^+ , NO_x , PO_4^{3-}) by transect (1-10). Concentrations are categorized in columns from left to right by season (May 2019, June 2018, July 2019, October 2018). The size of each pie chart is determined by the quartile value of the combined dataset (<1.2, 1.5, 2.5, 8.3). Individual nutrients are distinguished by color and represent their portion of the total average

concentration across a transect and sampling time. Maps are categorized by sampling depth; (A) surface, (B) chl *a* max, (C) bottom.

Figure 12: Average HAB concentrations (*Dinophysis* spp., *Karenia* spp., *Pseudo-nitzschia* spp.) and nutrient concentrations (TN, TP, NH₄⁺, NO_x, PO₄³⁻) by transect (1-10) from surface samples. The size of each pie chart is determined by the quartile value of the combined dataset—<1185-2166 cells L⁻¹ for HAB species and <12.2-18.9 μM for nutrients. Individual nutrients are distinguished by color and represent their portion of the total average concentration across a transect (top to bottom = north to south). Maps are categorized by sampling time; (A) May 2019, (B) June 2018, (C) July 2018, (D) July 2019, (E) October 2018.

Figure 13: Average HAB concentrations (*Dinophysis* spp., *Karenia* spp., *Pseudo-nitzschia* spp.) and nutrient concentrations (TN, TP, NH₄⁺, NO_x, PO₄³⁻) by transect (1-10) from chl *a* max samples. The size of each pie chart is determined by the quartile value of the combined dataset—<1185.0-2166.1 cells L⁻¹ for HAB species and <12.2-18.9 μM for nutrients. Individual nutrients are distinguished by color and represent their portion of the total average concentration across a transect (top to bottom = north to south). Maps are categorized by sampling time; (A) May 2019, (B) June 2018, (C) July 2018, (D) July 2019, (E) October 2018.

Figure 14: Matrix plots of raw data split into with three columns to categorize by depth and three rows to categorize by proximity to shore. Each plot within the matrix has individual data points from transects 1-10 along the x-axis and concentration values of chl *a* (μg L⁻¹) on the y-axis. The red line indicates the MCB threshold of 15

$\mu\text{g L}^{-1}$. (A) May 2019, (B) June 2018, (C) July 2018, (D) July 2019, (E) October 2018.

Figure 15: Matrix plots of raw data split into with three columns to categorize by depth and three rows to categorize by proximity to shore. Each plot within the matrix has individual data points from transects 1-10 along the x-axis and concentration values of TN ($\mu\text{M-N}$) on the y-axis. The red line indicates the MCB threshold of 46 $\mu\text{M-N}$. (A) May 2019, (B) June 2018, (C) July 2018, (D) July 2019, (E) October 2018.

Figure 16: Matrix plots of raw data split into with three columns to categorize by depth and three rows to categorize by proximity to shore. Each plot within the matrix has individual data points from transects 1-10 along the x-axis and concentration values of TP ($\mu\text{M-P}$) on the y-axis. The red line indicates the MCB threshold of 1.2 $\mu\text{M-P}$. (A) May 2019, (B) June 2018, (C) July 2018, (D) July 2019, (E) October 2018.

Figure 17: Matrix plots of raw data split into with three columns to categorize by depth and three rows to categorize by proximity to shore. Each plot within the matrix has individual data points from transects 1-10 along the x-axis and concentration values of NH_4^+ ($\mu\text{M-N}$) on the y-axis. (A) May 2019, (B) June 2018, (C) July 2018, (D) July 2019, (E) October 2018.

Figure 18: Matrix plots of raw data split into with three columns to categorize by depth and three rows to categorize by proximity to shore. Each plot within the matrix has individual data points from transects 1-10 along the x-axis and concentration

values of NO_x ($\mu\text{M-N}$) on the y-axis. (A) May 2019, (B) June 2018, (C) July 2018, (D) July 2019, (E) October 2018.

Figure 19: Matrix plots of raw data split into with three columns to categorize by depth and three rows to categorize by proximity to shore. Each plot within the matrix has individual data points from transects 1-10 along the x-axis and concentration values of PO_4^{3-} ($\mu\text{M-P}$) on the y-axis. (A) May 2019, (B) June 2018, (C) July 2018, (D) July 2019, (E) October 2018.

Figure 20: Matrix plots of raw data split into with two columns to categorize by depth (surface and chl *a* max) and three rows to categorize by proximity to shore. Each plot within the matrix has individual data points from transects 1-10 along the x-axis and concentration values of *Dinophysis* spp. (cells L^{-1}) on the y-axis. The red line indicates the MCB threshold of 10,000 cells L^{-1} . (A) May 2019, (B) June 2018, (C) July 2018, (D) July 2019, (E) October 2018.

Figure 21: Matrix plots of raw data split into with two columns to categorize by depth (surface and chl *a* max) and three rows to categorize by proximity to shore. Each plot within the matrix has individual data points from transects 1-10 along the x-axis and concentration values of *Karenia* spp. (cells L^{-1}) on the y-axis. The red line indicates the MCB threshold of 10,000,000 cells L^{-1} . (A) May 2019, (B) June 2018, (C) July 2018, (D) July 2019, (E) October 2018.

Figure 22: Matrix plots of raw data split into with two columns to categorize by depth (surface and chl *a* max) and three rows to categorize by proximity to shore. Each plot within the matrix has individual data points from transects 1-10 along the x-

axis and concentration values of *Karenia* spp. (cells L⁻¹) on the y-axis. (A) May 2019, (B) June 2018, (C) July 2018, (D) July 2019, (E) October 2018.

Figure 23: Matrix plots of raw data split into with two columns to categorize by depth (surface and chl *a* max) and three rows to categorize by proximity to shore. Each plot within the matrix has individual data points from transects 1-10 along the x-axis and concentration values of *Pseudo-nitzschia* spp. (cells L⁻¹) on the y-axis. The red line indicates the MCB threshold of 1,000,000 cells L⁻¹. (A) May 2019, (B) June 2018, (C) July 2018, (D) July 2019, (E) October 2018.

Figure 24: Average extracted chl *a* concentrations from bioassay experiments under nutrient treatments (Control, N+P, NH₄⁺, NO_x, PO₄³⁻) from the Ocean City Inlet. (A) Bioassay 1 - June 2019, (B) Bioassay 2 - July 2019, (C) Bioassay 3 – September 2019.

Figure 25: HAB species concentrations from bioassay experiments with nutrient treatments (Control, N+P, NH₄⁺, NO_x, PO₄³⁻). (A) *Dinophysis* spp., (B) *Karenia* spp., (C) *Pseudo-nitzschia* spp.

Figure 26: Seasonal diagram summarizing the chl *a* and dissolved nutrient (NH₄⁺, NO_x, PO₄³⁻) concentration patterns by depth and season. The size of each pie chart is determined by the quartile value of the combined dataset—<2.7-4.8 μg L⁻¹ for chl *a* and <1.7-15.1 μM for nutrients. Individual nutrients are distinguished by color and represent their portion of the total average concentration across the entire sampling grid. Columns are separated by season and rows are separated by depth. Spring consists of May 2019 and June 2018 sampling times; summer is July 2018 and July 2019, and Autumn is October 2018.

Figure 27: Diagram summarizing the chl *a* and dissolved nutrient (NH_4^+ , NO_x , PO_4^{3-}) concentration patterns by depth for July 2018 and July 2019. The size of each pie chart is determined by the quartile value of the combined dataset— $<2.6\text{-}4.6 \mu\text{g L}^{-1}$ for chl *a* and $<2.0\text{-}4.1 \mu\text{M}$ for nutrients. Individual nutrients are distinguished by color and represent their portion of the total average concentration across the entire sampling grid. Columns are separated by season and rows are separated by depth.

Figure 28: Conceptual diagram outlining the various chemical, biological, and physical processes that occur within the study region. Three columns are categorized by season, three rows categorized by depth.

INTRODUCTION:

Coastal Delmarva region

The study region for this project is a subsection of the coastal mid-Atlantic Ocean, offshore of the Delmarva Peninsula. This area is a climate boundary region that is undergoing ecological changes due to both anthropogenic climate change and eutrophication (Kaplan and Wolfe 2006). The coastal ocean is important both ecologically and economically to the region. Annually, the Maryland (MD) seafood industry contributes ~ \$600 million to the State's economy, and more than 8 million people visit Ocean City. As a popular tourist destination and important farming region in MD, the ecosystems surrounding Ocean City, MD, including Assateague Island National Seashore (ASIS) and the Maryland Coastal Bays (MCB), are impacted by human use through recreation, sewage outflow, and agricultural runoff (Figure 1) (Ocean City Chamber of Commerce). There is a need to understand water quality conditions in the region, and to establish baseline data on various parameters to assess threats to water quality. These threats include nutrient inputs and their effects on other water quality issues, including the presence of emergent harmful algal bloom species (HABs), which are increasing globally due to anthropogenic eutrophication and climate change (Heisler et al. 2008). Additionally, it is important to assess the potential for future threats to arise, given the region's importance both ecologically and economically of the region (Vilacoba 2017).

There has been prolific research and monitoring of the both the Chesapeake Bay and the MCBs, but less attention has been paid to the coastal regions off the

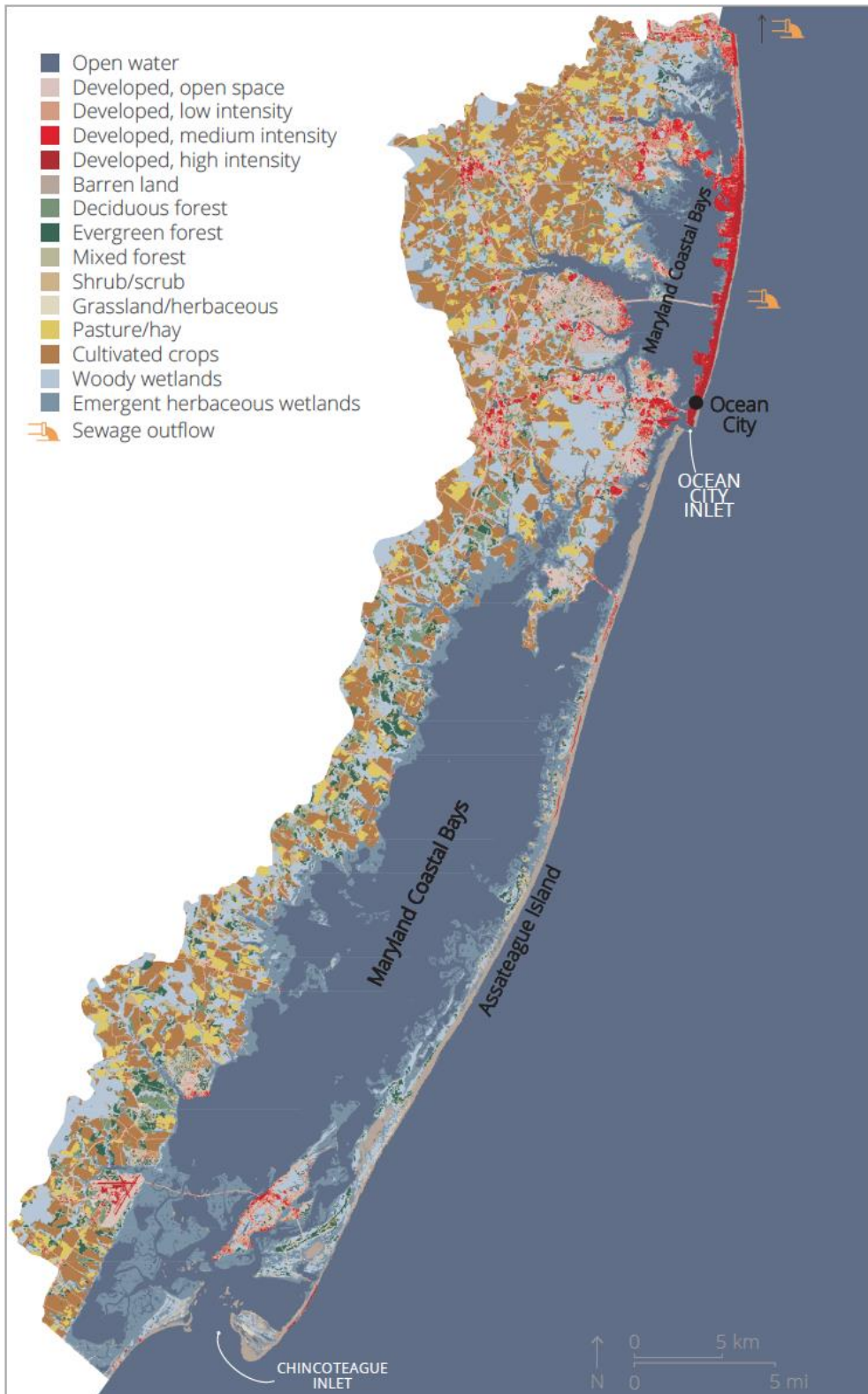


Figure 1: Land use land cover map of study region with areas of agricultural land, developed land, and barren land (Integration and Application Network - ian.umces.edu/media-library).

coast of MD and along the Delmarva Peninsula (DE, MD, VA) coastal region. Therefore, this study responded to the need for more information on seasonal and geographic data on water quality in the coastal Atlantic of this region. The sampling area for this study consists of 31 sampling stations along 10 transects from near the Delaware (DE) border in the north, south along the Maryland coast, and extending into the state of Virginia (VA) to the south. Sites ranged in proximity to shore at distances of ~0.8, 1.6 and 2.4 km offshore (Figure 2). These transects bracket the Delmarva regions of the Maryland coast from north to south covering different geographic, and nutrient sources described in more detail below. Specifically, this project sought to assess the state of water quality in the coastal Atlantic Ocean region of the Assateague Island National Seashore (ASIS) along the Delmarva Peninsula coast, in terms of nutrients (nitrogen and phosphorus), and emerging HABs of concern.

Anthropogenic influences

The Maryland coast has been influenced by humans since the indigenous Assateague people settled permanently on the Eastern Shore of Maryland in ~900 AD (Rountree and Davidson 1997). Starting in the 1600s, European settlers changed the landscape through farming and agriculture. Over time, the population grew and technology advanced, and the MCBs became a popular tourist destination. Currently the most densely populated area of the region is Fenwick Island, which is a barrier spit that is shared by the towns of Ocean City, MD, and South Bethany, DE (Figure 1) (US Census Bureau 2018). Sampling locations along transects 1 and 2 border



Figure 2: Map of the study area with data collection sites, transects, sewage outflow locations, and MCB inlet locations (Integration and Application Network - ian.umces.edu/media-library).

Ocean City, MD (Figure 2). The town of Ocean City is 7.1 km² of land, and this beachfront community is mostly seasonal with a population of ~7,000 year-round that expands to ~330,000 during the summer months (American Community Survey 2021) (Figure 1). The area has a boardwalk, hotels, restaurants, arcades, and other tourist attractions. Other than the beachfront, however, this area is covered almost entirely in impervious surfaces. (Figure 1).

In 1933, a hurricane created the Ocean City Inlet, separating Assateague Island from Fenwick Island. Transect 3 is directly adjacent to the Ocean City Inlet, which is one of two connections between the Atlantic Ocean and the MCBs (Figure 3). Increased development and population growth in the MCBs created the need for a municipal sewage treatment plant, and the newly formed Ocean City Inlet was an ideal place for wastewater release. Eventually the sewage treatment plant processing needs became too high for the Ocean City Inlet outfall, and an offshore outfall was created in 1969 (NewGen Strategies and Solutions 2020).

Currently, there are three major sewage outfall areas in the region. There is a sewage outfall release north of the sampling region in DE (38.72972 N, 75.05861 W). This sewage outfall releases 1829 m (~6000 ft) from shore through a pipe that connects to the Rehoboth Beach Wastewater Treatment Plant on Roosevelt St. (Figure 1) (*City of Rehoboth Beach Ocean Outfall Project Town Hall Q&A Workshop* 2017). The Rehoboth Beach Wastewater Treatment Plant treats approximately 7.6 million liters per day (2 million gallons a day) (MGD) but can reach up 26.5 million liters per day (7 MGD) during a peak tourist weekend. Additionally, the South Central Regional Waste-Water Treatment Facility (WWTF) in Bethany Beach, DE

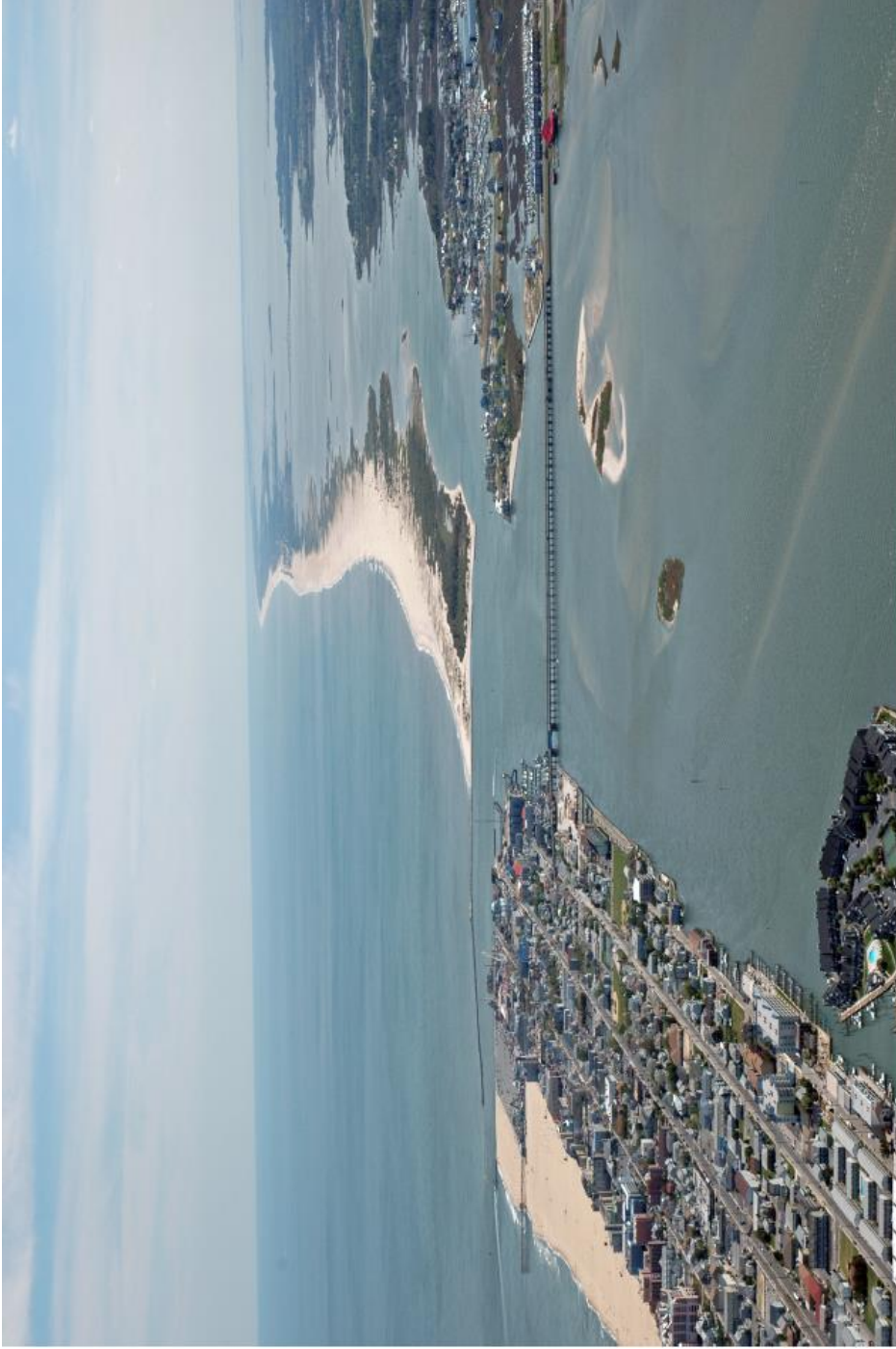


Figure 3: Aerial photograph of Ocean City with views of the Ocean City Inlet and Assateague Island. Photo by Jane Thomas-UMCES-IAN (CC BY-SA 4.0).

releases treated water into the Atlantic Ocean just north of Fenwick Island (38.5240 N, 74. 9567 W) (Figure 1) (Delaware Department of Natural Resources and Environmental Control 2020). The South Central WWTF releases between 9.5-11.3 million liters per day (2.5-3.0 MGD) through the ocean outfall location. Lastly, there is a sewage outflow that releases 1219 m (~4000 ft) offshore Fenwick Island (Figure 1). The sewage outflow releases directly north of the transect 2 sampling stations (38.38395 N, 75.05333W) and connects to the Ocean City, MD Wastewater Treatment Plant on 64th Street, Ocean City (Figure 2). Average daily flow from the sewage outfall ranges from 13.3 million liters per day (3.5 MGD) in the winter, to 39.7 million liters per day (10.5 MGD) in the summer. With more people visiting and developing Fenwick Island, more environmental stress has become evident (Dennison et al. 2009).

Sampling locations along transects 4-10 begin at the northern point of Assateague Island and stretch to the south at the Chincoteague Inlet (Figure 2). Assateague Island is 37-miles long and was originally connected to Fenwick Island. However, after the 1933 hurricane that separated the two barrier islands by an inlet, permanent jetties were installed to maintain the channel (Hayward 2007). The town of Chincoteague located near the Chincoteague Inlet, just south of the VA border, is another populated area. The town of Chincoteague has year-round residents with a population of ~3,000 – 15,000 (Town of Chincoteague 2015; Chincoteague: About Our Island). The major source of income for the town is tourism, but there is a highly developed seafood industry as well. Although much of the town is densely developed, there are many parks and undeveloped lands in the area. The Chincoteague Island

community takes pride in its rich history and preserves areas of historical and ecological importance. There is currently no WWTF on Chincoteague Island, but the Chincoteague Wastewater Advisory Committee continues to revisit wastewater treatment and management plans for the community (Papadopoulos et al. 2013; Chincoteague: About Our Island).

Between the Ocean City Inlet at the north and the Chincoteague Inlet at the south, Assateague Island consists of 37 miles of nearly undeveloped land (mostly sandy shoreline and herbaceous/wetland areas with scattered deciduous forest). Assateague Island is managed by three agencies: The National Parks Service (NPS) controls ASIS, the Maryland Department of Natural Resources (MD DNR) controls the Assateague State Park, and the U.S. Fish and Wildlife Service (USFWS) controls the Chincoteague National Wildlife Refuge. ASIS receives over 1 million visitors each year and is the largest section of the park. The national seashore allows daily visits, camping, and other recreational activities (National Parks Service 2018). The Assateague State park is a 3.2 km section of beachfront park that offers a similar experience managed by the state of MD (Maryland Parks Service 2020). The Chincoteague National Wildlife Refuge connects to ASIS via a bridge at the VA border and welcomes recreational visitors and tourists as well (US Fish and Wildlife Service 2015). ASIS is a popular tourist destination, and prior research regarding the National Park's coastal waters shows early indications of elevated nutrients and the presence of HABs, but there is no systematic coastal water quality monitoring. Therefore, continued coastal dissolved nutrient and HAB research is essential to understanding and managing the Assateague Island ecosystem.

The MCBs and waterways which surround the ASIS, are influenced by inputs from both land sources as well as from tides and currents from the Atlantic Ocean (Figure 1). There is a need to better understand the linkages between the coastal ocean and the MCBs, ecosystem changes and impacts of human activity. In the MCB watershed, urban development is increasing and taking over more natural lands and agricultural lands (Aighewi et al. 2013). Highly developed areas diminish ecosystem diversity by eliminating suitable habitat and resources for wildlife. Fenwick Island is experiencing high population growth, with projections for continued growth through 2030 (Nosakhare et al. 2012). High population density results in less natural land, hardening shorelines (i.e. riprap), and more impervious surfaces; all of which contribute to eutrophication of the MCB and coastal waters (Dillow and Greene 1999; Aighewi et al. 2013).

Land use in the MCB region is dominated by urban, forest, and agriculture (Figure 1) (Beckert et al. 2011). Agriculture is the primary source of the anthropogenic nutrient loading in the MCBs (Beaulac and Reckhow 1982; Dennison et al. 2009; Beckert et al. 2011). Agriculture contributes nutrients (specifically nitrogen and phosphorus) from land into the MCB waterways through fertilizer, crops, and animal waste (Boynton et al. 1993; Dennison et al. 2009). Most of the agricultural land is located on the western side of the coastal bays, but the impact from nutrient loading is still present in the coastal waters due to the MCB inlet connections. Physical movement of the water leaving the Ocean City Inlet does not necessarily get transported offshore (Kang et al. 2017; Mao and Xia 2018). Drifter

studies shows evidence of a small eddy formation to the south of the Ocean City Inlet that keeps the water and nutrients circulating close to shore (Mao and Xia 2018).

Impervious surfaces and runoff

In addition to sewage outfalls and agricultural nutrient loading, highly developed areas with impervious surfaces create environmental hazards in MD's coastal waters. The National Oceanic and Atmospheric Administration (NOAA) uses impervious surface land cover as a water quality indicator because impervious surfaces (in conjunction with excess nutrient pollution highly developed areas) limits water filtration capabilities. Runoff from impervious surfaces enter coastal waters, creating increased water pollutants and decreased water quality.

Continued monitoring of the MCB has provided thresholds to use for comparison of nutrient, chl *a* and HAB species concentrations (Table 1) (Dennison et al. 2009). Additionally, MD DNR has thresholds for emergent HAB species of concern for bloom levels of concern for the state of MD (Harmful algal bloom management in the Chesapeake and Coastal Bays 2014). However, the MCB and MD DNR thresholds are based on estuarine systems and are not necessarily suitable for coastal waters offshore. In this coastal setting, nitrogen and phosphorus are the primary limiting nutrients (Dennison et al. 2009). Unlike the MCB where there are numerous point sources for nutrient rich freshwater sources, the ocean system has only a few point sources for nutrients. Although there are multiple non-point sources of nutrients into these waterways, sewage outflows and inlets connecting the ocean to the MCB provide direct nutrient input into the coastal waters. Another potential

Table 1: MCB thresholds values for chl *a*, TN, TP, *Dinophysis* spp., *Karenia* spp., *Pseudo-nitzschia* spp.

Threshold Concentration (μM, $\mu\text{g L}^{-1}$, cells L^{-1})	
Total nitrogen	46
Total phosphorus	1.2
Chlorophyll <i>a</i>	15
<i>Dinophysis</i> spp.	10,000
<i>Karenia</i> spp.	10,000,000
<i>Pseudo-nitzschia</i> spp.	1,000,000

source of nutrient input into the coastal system is late-summer upwelling (Glenn et al. 2004b).

Management Initiatives

The Clean Water Act (1972) forced the MCBs to take a closer look at water quality and municipal wastewater pollution. As a result of water quality data from point-source and non-point source discharge, efforts were made to decrease nutrient input into the coastal waterways, including banning phosphate (PO_4^{3-}) use in 1985 (US Department of the Environment 2020). Numerous HAB incidents led to the MCBs being included on MD's impaired waters list in 1996 (Tango et al. 2004). As part of the Comprehensive Conservation and Management Plan released in 1999, the MD DNR conducts routine monitoring of the MCB water quality (Maryland Coastal Bays 1999). While nutrient thresholds have been established for the different salinity regions of the Chesapeake Bay (EPA 2001), as well as the MCB, and routine monitoring of the MCBs started in 2001, there are no monitoring or nutrient threshold regulations for offshore coastal waters. This knowledge gap is particularly problematic because of the sewage outfall locations which release offshore, nutrient loading from the dominant agriculture industry, and pollution runoff from impervious surfaces of highly developed areas. Several regulatory agencies are currently working on updating nutrient criteria (EPA 2001) and developing more specific offshore nutrient and chl *a* threshold concentrations (C. Wazniak pers com).

Eutrophication and Harmful Algal Blooms

HABs occur when algal growth is stimulated to such a degree that cell numbers accumulate and have some level of negative impact in the environment

ranging from nuisance, to toxic, depending on the species, but causing some level of detrimental impact to the ecosystem (Smayda 1997). HABs can change the color of the water, cause fish kills (physically or chemically), and potentially release toxins into the water and air that are damaging to the ecosystem and its inhabitants (Timmons et al. 2018). It has been observed that HABs have been increasing globally in spatial distribution and frequency as a result of climate change and eutrophication (Heisler et al. 2008). The MD DNR has identified three emergent HABs of concern in the region offshore Assateague Island and the MCB in recent years: *Karenia* spp., *Dinophysis* spp., and *Pseudo-nitzschia* spp. but little is known of their abundance over time nor their concentrations in the water column (Allen et al. 2014). Similarly, little is known about the potential production of toxin from these species. Therefore, these three genera were targeted for specific attention in this study.

Karenia spp.

Karenia spp. consist of unarmored dinoflagellate species, some of which can release a variety of toxins (Figure 4) (Basti et al. 2018). *Karenia brevis* (also known as the Red Tide in the Gulf of Mexico), *Karenia mikimotoi*, and *Karenia papilionacea* are among the species found in the region—however, this group of harmful algae is found more commonly at lower latitudes (Heil et al. 2014a). Toxin production is specific to each species, however all species within the genus *Karenia* have been identified as potentially toxic. *K. brevis* and *K. papilionacea* release brevetoxin which can cause respiratory illness and Neurotoxic Shellfish Poisoning (NSP) (Baden and Mende 1982; Fowler et al. 2020). *K. mikimotoi* releases multiple types of toxins—Gymnodimines which are associated with NSP, and Gymnocin-A,



Figure 4: Photomicrograph of *Karenia* spp. samples collected during research cruises in the MD coastal ocean. (A) *Karenia mikimotoi*, (B) *Karenia papilionacea*, (C) *Karenia brevis*. Photomicrographs taken by Jen Wolny-MD DNR.

Gymnocin-B which have unknown human effects, but can be fatal for fish and invertebrates (Seki et al. 1995; Satake et al. 2002; Brand et al. 2012). *K. selliformis* releases Brevetoxin and Gymnodimines (Miles et al. 2003; Brand et al. 2012).

These *Karenia* species can become abundant under various combinations of nutrient sources and do not necessarily require high nutrient conditions, and are known to have mixotrophic capabilities (Heil et al. 2014b). They are also adaptable to a high range of temperature and salinity conditions, which allow them to persist for multiple months in some regions of the Gulf of Mexico, in particular (Maier Brown et al. 2006; Vargo 2009; Errera and Campbell 2011).

Dinophysis spp.

Dinophysis spp. is a group of armored flagellate species which can release okadaic acid and dinophysistoxin (DTX) (Figure 5) (Basti et al. 2018). The lipophilic toxins released by *Dinophysis* spp. can cause Diarrhetic Shellfish Poisoning (DSP). In bloom conditions, DTX and okadaic acid result in dehydration, diarrhea and vomiting in humans after consuming contaminated shellfish. *Dinophysis* spp. have complex toxin profiles and can also release pectenotoxins along with other lipophilic toxins (yessotoxin, azaspiracids) (Reguera and Blanco 2019). However, the primary cause of poisoning associated with *Dinophysis* spp. is DSP from okadaic acid and DTX.

Dinophysis spp. are distributed globally across temperate latitudes in shallow waters (Morton et al. 2018). *Dinophysis acuta*, *Dinophysis acuminata*, *Dinophysis norvegica* and *Dinophysis caudata* are just some of the many species found in the study region, specifically during the summer months.

Pseudo-nitzschia spp.

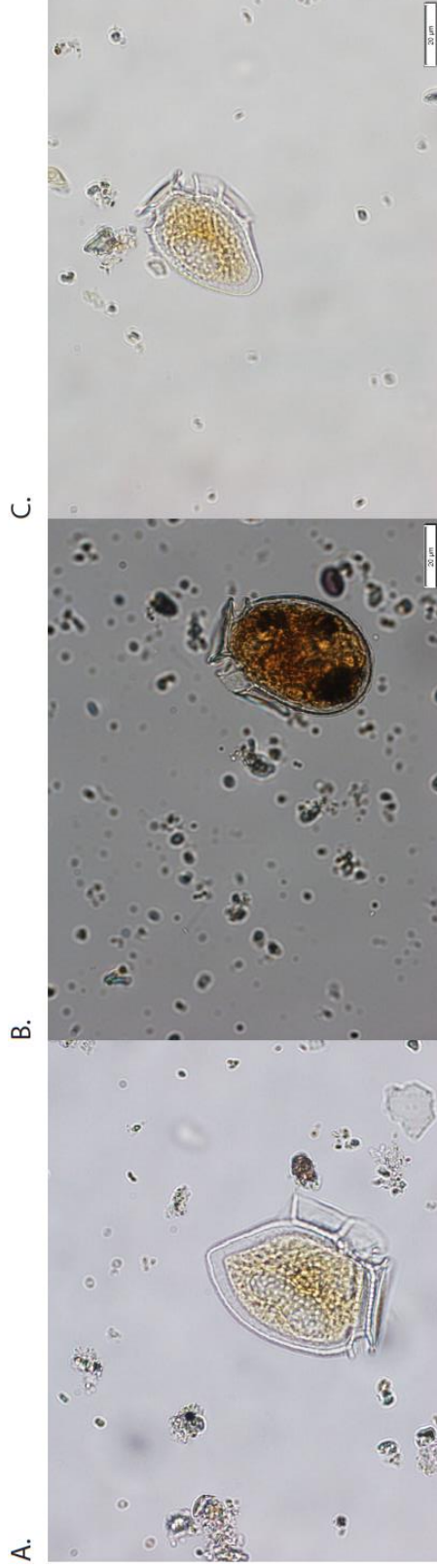


Figure 5: Photomicrograph of *Dinophysis* spp. samples collected during research cruises in the MD coastal ocean. (A) *Dinophysis norvegica*, (B) *Dinophysis acuminata*, (C) *Dinophysis acuminata*. Photomicrographs taken by Jen Wolny-MD DNR (used with permission).

Pseudo-nitzschia spp. are chain forming pennate diatoms and are known to form abundant blooms from multiple nutrient sources (specifically nitrogen and urea) (Figure 6) (Morton et al. 2018). Not all species of *Pseudo-nitzschia* are toxic, but toxigenic species of this harmful algae release domoic acid (DA) and previously have been noted as being most abundant in the springtime (Thessen and Stoecker 2007; Trainer et al. 2012). DA is associated with Amnesic Shellfish Poisoning (ASP) which, in humans, can lead to amnesia and memory loss (Basti et al. 2018). Toxic blooms are found mainly within eastern boundary current upwelling systems, but non-toxic or low-toxic blooms can be found globally (Morton et al. 2018). Conditions required to produce *Pseudo-nitzschia* spp. blooms are highly variable, but the toxigenic species found in the Chesapeake Bay region are generally more abundant with low temperature and high salinity (Thessen and Stoecker 2007). In 2020, DA was found in mussels in Ocean City Inlet just below concentrations of regulatory concerns. Mussels collected on September 15th, 2020 had DA concentrations of 7.6 - 10.6 ppb, much higher than typical water samples at that time of year (MD DNR unpublished data; Cath Wazniak pers comm).

Project aims and objectives

The potential anthropogenic nutrient and climate change threats to the region have led to a NPS funded project, of which this thesis is a part, with the following overall aims and objectives:

- To provide current data on nutrient and phytoplankton composition and potential HAB species to compare with previous MD DNR data along same sampling grid;



Figure 6: Photomicrograph of a *Pseudo-nitzschia* spp. sample collected during research cruises in the MD coastal ocean. Photomicrographs taken by Jen Wolny-MD DNR (used with permission).

- To use data acquired as a baseline for potential future monitoring of water quality and HAB species changes in terms of eutrophication and/or climate change;
- General overarching aim is to provide information to help protect the natural environment and natural resources in the ASIS and surrounding areas vital in the economic and cultural well-being of the region.

The primary objective of my thesis research, as part of this larger project, was to establish baseline concentrations of nutrients (Total Nitrogen [TN], Total Phosphorus [TP], Nitrate [$\text{NO}_3^{-1} + \text{NO}_2^{-1} = \text{NO}_x$], phosphate [PO_4^{3-}], ammonium [NH_4^+]) and investigate their impact on MD's emergent HAB species of concern (i.e. *Karenia* spp., *Dinophysis* spp., *Pseudo-nitzschia* spp.) in the coastal waters offshore ASIS and to assess the potential threats of these factors to water quality in the region. There are three primary hypotheses for this research that were tested using data collected from five cruises in 2018-2019:

- Nutrients and HAB species concentrations increase with high population density and human influence;
- Nutrients and HAB species concentrations vary seasonally in association with human influences;
- The population and use of Ocean City, MD and ASIS by seasonal visitors increase the concentrations of nutrient and HABs.

METHODS

Study Locations and Sampling Period

Water quality, phytoplankton community composition, chl *a* and nutrient (nitrogen and phosphorus) data were collected during five research cruises: June, July and October 2018; May and July 2019 aboard the University of Maryland Center for Environmental Science's (UMCES) R.V. *Rachel Carson*, and the University of DE's R.V. *Joanne Daiber*. Samples were collected at 31 stations located along 10 latitudinal transects (Figure 2, Table 2). Transects ranged from 38.4483⁰N to 37.82887⁰N, and from approximately 0.8 km offshore to 2.4 km offshore—a study area of ~2,500 km². The Ocean City Inlet, adjacent to transect 4; and the Chincoteague Inlet, adjacent to transect 10, provide estuarine influences from the MCBs. Additionally, the DE Bay is just north of the first transect and could provide additional estuarine mixing. Sampling location sites correspond to two previous sampling efforts (MD DNR 2011 survey; and MCB's Augmentative Grant Project, 2012) which established areas of concern to ASIS. Additionally, three bioassay experiments were performed in June, July and September of 2019 using water samples collected during flood tide from the *Oceanic Fishing Pier* adjacent to the Ocean City Inlet.

Field Sample Collection

Water at each station along the transects was sampled using CTD (Conductivity Temperature Depth) casts to determine the water profile with depth of various parameters, as well as to collect discrete water samples for nutrient analysis:

Table 2: List of research cruise dates and research vessels.

Field Data Collection	
Date	Ship
June 19-20, 2018	R.V. <i>Joanne Daiber</i>
July 28-29, 2018	R.V. <i>Rachel Carson</i>
October 9-10, 2018	R.V. <i>Rachel Carson</i>
May 20-21, 2019	R.V. <i>Rachel Carson</i>
July 16-17, 2019	R.V. <i>Rachel Carson</i>

TN, TP, NH_4^+ , NO_x , PO_4^{3-} and chl *a*. Discrete water samples for nutrient and chl *a* analyses were collected at the surface, the depth of the chlorophyll maximum (chl *a* max) determined by the CTD profile, and 1 m off of the bottom using a Rosette of 10 L Niskin bottles (Figure 7). Samples for nutrient, chl *a* and phytoplankton analyses were collected at the surface and chl *a* max depths. Samples were filtered through GF/F filters (nominal pore size 0.7 μm), which were retained for chl *a* analyses and the filtrate retained for nutrient analyses at the University of Maryland Center for Environmental Science – Horn Point Laboratory (UMCES-HPL) Analytical Services Laboratory. Chl *a* and nutrient samples were frozen aboard the ship and transported to HPL and kept frozen until analysis. Phytoplankton samples were fixed with 5% Lugol's iodine solution and maintained dark and cold, stored in a refrigerator until the time of analysis.

Water samples for nutrient bioassay experiments were collected in the Ocean City Inlet from the *Oceanic Fishing Pier* (710 S. Philadelphia Avenue, ~0.7 km NW of the inlet origination) during flood tides, to capture ocean water coming into the MCBs through the inlet. Water was collected using a submersible pump into 10 L cubitainers and placed into reduced light. Samples were covered with wet towels to maintain ambient temperature and transported back to HPL where the nutrient bioassay experiments were conducted (Figure 8). Water quality parameter values including water temperature, dissolved oxygen (DO), salinity, and conductivity were measured off the Oceanic Fishing Pier using a YSI Pro2030 DO, Conductivity, Salinity Instrument at each initial sampling date. Each experiment consisted of 5-6 L of site surface water, with triplicate cubitainer treatments. In the



Figure 7: Photograph of Rosette with CTD and 8, 10 L Niskin bottles deployed at each sample site to measure *in-situ* physical parameters and collect discrete water samples at the surface, chl *a* max and bottom depths. Photo by Max Hermanson-UMCES- IAN (used with permission).



Figure 8: Taylor Floats holding bioassay cubitainers used for incubating samples at ambient light and temperature in the Horn Point Laboratory Harbor. Photo by J.M. O'Neil-UMCES- HPL (used with permission).

second bioassay experiments, 200 μM mesh screening was used to remove meso-zooplankton such as copepods to assess grazing impacts.

Nutrient Analysis

In situ values of chemical and physical parameters were determined at each station and depth using the CTD's DO (mg L^{-1}), photosynthetic active radiation (PAR, $\mu\text{E m}^{-2} \text{s}^{-1}$), and fluorescence ($\mu\text{g L}^{-1}$) sensors. Discrete samples were taken at each depth for dissolved and particulate nutrient analyses (TN, TP, NH_4^+ , NO_x , and PO_4^{3-}) using standard methods of nutrient analysis at UMCES-HPL analytical services (D'Elia et al. 1977; Solórzano and Sharp 1980a; Solórzano and Sharp 1980b; Valderrama 1981; Parson et al. 1984; and, Clesceri et al. 1998). TN and TP concentrations are calculated using unfiltered water samples; therefore, total values are the sum of all dissolved and particulate constituents for each of these elements. TN and TP are indicators of total loading of nitrogen and phosphorus, whereas dissolved nutrients (NH_4^+ , NO_x , and PO_4^{3-}) are what phytoplankton are capable of direct uptake. N:P ratios were calculated based on the molar TN and TP concentrations, and dissolved N:P ratios were calculated based on the concentrations of $\text{NO}_x + \text{NH}_4^+$, and PO_4^{3-} .

Chlorophyll Extraction

Chl *a* concentrations from discrete water samples collected at the surface, chl *a* max, and bottom depths were processed using EPA Standard Method 445.0 for *in vitro* determination of chl *a* in which samples were extracted in 10 mL of 90% acetone for 24 hours, while refrigerated (Arar and Collins 2021). Samples were then

centrifuged for 10 minutes at 1000 g, fluorescence measured for chlorophyll and then acidified to obtain phaeopigment concentrations, using a *Turner Designs* fluorometer and standardized to $\mu\text{g chl } a \text{ L}^{-1}$.

Phytoplankton Community Analysis and Cell Counts

Phytoplankton community analysis was performed for all samples at the surface and chl *a* max depths by MD DNR. Phytoplankton samples from bioassays were analyzed at UMCES-HPL microscopy lab. In all cases, samples were examined using a Zeiss Axiovert 200 inverted microscope using a modified Utermohl method in which a 9 mL sample was allowed to settle for 24 hours. Subsequently, a minimum of 5 optical fields were examined at 400X to identify and enumerate small and numerous species. Additional optical fields were examined until a minimum of 200 cells were enumerated. The entire chamber was scanned at 100X to allow for the identification and enumeration of large and rare species. Species were identified to the lowest taxon possible (Dodge 1982; Steidinger et al. 1997; Tomas 1997). The following emergent HAB species were enumerated: *Dinophysis acuminata*, *D. acuta*, *D. norvegica*, *D. punctata*, *D. fortii*, *D. hastata*, *D. odiosa*, *D. ovum*, *D. sp.*; *Karenia brevis*, *K. mikimotoi*, *K. papilionacea*, *K. selliformis*, *D. sp.*; *Pseudo-nitzschia brasiliiana*, *P. sp.* However, for the purposes of this analysis, HAB species will be combined at the genus level; *Dinophysis* spp., *Karenia* spp., *Pseudo-nitzschia* spp.

Synthesis of Nutrients, HABs, Environmental Factors

For seasonal and geographical variation comparisons, nutrient and HAB species data was integrated along transects by calculating the mean concentration for




each nutrient (TN, NH₄⁺, NO_x, TP, PO₄³⁻), HAB species (*Dinophysis* spp., *Pseudo-nitzschia* spp., and *Karenia* spp.) and environmental factors (DO, temperature, salinity, chl *a*) at each sampling depth. Additionally, the average concentrations at each transect were summed to create a total nutrient, total HAB species, and total chl *a* concentration for each sampling date and sampling depth. Total concentrations of all variables are categorized by quartile. For all analyses the data is presented to show seasonal variation by using the following order: May 2019, June 2018, July 2018, July 2019, October 2018.

Statistical significance of correlation between nutrients, HAB species, depth and environmental factors was determined using a linear regression model in R (Tables 3-4) (Wilkinson and Rogers 1973; Chambers 1992). Each regression was run using individual sampling locations, rather than integrating the data along transects. Additionally, N:P ratios and dissolved N:P ratios were included in the statistical testing.

Principal Component Analysis

Multiple principal component analyses (PCA) were completed using R software (Venables and Ripley 2002; Martin and Maes 2008). PCAs were run with the following variables: depth, TN, NH₄⁺, NO_x, TP, PO₄³⁻, dissolved N:P ratio, total N:P ratio, DO, temperature, salinity, chl *a*, *Dinophysis* spp. concentration, *Pseudo-nitzschia* spp. concentration, and *Karenia* spp. concentration. Two kinds of PCAs were run, PCAs for each sampling period and PCAs for each HAB species. PCAs for each sampling period (including one that combined data from all sampling periods) included physical variables and nutrient concentrations at the surface, chl *a* max and

Table 3: Statistical significance of the differences between HAB concentrations and nutrients/physical parameters. Statistical significance of linear regression model is defined by p-value<0.05 for t-test (Integration and Application Network ian.umces.edu/media-library).

Species	Nutrient	P-Value	Adjusted R-Squared	Slope	Intercept
<i>Dinophysis</i> spp. 	TN-TP Ratio	0.84	-0.005	>-0.01	11.9
	Dissolved N-P Ratio	<0.01	0.038	>-0.01	10.4
	TN	0.25	<0.01	<0.01*	10.7
	NO _x	0.23	<0.01	>-0.01	0.4
	NH ₄ ⁺	<0.01	0.031	>-0.01	1.4
	TP	0.29	<0.01	<0.01*	0.9
	PO ₄ ³⁻	0.97	>-0.01	>-0.01	0.3
	Temperature	<0.01	0.081	>-0.01	20.5
	Salinity	0.24	<0.01	>-0.01	30.5
DO	0.05	0.016	>-0.01	6.5	
<i>Karenia</i> spp. 	TN-TP Ratio	0.46	-0.003	>-0.01	12.5
	Dissolved N-P Ratio	0.18	<0.01	>-0.01	8.3
	TN	0.42	>-0.01	>-0.01	11.0
	NO _x	0.42	>-0.01	>-0.01	0.0
	NH ₄ ⁺	0.78	>-0.01	>-0.01	1.1
	TP	0.87	>-0.01	>-0.01	0.9
	PO ₄ ³⁻	0.90	>-0.01	<0.01*	0.3
	Temperature	0.25	<0.01	>-0.01	21.8
	Salinity	0.61	>-0.01	<0.01*	30.4
DO	0.46	0.003	>-0.01	6.8	
<i>Pseudo-nitzschia</i> spp. 	TN-TP Ratio	0.05	0.021	>-0.01	12.5
	Dissolved N-P Ratio	0.15	<0.01	>-0.01	7.8
	TN	0.67	>-0.01	<0.01*	12.2
	NO _x	0.97	>-0.01	>-0.01	0.7
	NH ₄ ⁺	0.65	>-0.01	>-0.01	1.2
	TP	0.09	0.014	<0.01*	1.0
	PO ₄ ³⁻	<0.01	0.042	<0.01*	0.4
	Temperature	0.36	>-0.01	<0.01*	23.0
	Salinity	0.21	<0.01	<0.01*	30.5
DO	0.86	>-0.01	<0.01*	7.0	

Statistically significant (p-value<0.05)

* Positive slope

Table 4: Statistical significance of the differences between sampling depth of HAB concentrations (surface, chl *a* max, bottom). Statistical significance of linear regression model is defined by p-value<0.05.

Species	P-Value	Adjusted R-Squared	Slope	Intercept
<i>Dinophysis</i> spp.	<0.01	0.44	0.53*	-209.2
<i>Karenia</i> spp.	0.29	<0.01	0.01*	1403
<i>Pseudo-nitzschia</i> spp.	<0.01	0.11	0.3171*	1519.9
Statistically significant (p-value<0.05)				

* Positive slope

bottom. PCAs for each HAB species included physical variables, nutrient concentrations and HAB species concentrations at the surface and chl *a* max.

Nutrient Bioassay

Three nutrient bioassay experiments were conducted in June, July, and September 2019 (Table 5). The June bioassay experiment ran for 7 days, but chl *a* concentrations declined after day 3, so the July and September bioassays ran for 3 days. Bioassays were incubated in situ at HPL in “Taylor Floats” at ambient water temperature under 1-2 layers of neutral density screening in order to reduce photo-inhibition and simulate the light level experienced at ocean surface (Figure 8). In the June and September bioassays, triplicate samples for all bioassay treatments included concentrations of 10 μM NH_4^+ , 10 μM NO_3^- , 5 μM PO_4^{3-} , a combined treatment of 10 μM NO_3^- + 5 μM PO_4^{3-} (N+P); and a control treatment of 10 mL deionized water added daily. In the July bioassay, a second control was added with a filter to remove zooplankton grazers. Samples were taken to determine absolute chl *a* values every 3rd day in June, and every day in July and September. Chl *a* was extracted using the same methods as field samples. Additionally, samples were collected to measure HAB species (*Dinophysis* spp., *Pseudo-nitzschia* spp., and *Karenia* spp.) concentrations. HAB species concentration samples were taken in June on days 0, 1, 3; in July on days 0, 1, 3; and in September on days 0, 1, 2, 3 and analyzed using the same methods as field samples.

Table 5: List of nutrient bioassay dates and treatments.

Nutrient Bioassay Experiments		
Bioassay #	Experiment Dates	Treatments
Bioassay 1	June 18-25, 2019	Control, NH4+, PO43-, NO3+PO43
Bioassay 2	July 9-12, 2019	Control, Grazer Control, NH4+, PO43-, NO3 + PO43
Bioassay 3	September 3-6, 2019	Control, NH4+, PO43-, NO3+PO43

RESULTS

Nutrients and Physical Characteristics

NO_x and NH_4^+ were the primary components that explained the most variation (20.8% and 27.6%, respectively) when integrating nutrient data across surface, chl *a* max and bottom sampling depths, 31 sampling locations, and sampling times in June, July and October 2018, and May, July 2019 (Figure 9a). At each sampling time, the percentage of explained variability changed, but the principal components themselves remained the same during all cruises. In May there was a positive relationship between NH_4^+ and salinity and PO_4^{3-} , and a negative relationship between NH_4^+ and temperature, total nutrients (nitrogen and phosphorus), N:P ratios (total and dissolved) (Figure 9b). During this sampling period there was also a negative relationship between NO_x and dissolved N:P ratios, TP, and NH_4^+ . There was very little depth stratification in May, but the surface became more differentiated from the mid and bottom depths in June (Figure 9c). In June, the strength of the relationship between NH_4^+ and salinity decreased, but there was a positive relationship between NO_x and salinity. The correlation between NH_4^+ and total nutrients (nitrogen and phosphorus), as well as chl *a* also increased compared to May.

The summer months (July 2018, July 2019) had a higher percentage of explained variation by NH_4^+ (49.8% and 54.4%, respectively) and had more depth stratification. However, there were a few commonalities in physical characteristics between July 2018 (Figure 9d) and 2019 (Figure 9e). In July 2018, there was a positive relationship between NH_4^+ and total nutrients, dissolved nutrients, salinity,

and dissolved N:P ratios; and a negative relationship between NH_4^+ and total N:P ratios, temperature, and chl *a*. Alternatively, in July 2019, the relationship between NH_4^+ and total nutrients, dissolved nutrients, and salinity was negative. NH_4^+ and chl *a* had a negative relationship, and NH_4^+ and DO had a positive relationship in both July 2018 and 2019.

In October (just after a strong mixing event due to the impact of Hurricane Florence) there was very little depth stratification. The explained variation by NH_4^+ was still high (46.1%) and the NO_x was still lower than in the spring months (18.1%) (Figure 9f). The relationship between NH_4^+ and total nutrients, dissolved nutrients, and N:P ratios (total and dissolved) was positive; and the relationships between NH_4^+ and temperature, chl *a*, and salinity were negative. Additionally, there was a positive relationship between NO_x and temperature, chl *a*, and total N:P ratios, but a negative relationship between NO_x and salinity, DO, TP, and PO_4^{3-} .

Nutrients and Harmful Algal Bloom Species

Linear regression correlation models were used, and statistical significance levels were established for each HAB species, each nutrient, temperature, salinity, and N:P ratios (total and dissolved) (Table 3). Using a p-value of <0.05 to reject the null hypothesis, a significant correlation was determined for the following pairs: *Dinophysis* spp. and dissolved N:P ratio, *Dinophysis* spp. and NH_4^+ , *Dinophysis* spp. and temperature, *Pseudo-nitzschia* spp. and PO_4^{3-} . All of the statistically significant relationships with *Dinophysis* spp. had negative relationships. PO_4^{3-} paired with *Pseudo-nitzschia* spp. had a positive relationship.

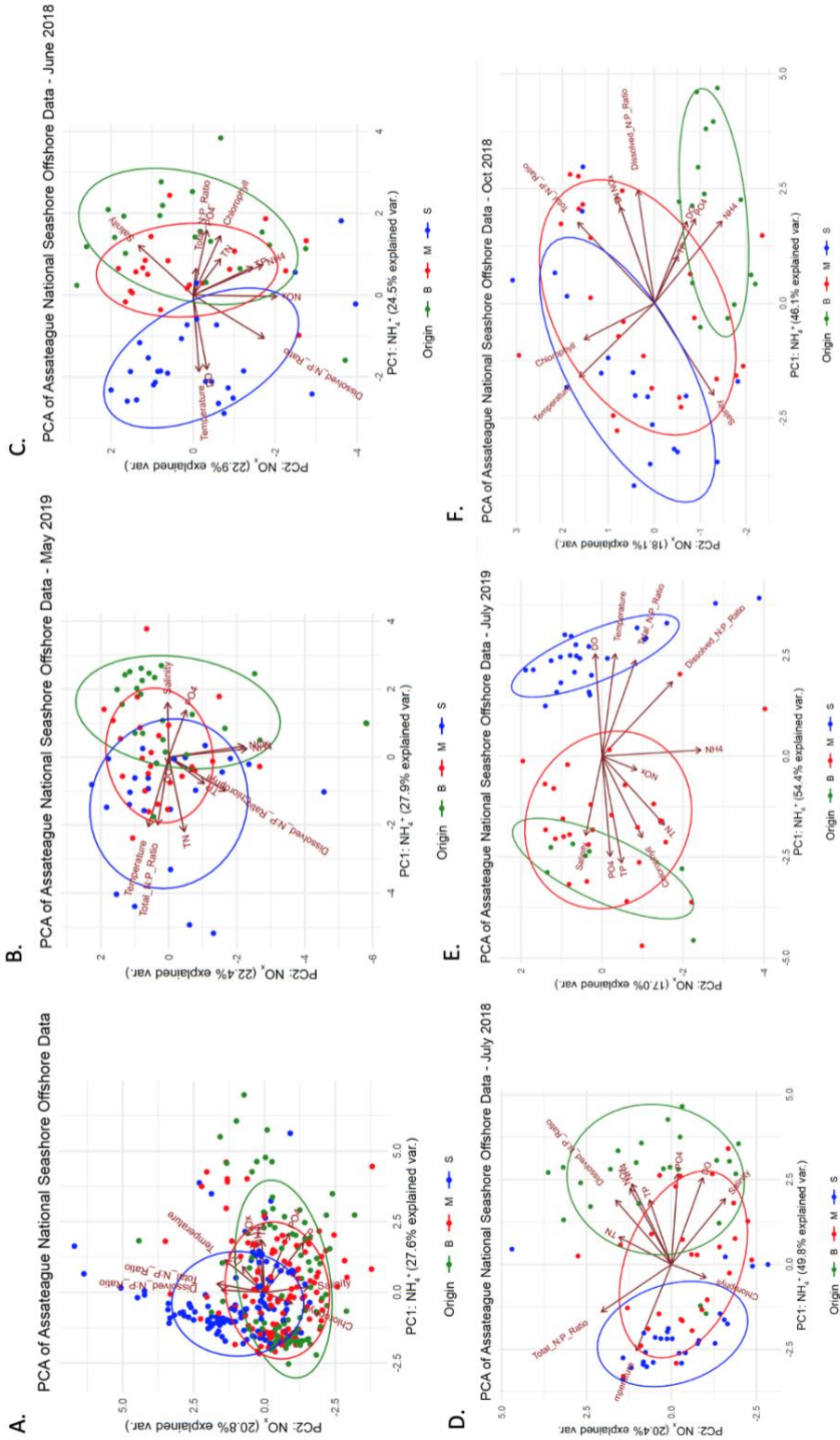


Figure 9: PCA bi-plots categorized by depth to include physical variables (temperature, salinity, DO), N:P ratios (dissolved and total), chl *a* and nutrient concentrations (TN, TP, NH_4^+ , NO_x , PO_4^{3-}). (A) Combined data from all sampling times (June, July, October 2018; May, July 2019), (B) data from May 2019, (C) data from June 2018, (D) data from July 2018, (E) data from July 2019, (F) data from October 2018.

A principal component analysis (PCA) was run for each of the three emergent HAB species of concern, to assess the determinant environmental variables and nutrients when each species is present. Each species' PCA combines all the data points (including HAB species concentrations) from the five sampling cruises and two sampling depths (surface and chl *a* max) when the species was present (Figure 10). For every HAB species, the principal components that explained the most variation in the dataset were NH_4^+ and NO_x . Temperature, DO, and N:P ratios (dissolved and total) have a positive relationship with NH_4^+ , and chl *a*, salinity, TP, PO_4^{3-} , TN, and NO_x had a negative relationship with NH_4^+ . Nearly all of the nutrients and environmental variables had a negative relationship with NO_x , except for chl *a* and salinity.

For the datapoints in which *Dinophysis* spp. were present, 23.4% of the variation was explained by NH_4^+ and 21.7% was explained by NO_x (Figure 10a). *Dinophysis* spp. has a very small negative relationship with NH_4^+ , but a moderate positive relationship with NO_x . When *Karenia* spp. were present, 23.3% of the variation was explained by NH_4^+ , and 20.5% was explained by NO_x (Figure 10b). Since all sampled *Karenia* spp. concentrations were small, the relationships between *Karenia* spp. and nutrients and environmental variables were also small. *Karenia* spp. did have a slight positive relationship with both NO_x and NH_4^+ , and a negative relationship with TN, and TP. The explained variation by NH_4^+ and NO_x when *Pseudo-nitzschia* spp. was present was 23.7% and 20.6%, respectively. (Figure 10c). *Pseudo-nitzschia* spp. had a negative relationship with both NH_4^+ and NO_x , but a relatively strong relationship with PO_4^{3-} , TP and TN.

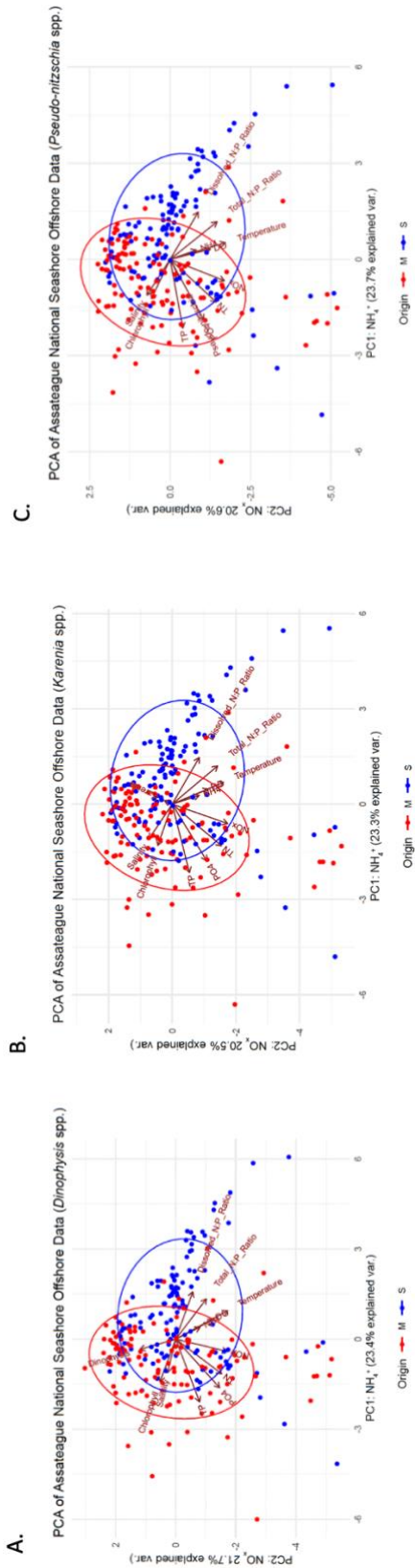


Figure 10: PCA bi-plots categorized by depth (surface, chl α max, bottom) to include physical variables (temperature, salinity, DO), N:P ratios (dissolved and total), HAB species concentrations (*Dinophysis* spp., *Karenia* spp., and *Pseudo-nitzschia* spp.), chl α and nutrient concentrations (TN, TP, NH₄⁺, NO_x, PO₄³⁻). (A) Combined data from all sampling times with the presence of *Dinophysis* spp., (B) combined data from all sampling times with the presence of *Karenia* spp., (C) combined data from all sampling times with the presence of *Pseudo-nitzschia* spp.

Correlation tests to assess the statistical significance of differences between surface and chl *a* max concentrations were established for each emergent HAB species of concern (Table 4). For *Dinophysis* spp. there was a large statistically significant difference between surface and chl *a* max samples (p-value = <0.01) with higher abundances in the chl *a* max layer. *Pseudo-nitzschia* spp. also had a statistically significant difference between surface and chl *a* max samples (p-value = <0.01), also with higher values in the chl *a* max layer. However, the difference in depth of *Karenia* spp. samples was not statistically significant (p-value = 0.3). The highest concentrations of *Karenia* spp. occurred at the chl *a* max depth, but there were more sites with *Karenia* spp. presence at the surface.

Dissolved nutrient variations

The dissolved nutrient concentrations and the nutrient species with the highest concentration percentage varied seasonally, geographically and by depth (Figure 11). The highest combined dissolved nutrient concentration ranges were found at the chl *a* max layer (up to 19 μM), with both the surface and bottom concentration peaks significantly lower (up to 8.4 μM at the surface and 12.1 μM at the bottom). At the surface, the highest concentrations were found in July 2019 and October 2018 and the lowest concentrations were found in July 2018. Overall, surface dissolved nutrients were primarily dominated by NH_4^+ , with increased PO_4^{3-} concentrations in July and October 2018. At the chl *a* max, May 2019 and October 2018 had the highest combined dissolved nutrient concentrations, and there was an overall higher portion of PO_4^{3-} than in surface samples for every sampling period. At the bottom, the highest

combined concentrations were found in July 2018, July 2019 and October 2018, with many samples being coincident with the chl *a* max depth.

In May 2019, the dominant dissolved combined nutrient species was NH_4^+ , and there was a relatively equal distribution of NO_x and PO_4^{3-} (Figure 11a). In June 2018, there was a more even distribution of NO_x to NH_4^+ , with a couple of transects (transects 4, 10) having higher PO_4^{3-} concentrations. Geographic variation in June was much stronger—higher total nutrient concentrations in the northernmost and southernmost transects. July 2018 shifted to a much stronger dominance of NH_4^+ and PO_4^{3-} across all transects. The geographic variation for July 2018 was the opposite of June in that the lowest total dissolved nutrient concentrations were located in the northernmost and southernmost transects, with the more average concentrations at the central sampling locations. Similarly, July 2019 geographic variation had higher total concentrations of dissolved nutrients in all sites except for the two northernmost transects (transects 1, 2). NH_4^+ had the highest percentage of combined nutrient concentrations in July 2019, with a small percentage of NO_x and little PO_4^{3-} present. Lastly, October 2018 was very different than the spring and summer months—there were high total concentrations of dissolved nutrients at all locations, and a more balanced nutrient profile. NO_x and NH_4^+ were both dominant, but PO_4^{3-} concentrations were higher as well.

At the chl *a* max, there were seasonal and geographic variations that were unique from those of the surface concentrations (Figure 11b). In May 2019, the total concentration of dissolved nutrients across all transects was higher than at any other sampling time. NH_4^+ had the highest percentage distribution, but there were moderate

amounts of NO_x and PO_4^{3-} as well. In June 2018, the dissolved concentrations were very low across all transects, except the northernmost transect. Similar to May 2019, NH_4^+ was the dominant nutrient, but NO_x and PO_4^{3-} were also present in moderate concentrations. In July 2018 the overall concentration of dissolved nutrients was moderate, with a lower concentration at transect 6 and higher concentrations at transects 8, 9. PO_4^{3-} made up a higher percentage of the dissolved nutrient profile, but NH_4^+ still made up the largest portion of the nutrient pool. In July 2019 there was much more geographic variation, with very low nutrient concentrations at transects, 1, 2 and higher concentrations south of the Ocean City inlet. NH_4^+ was the largest contributor to the dissolved nutrient pool, but at transects 1, 2, 6, and 8, there was a more even distribution of PO_4^{3-} , NO_x and NH_4^+ . October 2018 had a strong geographic variation—northern sites had higher concentrations and were dominated by NO_x , whereas southern sites had lower concentrations and were more evenly distributed with NH_4^+ dominance.

At the bottom depths, nutrient concentrations early in the season were lower than July and October (Figure 11c). May 2019 had generally low concentrations of dissolved nutrients with slightly higher concentrations at transects 6 and 10. NH_4^+ had the highest percentage of the total dissolved nutrients, with small concentrations of PO_4^{3-} . In June 2018, the dissolved nutrient concentrations were low at all transects except for transects 1, 2, 4, 10. NO_x had a higher percentage of the nutrient profile at transects 1, 2, but NH_4^+ was higher at all other locations. In July 2018 there were very high concentrations of dissolved nutrients at all transects except transect 6—again, NH_4^+ made up the largest portion of the nutrients in all locations. In July there were

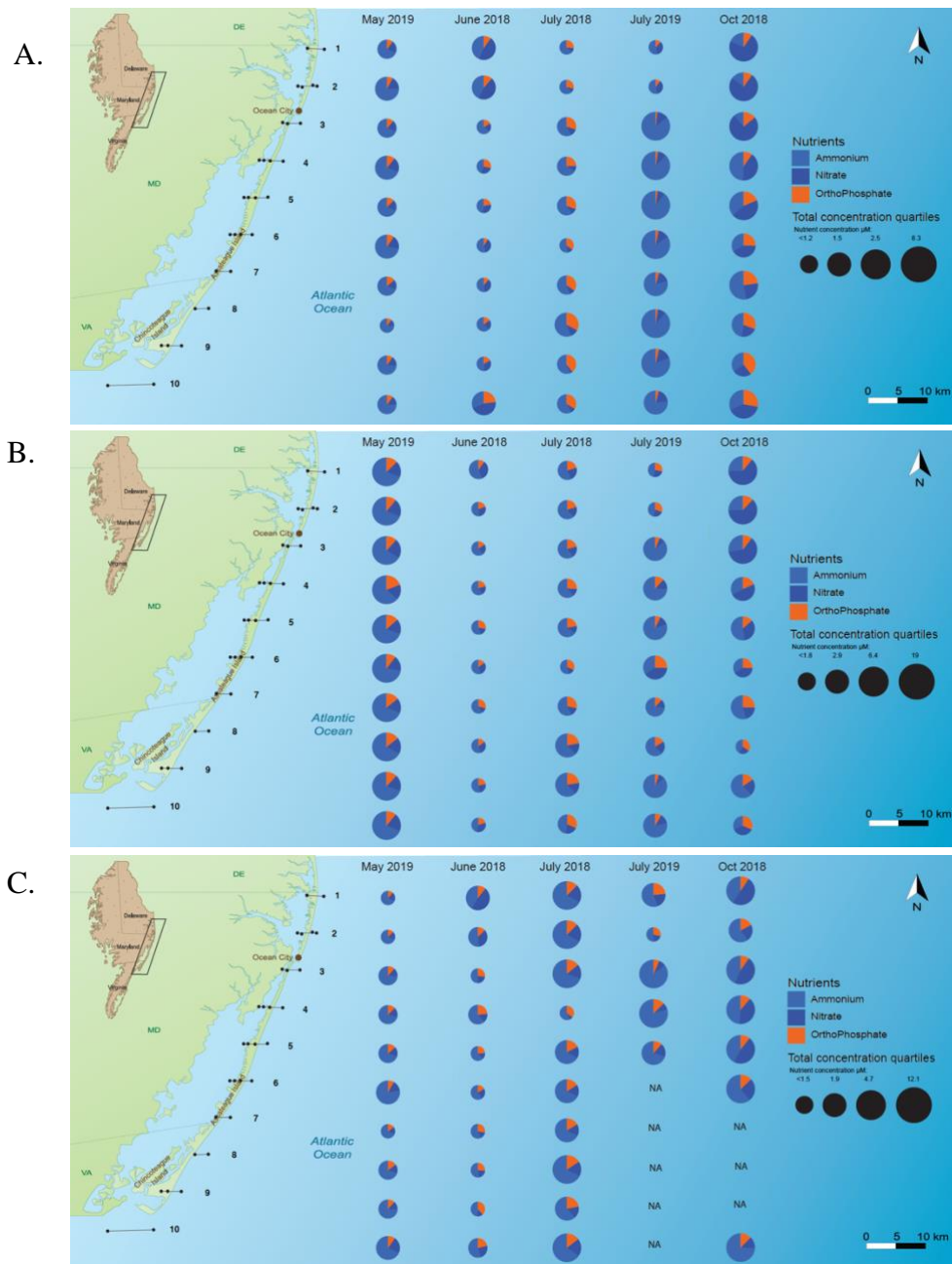


Figure 11: Average dissolved nutrient concentrations (NH_4^+ , NO_x , PO_4^{3-}) by transect (1-10). Concentrations are categorized in columns from left to right by season (May 2019, June 2018, July 2019, October 2018). The size of each pie chart is determined by the quartile value of the combined dataset (<1.2, 1.5, 2.5, 8.3). Individual nutrients are distinguished by color and represent their portion of the total average concentration across a transect and sampling time. Maps are categorized by sampling depth; (A) surface, (B) chl *a* max, (C) bottom.

missing data points within transects 6 through 10, but the northern transects had high concentrations overall with large portions of NH_4^+ . In October 2018 NO_x and NH_4^+ both comprised high percentages of the nutrient profile, and there were high concentrations at all sampling locations (there are missing data points within transects 7, 8, 9).

Nutrient and Harmful Algal Bloom species variations at the surface

The nutrient concentrations followed a similar pattern to that of the HAB species, with highest concentrations at the northern sites and decreasing concentrations towards the southern transects. Unlike the HAB species concentrations though, the nutrient concentrations spiked at the southernmost transect. The nutrient composition at most sites was consistent.

At the surface in July 2018, total average HAB concentrations ranged from 1462-4895 cells L^{-1} , and total average nutrient concentrations ranged from 10.7-25.5 μM (Figure 12c). *Pseudo-nitzschia* spp. and *Karenia* spp. were more prominent in the northern transects (1-7), but *Dinophysis* spp. was high at transect 8. In one sampling location along transect 8, *Dinophysis* spp. exceeded MD DNR guideline's bloom level of concern values, with a concentration of $\sim 11,000$ cells L^{-1} . TN had the highest portion of the nutrient pool at all sampling locations in July 2018, but TP and PO_4^{3-} concentrations were elevated at transects 3, 6, 8, and 10.

In July 2019, nutrient concentrations were highest in the northern half of the sampling grid (1-5) with a range of 11.5-16.3 μM (Figure 12d, Table 6a). TN made up the highest portion of the nutrient pool across all transects, but NH_4^+ made up over

25% of the total nutrient pool at transects 3, 4, 5, 7, 8. TP was the next largest portion of the combined nutrients, followed by NO_x, and then PO₄³⁻.

HAB concentrations in July 2019 were unique because all three HAB species were present, but not simultaneously at any single transect (Figure 12d). Transect 1, 3, 4, and 5 contained small concentrations of *Dinophysis* spp.; transects 2 and 10 contained only *Karenia* spp.; and transect 8 had small concentrations of *Pseudo-nitzschia* spp. (125-1050 cells L⁻¹). Transects 7 and 9 had no detected emergent HAB species (Table 6a).

In October 2018, sampling took place following Hurricane Florence which impacted the mid-Atlantic Coast from September 9-17th, 2018 (Dance 2018). The combined average nutrient concentrations at the surface across all transects were relatively high with a range of 15.8-29.9 μM; the HAB concentrations had a very wide range of 725-17,120 cells L⁻¹ (Figure 12e). The geographic variation of the nutrients showed higher concentrations in northern locations and incrementally decreasing concentration towards southern locations. The same was true of HAB species concentrations, with the exception of transect 9 that showed a spike in *Pseudo-nitzschia* spp. TN was still the dominant nutrient, but there was a higher concentration of NO_x (in comparison to other sampling times) in the northern sites (1-4). Overall, *Pseudo-nitzschia* spp. was the primary HAB species, but *Karenia* spp. and *Dinophysis* spp. were also present in low concentrations in northern sites.

Nutrient and Harmful Algal Bloom species variations at the chlorophyll max

The chl *a* max depth combined HAB species counts from May 2019 had the

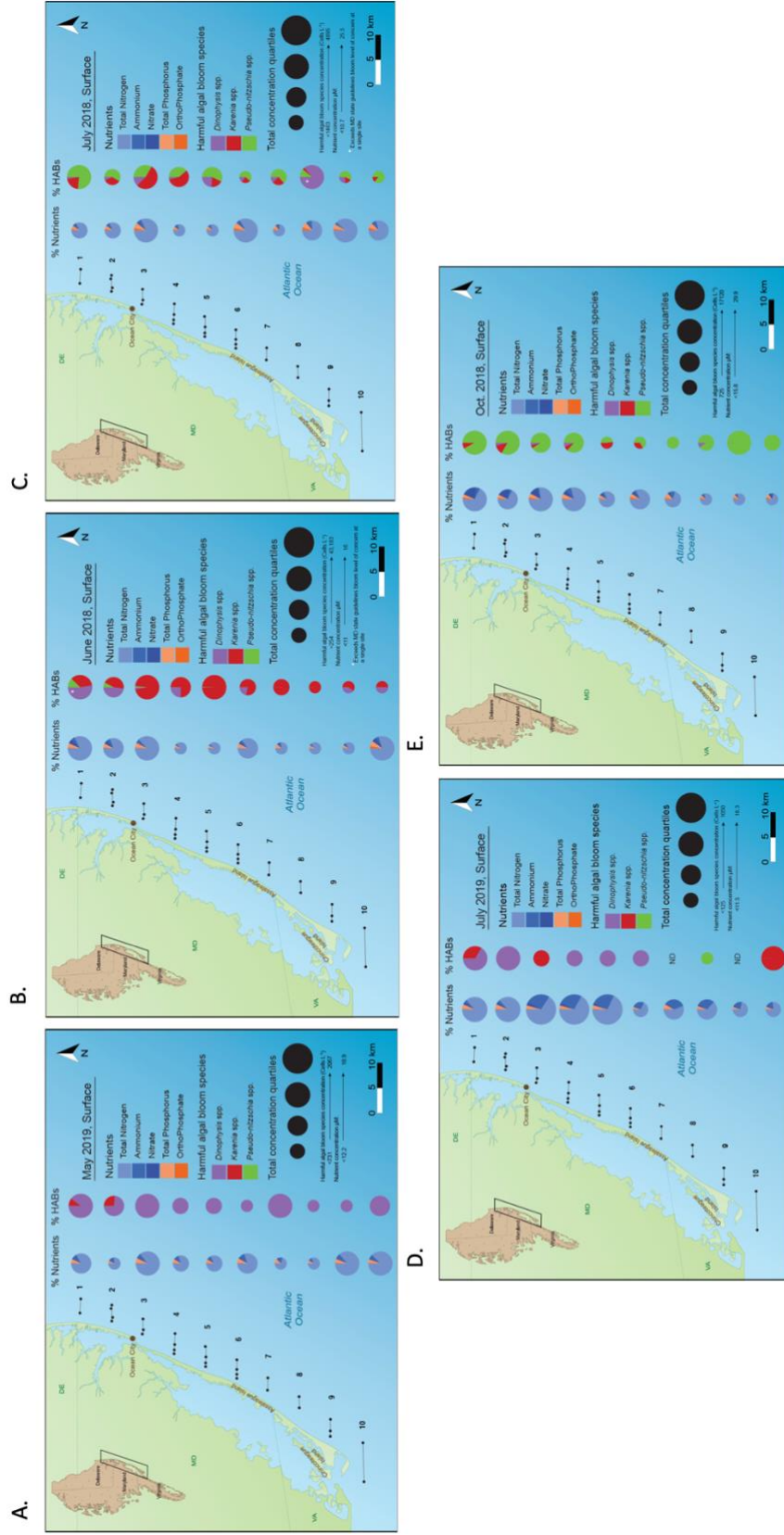


Figure 12: Average HAB concentrations (*Dinophysis* spp., *Karenia* spp., *Pseudo-nitzschia* spp.) and nutrient concentrations (TN, TP, NH₄⁺, NO_x, PO₄³⁻) by transect (1-10) from surface samples. The size of each pie chart is determined by the quartile value of the combined dataset—<1185.0-2166.1 cells L⁻¹ for HAB species and <12.2-18.9 µM for nutrients. Individual nutrients are distinguished by color and represent their portion of the total average concentration across a transect (top to bottom = north to south). Maps are categorized by sampling time; (A) May 2019, (B) June 2018, (C) July 2018, (D) July 2019, (E) October 2018.

Table 6: The 1st and 4th quartile concentration values of the average transect concentrations of combined nutrients (TN, TP, NH₄⁺, NO_x, PO₄³⁻) and combined HAB species (*Dinophysis* spp., *Karenia* spp., *Pseudo-nitzschia* spp.) for each sampling month (June, July, October 2018; May, July 2019). (A) Surface, (B) Chl *a* max sampling depths.

A. SURFACE	Combined HAB Species Concentrations		Combined Nutrient Species Concentrations	
Sampling Time	<1st Quartile	<4th Quartile	<1st Quartile	<4th Quartile
May-19	731.2	2066.7	12.2	18.9
Jun-18	254.1	43183.3	11	16
Jul-18	1462.5	4895	10.7	25.5
Jul-19	125	1050	11.5	16.3
Oct-18	725	17120	15.8	20.1

B. CHLA MAX	Combined HAB Species Concentrations		Combined Nutrient Species Concentrations	
Sampling Time	<1st Quartile	<4th Quartile	<1st Quartile	<4th Quartile
May-19	1185	2166.1	12.2	18.9
Jun-18	5279.4	87760	11.5	15.5
Jul-18	2716.6	21537.2	12.7	22.4
Jul-19	249.9	11414.3	15.2	24
Oct-18	866.6	19433.3	20.1	30.1

smallest and lowest range of any sampling periods (1185-2188 cells L⁻¹) (Table 6b, Figure 13a). The higher combined HAB species counts were located in the northern half of the sampling grid (transects 1, 2, 4). The primary HAB species present was *Dinophysis* spp., but *Karenia* spp. was present in lower concentrations at every transect except for transect 8. *Pseudo-nitzschia* spp. was present only in the northernmost transect and had the smallest portion of the HAB species concentration.

In May 2019, the higher combined nutrient concentrations were at the southernmost transects (9, 10) along with the transect immediately adjacent to the Ocean City Inlet (transect 3) (Figure 13a). The combined concentration of nutrients at the chl *a* max depth had the same range as the surface sampling depth (12.2-18.9 μM). TN comprised the largest portion of the nutrient pool, and PO₄³⁻ and NH₄⁺ had the next highest portions.

In June 2018, chl *a* max depth samples of HAB species had the highest range of concentrations of all sampling times and depths (5270-87760 cell L⁻¹) (Figure 13b, Table 6b). The highest combined concentrations of all HAB species were located along transects 3-7—transect 3 was located directly adjacent to the Ocean City Inlet. *Karenia* spp. was present at all transects except for the southernmost transect (10) and comprised the largest portion of the combined HAB species concentration at all transects except 8 and 10. *Dinophysis* spp. was present primarily along the northernmost (1, 2), and southernmost (7-10) transects. While *Dinophysis* spp. did not make up the largest portion of the combined HAB concentrations, it did have a large enough concentration at a single site along transects 1, 2, and 9 to exceed the MD state bloom level of concern guidelines (Table 1). *Pseudo-nitzschia* spp. was only

present at transects 1, 2 and had the smallest portion of the combined HAB species concentration along both transects.

July 2018 chl *a* max nutrient concentration ranges (12.7-22.4 μM) were very similar to the July 2018 surface ranges (10.7-25.5 μM) (Table 6b). The highest concentrations of combined nutrients were at the northern transects 1-3 and the southern transects 8, 9 (Figure 13b). The nutrient species proportions of the total combined concentrations remained similar regardless of geography: TN comprised the largest portion, then NH_4^+ , TP, PO_4^{3-} , and NO_x .

The combined HAB species concentrations in July 2018 (2720 – 21540 cells L^{-1}) were much lower than those at the surface (1460 – 4895 cells L^{-1}) (Table 6b). The higher combined concentrations were located along the more central transects (2-6) (Figure 13c). *Pseudo-nitzschia* spp. was present along all transects and comprised the largest portion of the combined concentrations of HAB species at transects 1, 3, 4, 9, and 10. *Karenia* spp. were present along every transects except for transect 8, but *Karenia* spp. had the highest portion of the combined concentrations along transects 2, 5, and 6. Neither *Karenia* spp. nor *Pseudo-nitzschia* spp. had concentrations that exceeded MD state's bloom level of concern at any single site. *Dinophysis* spp. did however have concentrations that exceeded MD's bloom level of concern at a single site along transect 8 (Table 1). *Dinophysis* spp. was also present along all transects and takes up the largest portion of the combined concentrations at transects 7, 8.

In July 2019, combined nutrient concentration ranges at the chl *a* max (15.2-24 μM) were much higher than that of the surface (11.5-16.3 μM) (Table 6b). The highest combined nutrient concentrations in July 2019 at the chl *a* max were along

transects 3, 5, 6, 9, 10 (Figure 13d). TN had the highest portion of the combined nutrient concentrations along all transects. Additionally, the transects with the highest combined nutrient concentrations had a larger portion of NH_4^+ than at of the other transects.

July 2019 combined HAB species concentrations were very different from the surface samples as well as all samples from July 2018 (Table 6b). The combined HAB species concentrations ranged from 250-11400 cells L^{-1} which was significantly higher than the surface concentration ranges (125-1050 cells L^{-1}) and significantly lower than the July 2018 chl *a* max concentration ranges (2720-21540 cells L^{-1}). The higher combined concentrations of HAB species were in the north and south (transects 1, 2, 10). At the chl *a* max in July 2019, *Dinophysis* spp. was the only HAB species present along all transects (Figure 13d). *Karenia* spp. was present along transects 1 and 2 and had the largest portion of the combined concentrations along transect 1. However, no concentration at a single sampling location was higher than the MD bloom level of concern thresholds for any emergent HAB species.

In October 2018, the combined nutrient concentrations at the chl *a* max (20.1-30.1 μM) were slightly higher than the surface (15.8-20.1 μM) 2018 (Table 6b). The combined concentrations of nutrients were higher in the northern half (transects 1-4) and lower in the southern half (transects 5-10) of the sampling grid. October 2018 was different from all other sampling times because it had a significant amount of NO_x and TP in comparison to other months. TN still was the dominant form of the combined nutrient pool along each transect (Figure 13e). NH_4^+ had the second highest portion of the total combined nutrient pool at transects 1-3, but NO_x had the second

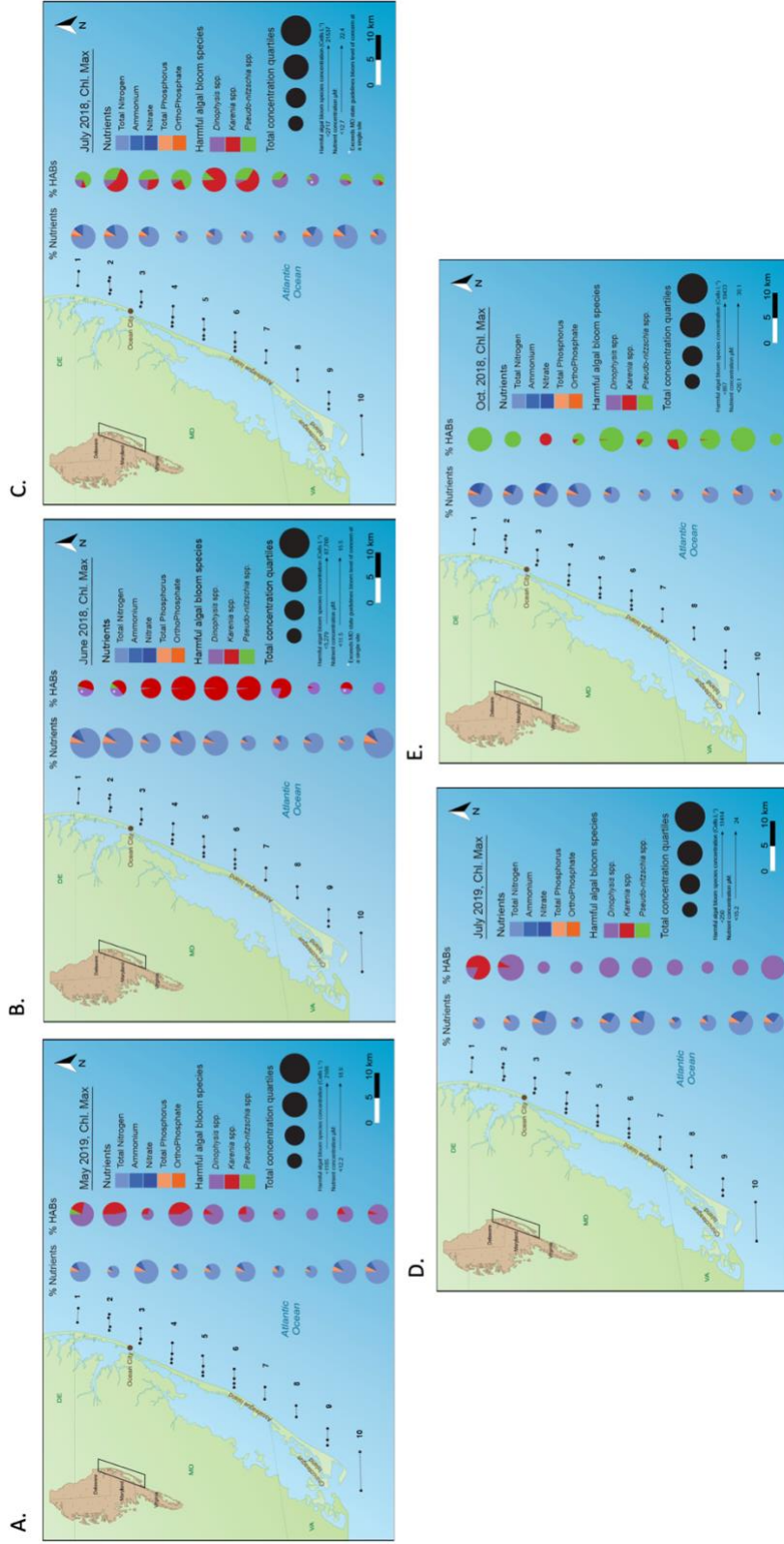


Figure 13: Average HAB concentrations (*Dinophysis* spp., *Karenia* spp., *Pseudo-nitzschia* spp.) and nutrient concentrations (TN, TP, NH_4^+ , NO_x , PO_4^{3-}) by transect (1-10) from chl α max samples. The size of each pie chart is determined by the quartile value of the combined dataset — $<1185\text{-}2166$ cells L^{-1} for HAB species and $<12.2\text{-}18.9$ μM for nutrients. Individual nutrients are distinguished by color and represent their portion of the total average concentration across a transect (top to bottom = north to south). Maps are categorized by sampling time; (A) May 2019, (B) June 2018, (C) July 2018, (D) July 2019, (E) October 2018.

highest portion at transects 7 and 9. TP contributed a more significant amount to the nutrient pool than in any other month and did not vary significantly by geography. PO_4^{3-} proportions of total dissolved nutrients were the smallest and did not change geographically.

The chl *a* max combined HAB species counts were also unique in October 2018. The concentration ranges at the chl *a* max depths (870-19430 cells L^{-1}) were very similar to those at the surface (725-17120 cells L^{-1}) (Table 6b). With the exception of transect 3, 4 and 10, the combined HAB concentrations were at the higher end of the concentration range (Figure 13e). Transects 1, 5 and 9 had the highest combined concentrations. Unlike any of the other sampling times, *Pseudo-nitzschia* spp. was the primary emergent HAB species present. *Pseudo-nitzschia* spp. had the highest portion of the total combined concentrations across all transects except for transect 3. *Karenia* spp. is the only other HAB species present at the chl *a* max in October 2018. *Karenia* spp. had the highest portion of the combined concentrations at transect 3, and had a portion at transects 4, 6 and 7, but transects 2 and 10 contained only *Pseudo-nitzschia* spp.

Nutrient, chlorophyll and Harmful Algal Bloom species threshold comparisons

In order to assess the nutrient, chl *a*, and HAB species concentrations in more detail, scatter plot matrices for each variable (TN, TP, NH_4^+ , NO_x , PO_4^{3-} , chl *a*, *Dinophysis* spp., *Karenia* spp., and *Pseudo-nitzschia* spp.) were compared to threshold values from the MCB standards (for total nutrients and chl *a*) and the MD state guidelines for bloom levels of concern for HAB species (Figure 14-16, Table 7-

8). There were no threshold values for dissolved inorganic nutrients, but scatter plots still revealed patterns based on depth, proximity to shore, and latitude (Figure 17-19).

Chl *a* concentration patterns did not show strong variation with proximity to shore during any sampling time or at any transect (Figure 14). The highest overall concentrations of chl *a* occurred in May 2019 and July 2019 (with concentrations of $\sim 8 \mu\text{g chl } a \text{ L}^{-1}$) (Figure 14a, 14d). Moderate concentrations across the sampling grid occurred in June 2018, July 2018 and October 2018 (Figure 14b, 14c, 14e). The highest individual concentration was found in October 2018 at the bottom depth, offshore, transect 3 ($\sim 9 \mu\text{g chl } a \text{ L}^{-1}$). Many of the chl *a* max depth samples were coincident with either surface or bottom samples (shown by missing data points in the “Chlorophyll Max” column of the matrix). Coincident samples were most frequent in July 2018, July 2019 and October 2018 at the midshore locations (Figure 14c, 14d, 14e). None of the chl *a* concentrations exceeded the MCB maximum threshold of $15 \mu\text{g chl } a \text{ L}^{-1}$.

The TN concentrations had more seasonal variation than the chl *a* concentrations (Figure 15). May and July 2019 had the lowest concentrations, and most samples were $\sim 10 \mu\text{M-N}$, and higher concentrations to the south (inshore) $\sim 18 \mu\text{M-N}$ (Figure 15a). June 2018 had a broader range of TN concentrations (~ 10 - $22 \mu\text{M-N}$), and the highest concentration was at the midshore site along transect 6 at the bottom depth ($\sim 39 \mu\text{M-N}$) (Figure 145b). In July 2018, the majority of the concentrations were low (~ 10 - $15 \mu\text{M-N}$) but there were several peaks in the midshore samples (Figure 15c). The highest July 2018 sample was at the midshore site along transect 9 at the surface, and at $\sim 52 \mu\text{M-N}$ it did exceed the MCB threshold value of

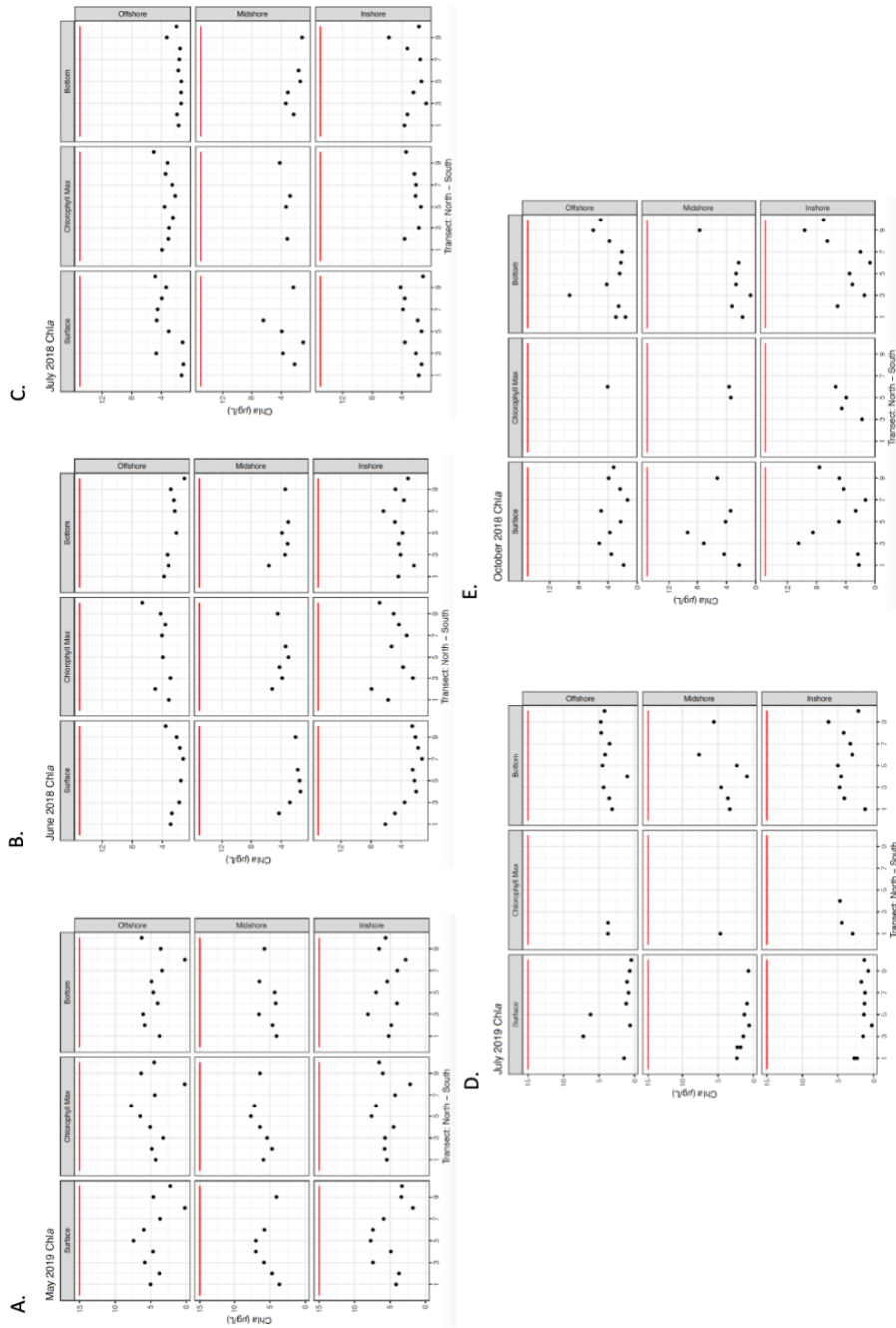


Figure 14: Matrix plots of raw data split into with three columns to categorize by depth and three rows to categorize by proximity to shore. Each plot within the matrix has individual data points from transects 1-10 along the x-axis and concentration values of chl a ($\mu\text{g L}^{-1}$) on the y-axis. The red line indicates the MCB threshold of $15 \mu\text{g L}^{-1}$. (A) May 2019, (B) June 2018, (C) July 2018, (D) July 2019, (E) October 2018.

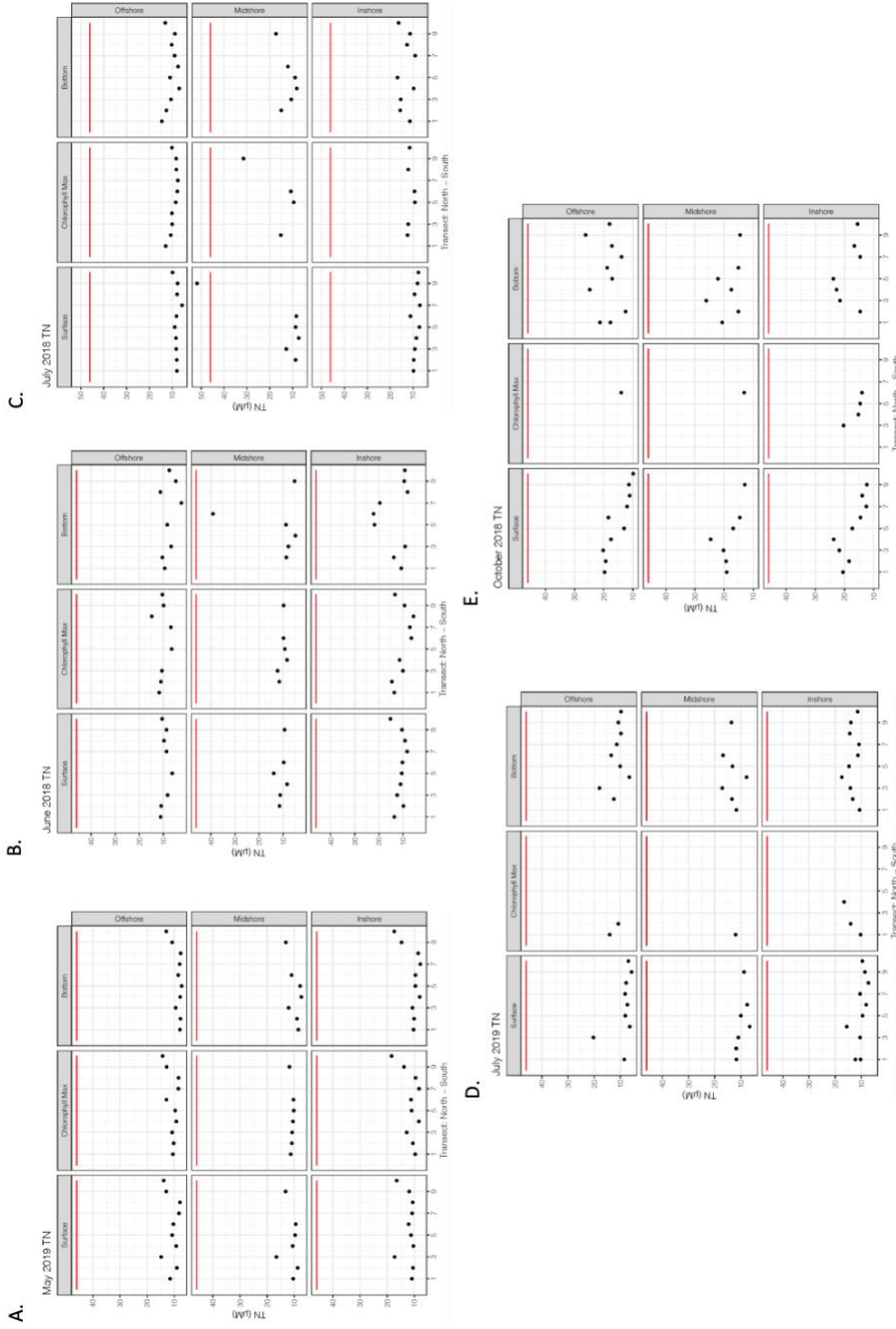


Figure 15: Matrix plots of raw data split into with three columns to categorize by depth and three rows to categorize by proximity to shore. Each plot within the matrix has individual data points from transects 1-10 along the x-axis and concentration values of TN ($\mu\text{M-N}$) on the y-axis. The red line indicates the MCB threshold of $46 \mu\text{M-N}$. (A) May 2019, (B) June 2018, (C) July 2018, (D) July 2019, (E) October 2018.

46 $\mu\text{M-N}$ (Table 7). Another spike in the TN concentrations during July 2018 was located at the chl *a* max midshore site along transect 9 with a concentration of ~ 31 $\mu\text{M-N}$ (Figure 15d). October 2018 concentrations had consistently higher concentrations across all sampling locations with a range of ~ 10 -28 $\mu\text{M-N}$ (Figure 15e).

The TP MCB threshold is 1.2 $\mu\text{M-P}$ and there were numerous locations from every sampling time that exceeded the threshold value (Figure 16, Table 7). May 2019 and June 2018 both had the lowest ranges of the sampling times, going from ~ 0.1 -1.4 $\mu\text{M-P}$ (Figure 16a, 16b). In May 2019, the locations that exceeded the MCB threshold were located at the surface and bottom inshore and midshore along transect 3, as well as the chl *a* max (inshore and offshore) and bottom (inshore) along transect 10 (Figure 16a). June 2018 was different than May 2019 because the range of concentrations across all sampling locations was generally higher (~ 0.4 -1.3 $\mu\text{M-P}$) but there are fewer sites that exceeded the MCB threshold. All of the threshold exceedances occurred at the inshore sites; along transect 10 at the surface and chl *a* max, and along transect 2 at the bottom site (Figure 16b). July 2018 had a large portion of the sampling locations above the MCB threshold, and some of the locations had concentrations values more than double the threshold (Figure 16b). At the surface in July 2018 there was one location that exceeded the MCB threshold, midshore transect 9 with a concentration of 2.6 $\mu\text{M-P}$. At the chl *a* max. there were numerous locations that exceeded the threshold value of 1.2 $\mu\text{M-P}$; transect 1 offshore, transect 2 midshore, transect 8 inshore, transect 9 midshore and offshore, and transect 10 inshore and offshore. In July 2018's bottom samples there were more samples that

Table 7: List of MCB threshold exceedances of TN and TP, sampling location, depth and sampling time.

Date	Depth	Transect	Station	NH ₄ ⁺	NO _x	NO ₃ ⁻	TN	PO ₄ ³⁻	TP	Chl <i>a</i>
July, 2018	S	9	28	1.1	0.15	51.8	15.2	0.54	2.56	2.34
June, 2018	S	10	30	0.76	1.53	15.2	15.2	0.79	1.24	2.51
June, 2018	M	10	30	0.63	0.47	13.3	13.3	0.39	1.25	6.85
June, 2018	B	2	4	1	1.12	13.8	13.8	0.24	1.21	2.28
July, 2018	S	6	20	0.51	0.14	13.9	13.9	0.39	1.21	1.69
July, 2018	S	9	28	1.1	0.15	51.8	15.2	0.54	2.56	2.34
July, 2018	M	2	5	2.895	0.86	15.2	15.2	0.63	1.21	3.16
July, 2018	M	5	16	3.9	0.8	11.8	11.8	0.75	1.36	4.34
July, 2018	M	8	25	2.82	0.67	12.1	12.1	0.73	1.47	2.3
July, 2018	M	9	28	0.85	0.04	31.5	31.5	0.64	3.39	4.18
July, 2018	M	10	30	1.3	0.37	11.5	11.5	0.68	1.26	3.42
July, 2018	M	10	31	0.81	0.53	10.2	10.2	0.73	1.24	5.01
July, 2018	B	1	3	4.69	1.4	14.6	14.6	0.86	1.26	1.66
July, 2018	B	2	4	3.85	1.08	15.6	15.6	0.65	1.41	3.25
July, 2018	B	2	5	4.78	1.52	15	15	0.74	1.36	2.3
July, 2018	B	2	6	4.18	1.4	12.6	12.6	0.81	1.265	1.88
July, 2018	B	3	8	3.56	0.77	15.4	15.4	0.64	1.51	0.72
July, 2018	B	3	10	3.18	0.84	10.6	10.6	0.74	1.2	1.32
July, 2018	B	4	12	1.79	0.31	10.4	10.4	0.6	1.2	3.21
July, 2018	B	5	15	3.73	0.89	16.8	16.8	0.74	1.81	1.36
July, 2018	B	5	16	4.41	0.9	12.6	12.6	0.8	1.54	1.86
July, 2018	B	5	18	1.78	0.33	11	11	0.69	1.38	1.3
July, 2018	B	6	20	3.64	0.96	13.1	13.1	0.77	1.29	1.3
July, 2018	B	6	21	3.13	0.71	12.1	12.1	0.75	1.21	1.63
July, 2018	B	7	24	2.685	0.625	8.99	8.99	0.75	1.3	1.56
July, 2018	B	8	25	3.47	0.84	12.6	12.6	0.8	1.31	3.26
July, 2018	B	8	26	3.6	0.93	10.3	10.3	0.85	1.35	1.46
July, 2018	B	9	27	2.63	0.81	11.3	11.3	0.79	1.41	5.75
July, 2018	B	9	28	3.15	0.79	17.3	17.3	1.04	2.044	1.16
July, 2018	B	9	29	2.57	0.72	8.86	8.86	1.01	1.28	3.25
July, 2018	B	10	30	3.17	0.95	16.3	16.3	0.46	1.67	1.69
July, 2018	B	10	31	3.545	1.075	13.1	13.1	1.015	1.595	1.95

Threshold Exceedance

Date	Depth	Transect	Station	NH ₄ ⁺	NO _x	NO ₃ ⁻	TN	PO ₄ ³⁻	TP	Chl <i>a</i>
October, 2018	S	1	1	1.28	5.76	20.5	20.5	0.71	1.2	2.21
October, 2018	S	2	4	1.11	5.62	18.4	18.4	0.73	1.2	2.35
October, 2018	S	2	5	1.21	5.93	19.3	19.3	0.84	1.29	4.31
October, 2018	S	2	6	1.61	3.81	19.3	19.3	0.69	1.25	3.55
October, 2018	S	2	7	1.58	6.02	18.7	18.7	0.89	1.24	4.56
October, 2018	S	3	8	0.49	4.4	21.75	21.75	0.78	1.49	10.46
October, 2018	S	3	9	1.59	5.5	20.2	20.2	0.89	1.4	7.1
October, 2018	S	3	10	0.56	2.54	20.2	20.2	0.54	1.44	5.2
October, 2018	S	4	11	2.26	1.89	23.7	23.7	0.45	1.68	8.5
October, 2018	S	4	13	0.42	0.88	24.6	24.6	0.54	1.715	9.32
October, 2018	S	5	15	0.52	1.31	17.3	17.3	0.56	1.24	4.94
October, 2018	S	5	17	1.36	0.94	16.9	16.9	0.44	1.21	4.12
October, 2018	S	6	19	1.02	1.04	14.5	14.5	0.68	1.2	2.66
October, 2018	S	6	22	0.63	0.97	18.4	18.4	0.52	1.27	4.94
October, 2018	S	6	27	0.45	0.33	12.3	12.3	0.7	1.22	4.88
October, 2018	S	9	28	0.38	0.23	12.9	12.9	0.69	1.29	5.26
October, 2018	S	10	31	0.76	0.59	9.89	9.89	0.72	1.26	3.23
October, 2018	M	3	8	2.08	5.74	20.3	20.3	0.95	1.4	1.78
October, 2018	M	6	19	0.5	0.8	14	14	0.46	1.205	5.39
October, 2018	B	1	1	4.26	6	21.3	21.3	1.05	1.37	1.61
October, 2018	B	1	2	4.25	4.34	20.65	20.65	0.9	1.385	1.79
October, 2018	B	1	3	3.26	1.07	17.7	17.7	0.79	1.52	2.92
October, 2018	B	2	5	3	1.27	15.1	15.1	0.74	1.27	3.23
October, 2018	B	3	8	5.59	5.22	21.5	21.5	1.22	1.53	1.46
October, 2018	B	3	9	4.95	6.13	26.1	26.1	1.13	2	0.7
October, 2018	B	4	11	4.21	2.98	22.7	22.7	0.94	1.87	3.11
October, 2018	B	4	13	4.95	3.46	17.5	17.5	1.03	1.31	2.69
October, 2018	B	4	14	2.86	3.56	24.8	24.8	0.8	1.98	4.18
October, 2018	B	5	15	3.86	5.1	23.8	23.8	1.06	1.85	3.49
October, 2018	B	5	17	3.985	3.555	22.1	22.1	0.93	1.62	2.68
October, 2018	B	5	18	1.88	1.31	17.1	17.1	0.48	1.3	2.4
October, 2018	B	6	21	3.91	2.15	15.1	15.1	1	1.39	2.32
October, 2018	B	6	22	3.71	1.255	18.8	18.8	0.64	1.68	2.23
October, 2018	B	7	23	1.315	0.53	14.6	14.6	0.82	1.42	2
October, 2018	B	7	24	1.87	0.65	13.9	13.9	0.66	1.27	2.1
October, 2018	B	8	25	0.74	0.46	16.6	16.6	0.59	1.7	6.53
October, 2018	B	8	26	0.74	0.41	17.2	17.2	0.63	1.69	3.8
October, 2018	B	9	28	3.89	1.32	14.5	14.5	0.63	1.21	7.67
October, 2018	B	9	29			26.2	26.2		2.86	6.02
October, 2018	B	10	30	0.88	1.03	15.5	15.5	0.88	1.8	7.04
October, 2018	B	10	31	4.18	0.74	18	18	0.69	1.57	5.01

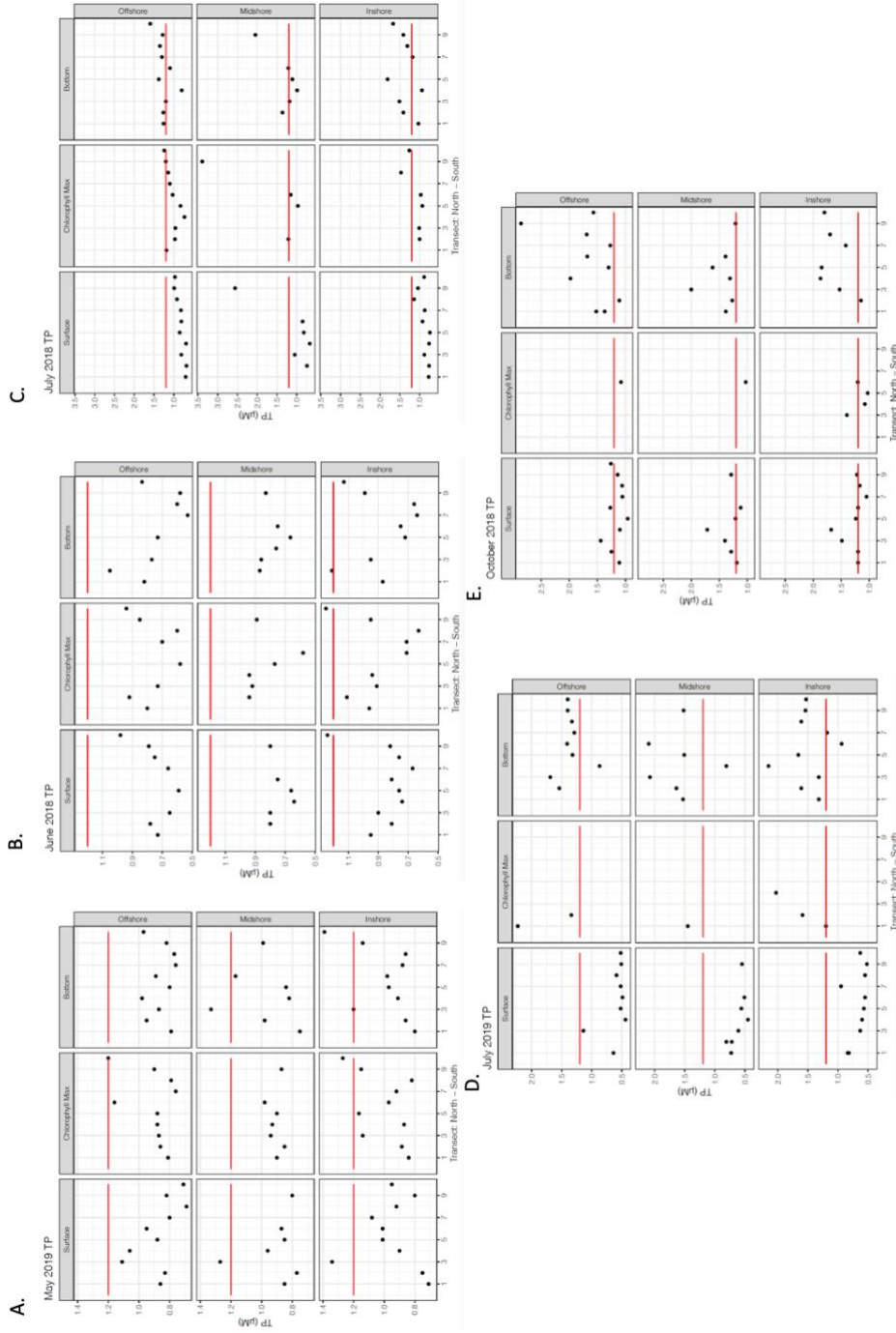


Figure 16: Matrix plots of raw data split into with three columns to categorize by depth and three rows to categorize by proximity to shore. Each plot within the matrix has individual data points from transects 1-10 along the x-axis and concentration values of TP ($\mu\text{M-P}$) on the y-axis. The red line indicates the MCB threshold of $1.2 \mu\text{M-P}$. (A) May 2019, (B) June 2018, (C) July 2018, (D) July 2019, (E) October 2018.

exceeded the MCB threshold than did not. Inshore sites along transect 2, 3, 5, 8, 9, and 10; midshore sites along transects 2, 3, 6, and 9; and offshore sites along transects 1, 2, 3, 5, 7, 8, 9, and 10 all had concentrations higher than 1.2 $\mu\text{M-P}$ (Figure 16b). October 2018 and July 2019 had the highest concentration ranges of all sampling times ($\sim 0.4\text{-}2.8$ $\mu\text{M-P}$) (Figure 16d, 16e). At the surface, inshore sites along transect 1, 2, 3, 4, 5, 6, and 9; midshore sites along transects 2, 3, 4, 5, and 9; and offshore sites along transects 2, 3, 6, and 10 all exceeded the MCB thresholds in October 2018 (Figure 16e). Despite having many coincident values with the chl *a* max and surface/bottom depths, the inshore site along transects 3 and 6 also exceeded the 1.2 $\mu\text{M-P}$ threshold. At the bottom sampling depth, nearly every site exceeded the MCB threshold except for the inshore and offshore sites along transect 2. In July 2019, nearly all bottom sampling sites exceeded the MCB threshold regardless of proximity to shore (Figure 16d). Additionally, non-coincident chl *a* max sites all exceeded the MCB threshold for TP in July 2019.

The dissolved inorganic nutrients did not have thresholds set for MD's coastal ocean, but there was drastic depth, geographic and seasonal variation specific to each nutrient species (Figure 17-19). NH_4^+ was highest in July 2019 and October 2018 with the highest concentrations (up to 7.1 $\mu\text{M-N}$) (Figure 17d, 17e). NO_x also had its highest concentrations in July 2019, and October 2018 with a high of ~ 2.1 $\mu\text{M-N}$ in July and ~ 6.0 $\mu\text{M-N}$ in October (Figure 18c, 18e). There was also a distinct geographic pattern during all sampling times; NO_x concentrations were higher in the northern and southern sites (1, 2, 9, 10) with a narrow peak at central sites (3, 4)—all of which were associated with anthropogenic influences near the outfalls and inlets

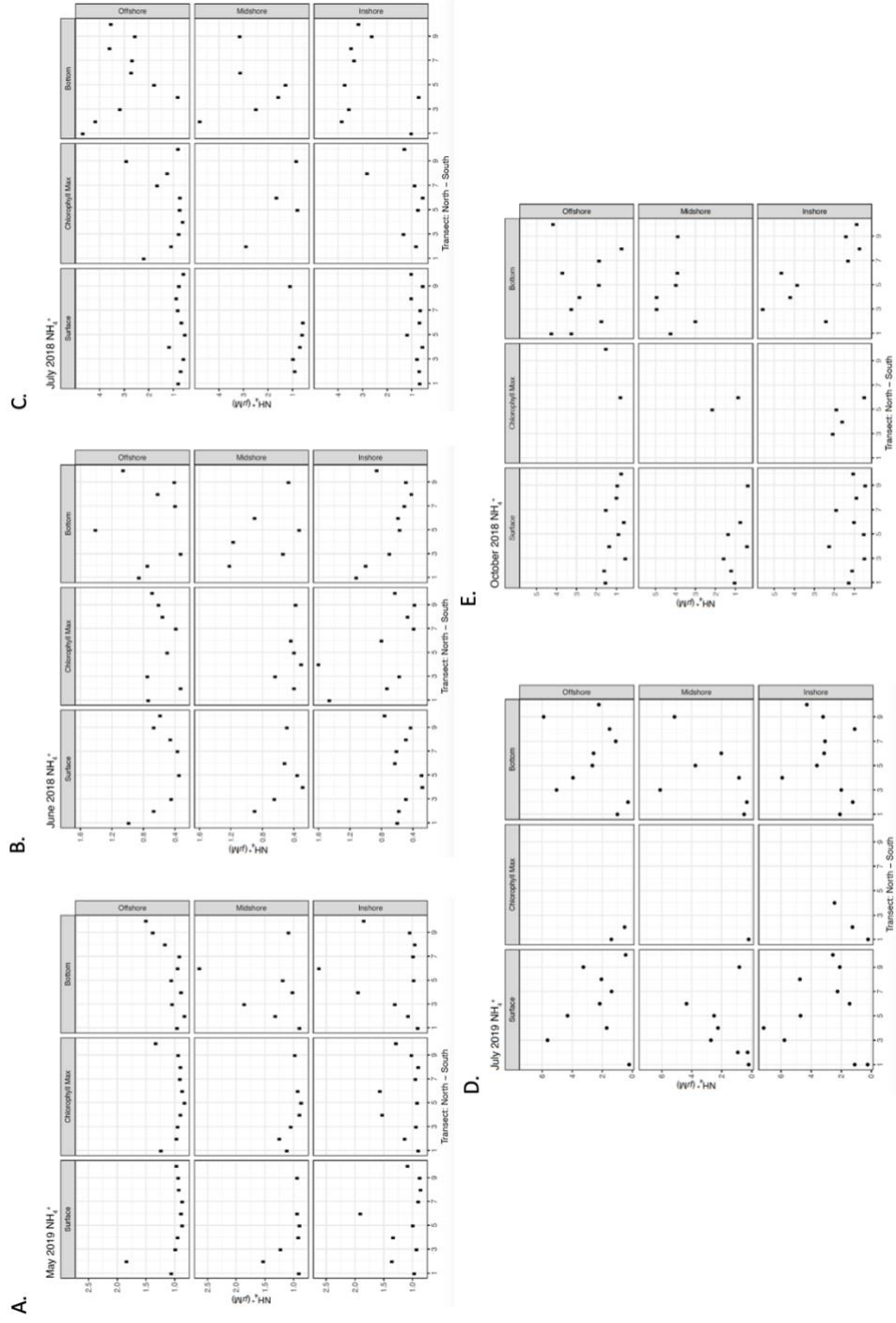


Figure 17: Matrix plots of raw data split into with three columns to categorize by depth and three rows to categorize by proximity to shore. Each plot within the matrix has individual data points from transects 1-10 along the x-axis and concentration values of NH_4^+ (μM -N) on the y-axis. (A) May 2019, (B) June 2018, (C) July 2018, (D) July 2019, (E) October

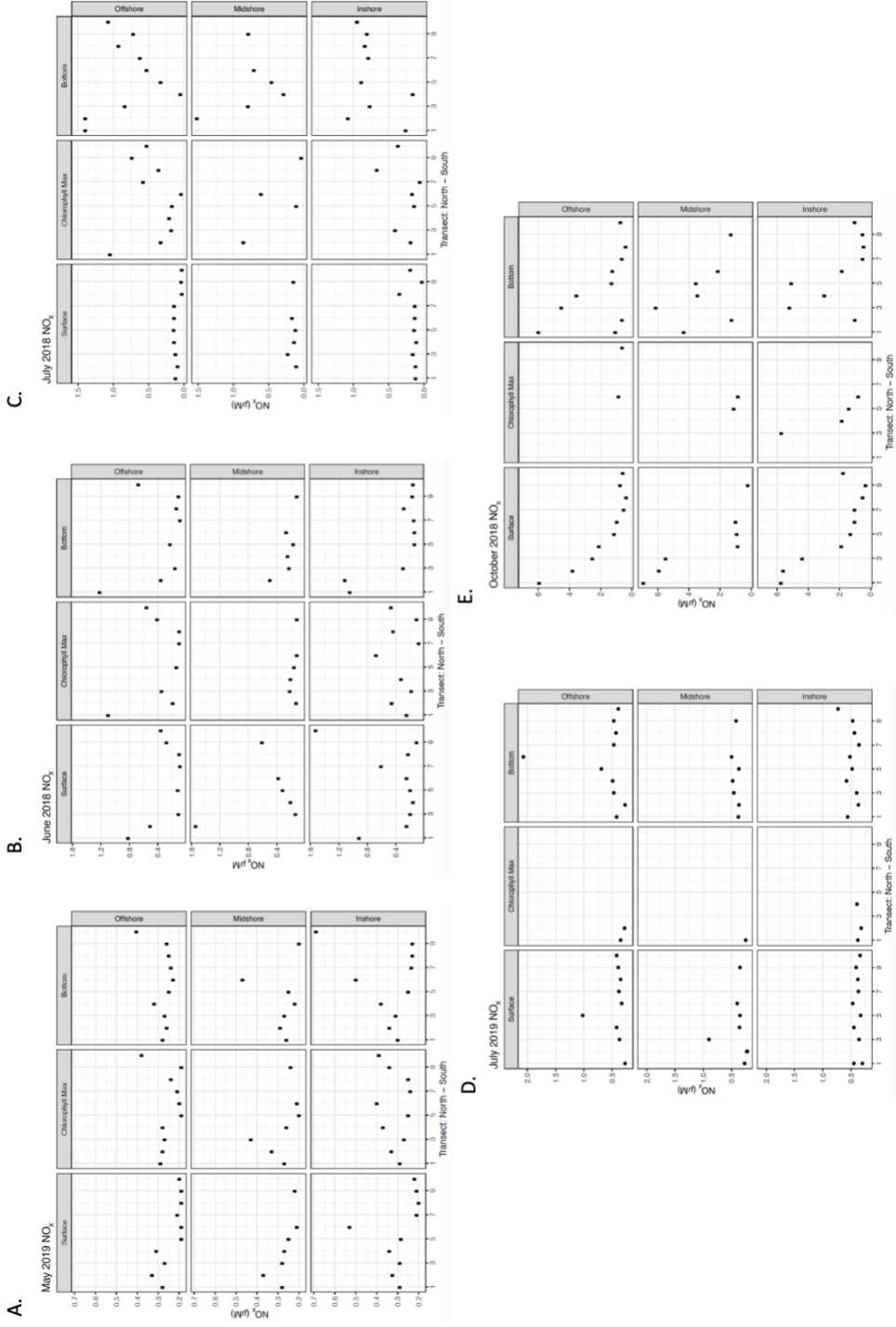


Figure 18: Matrix plots of raw data split into with three columns to categorize by depth and three rows to categorize by proximity to shore. Each plot within the matrix has individual data points from transects 1-10 along the x-axis and concentration values of NO_x (µM-N) on the y-axis. (A) May 2019, (B) June 2018, (C) July 2018, (D) July 2019, (E) October 2018.

(Figure 18). PO_4^{3-} concentrations were generally higher at the bottom sampling depth across all sampling times and locations (Figure 19). The highest concentrations were in July 2018 and October 2018, however October had overall higher concentrations (up to $1.2 \mu\text{M-P}$) across all sites rather than a single peak concentration (Figure 19c, 19e).

Dinophysis spp. was the only emergent HAB species of concern that had sample locations which exceeded the MD state guidelines for bloom levels of concern ($10,000 \text{ cells L}^{-1}$) (Figure 20, Table 8). No samples in May 2019, July 2019, nor October 2018 exceeded the threshold, but four samples in June 2018 and two samples in July 2018 were higher than $10,000 \text{ cells L}^{-1}$. In June 2018 the inshore surface sample along transect 1 had a concentration of $\sim 1400 \text{ cells L}^{-1}$ (Figure 20b). Chl *a* max samples from June 2018 exceeded the bloom level of concern threshold at inshore sites along transects 1, 2 and 9. July 2018 samples were very similar to June 2018 with an inshore surface and chl *a* max sample above $10,000 \text{ cells L}^{-1}$ along transect 8 (Figure 20c). May 2019 had values that reached up to $5000 \text{ cells L}^{-1}$ at the surface along inshore transects 2 and 7, and offshore transect 1; and at the chl *a* max along midshore transect 1, and offshore transects 1 and 4 (Figure 20a). In July 2019, the *Dinophysis* spp. concentrations ($\sim 0-2600 \text{ cells L}^{-1}$) with only one single site at the chl *a* max offshore transect 1 was higher than $5000 \text{ cells L}^{-1}$ (Figure 20d). In October 2018, only five samples include *Dinophysis* spp. concentrations at all and they were all less than 500 cells L^{-1} ; surface samples inshore along transect 2, 3 and 4, as well as midshore along transect 9 and offshore along transect 8 (Figure 20e).

Table 8: List of MCB threshold exceedances of HAB species, sampling location, depth and sampling time.

Date	Depth	Transect	Station	HAB Species	Cells L⁻¹
Jun-18	Surface	1	1	<i>Dinophysis</i> spp.	14,900
Jun-18	Chl <i>a</i> Max	1	1	<i>Dinophysis</i> spp.	14,900
Jun-18	Chl <i>a</i> Max	2	4	<i>Dinophysis</i> spp.	12,000
Jun-18	Chl <i>a</i> Max	9	29	<i>Dinophysis</i> spp.	14,800
Jul-18	Surface	8	25	<i>Dinophysis</i> spp.	10,700
Jul-18	Chl <i>a</i> Max	8	25	<i>Dinophysis</i> spp.	12,200

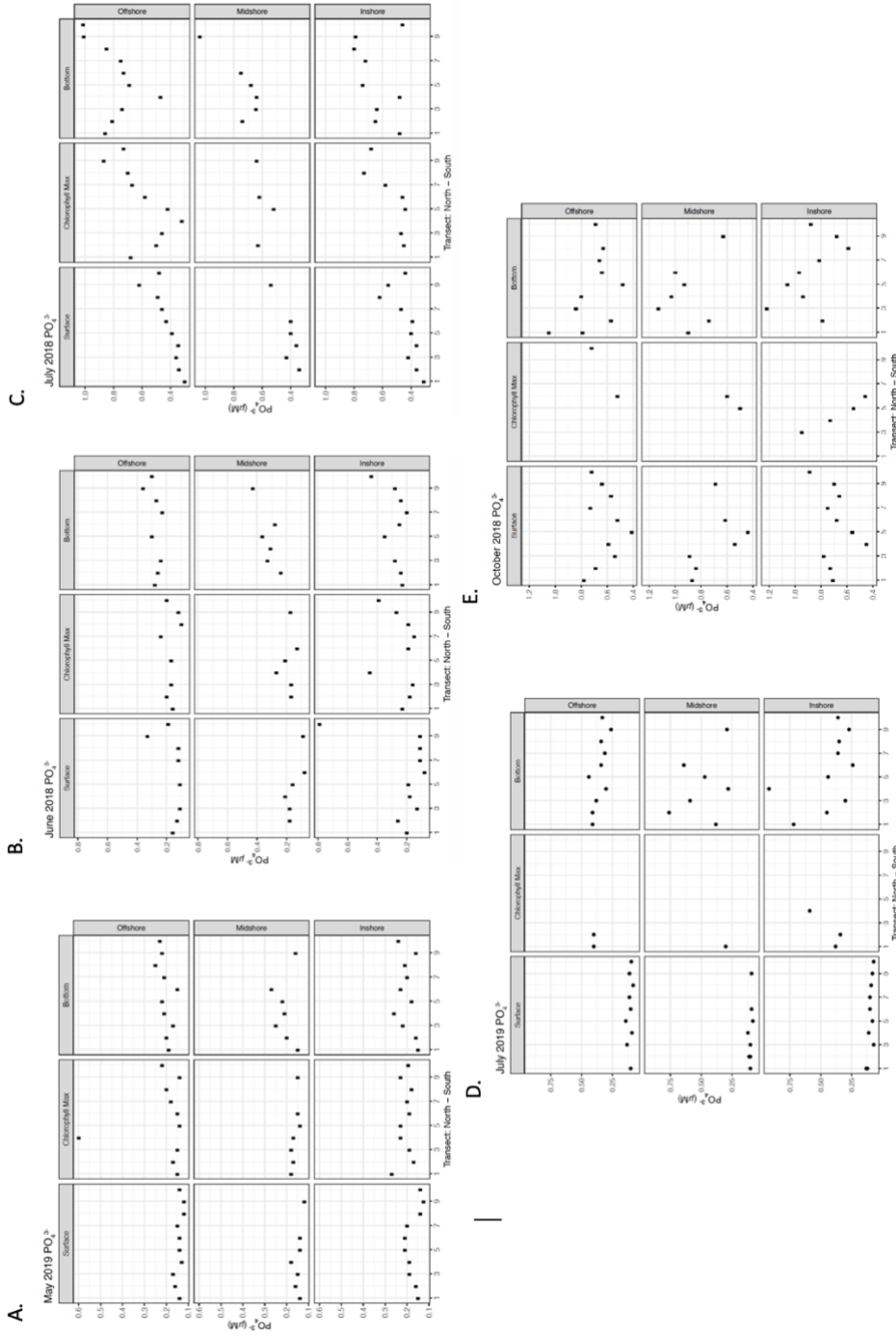


Figure 19: Matrix plots of raw data split into with three columns to categorize by depth and three rows to categorize by proximity to shore. Each plot within the matrix has individual data points from transects 1-10 along the x-axis and concentration values of PO_4^{3-} (μM -P) on the y-axis. (A) May 2019, (B) June 2018, (C) July 2018, (D) July 2019, (E) October 2018.

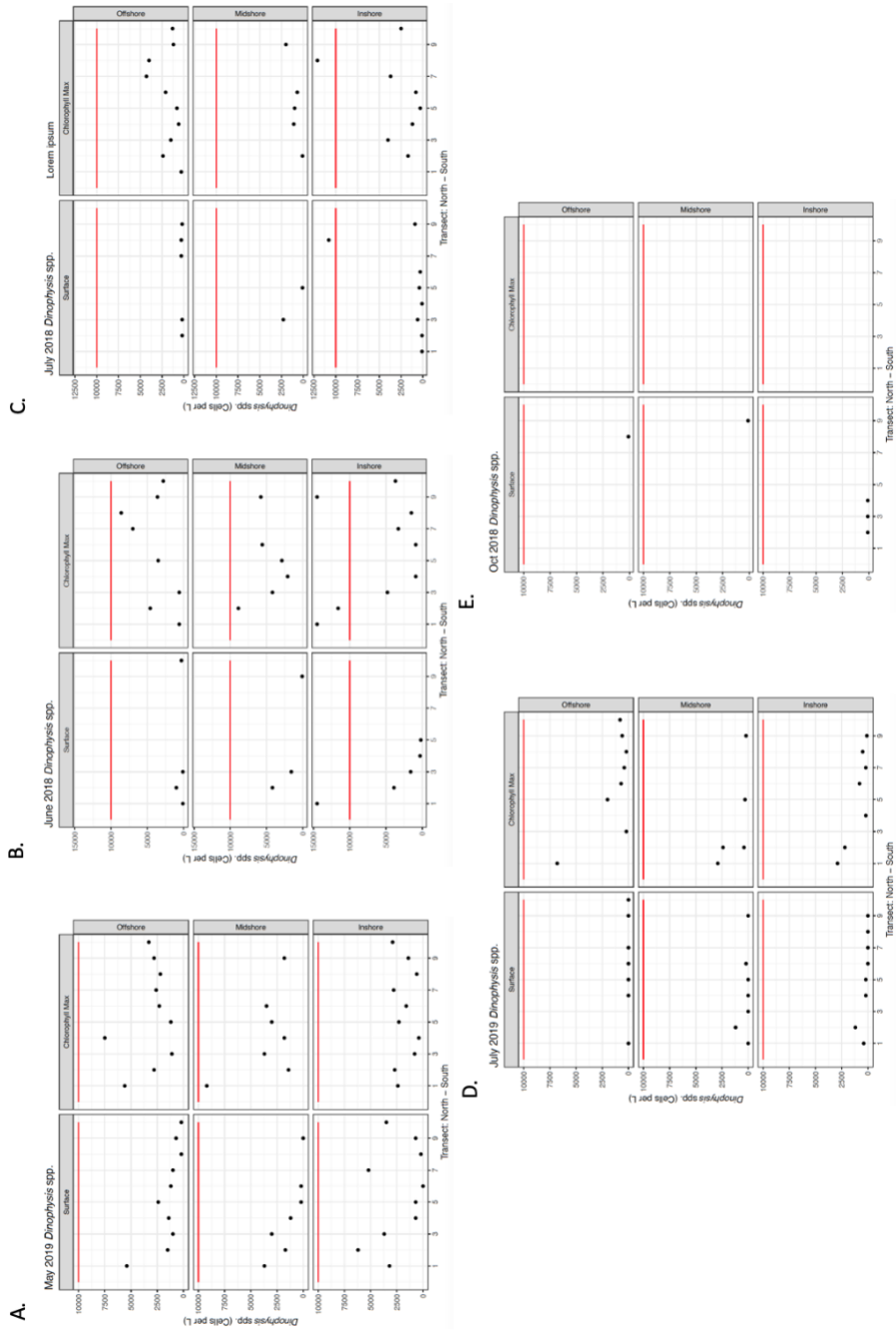


Figure 20: Matrix plots of raw data split into with two columns to categorize by depth (surface and chl a max) and three rows to categorize by proximity to shore. Each plot within the matrix has individual data points from transects 1-10 along the x-axis and concentration values of *Dinophysis* spp. (cells L^{-1}) on the y-axis. The red line indicates the MCB threshold of 10,000 cells L^{-1} . (A) May 2019, (B) June 2019, (C) July 2019, (D) July 2018, (E) October 2018.

Karenia spp. had no samples that exceeded the MD state guidelines for bloom levels of concern (10,000,000 cells L⁻¹) (Figure 21). The highest concentration of any *Karenia* spp. sample was around 30,000 cells L⁻¹ (Figure 22). In May 2019, nearly all *Karenia* spp. concentrations were from the chl *a* max sampling depth and the highest concentrations were located offshore along transects 1 and 4 (Figure 22). June 2018 had more abundance at the surface and chl *a* max with samples reaching up to ~19,000 cells L⁻¹ at the chl *a* max midshore sample along transect 5 (Figure 22b). July 2018 also had *Karenia* spp. presence at the surface and chl *a* max, with one single location at the chl *a* max along offshore transect 2 reaching over 30,000 cells L⁻¹—the highest concentration of *Karenia* spp. found at any sampling time (Figure 22c). July 2019 had very few samples with *Karenia* spp. presence, mostly at surface samples. However, the inshore sample at the chl *a* max along transect 1 did have the highest concentration of this sampling time (~1,650 cells L⁻¹) (Figure 22d). October 2018 had few samples at the surface and chl *a* max with *Karenia* spp. present, but the highest concentration was a chl *a* max depth inshore site along transect 7 (with only 1,000 cells L⁻¹ (Figure 22e).

Pseudo-nitzschia spp. also had no samples that exceeded the MD state guidelines for bloom levels of concern (1,000,000 cells L⁻¹) (Figure 23). In May 2018, only the chl *a* max inshore and offshore sites contained any appreciable concentrations of *Pseudo-nitzschia* spp. (with a high of ~300 cells L⁻¹) (Figure 23a). June 2018 had small concentrations (up to ~1,600 cells L⁻¹) at inshore, midshore, and offshore sites along transects 1-6 (Figure 23b). July 2018 had *Pseudo-nitzschia* spp. presence at nearly every sampling location, but with low concentrations, up to ~6200

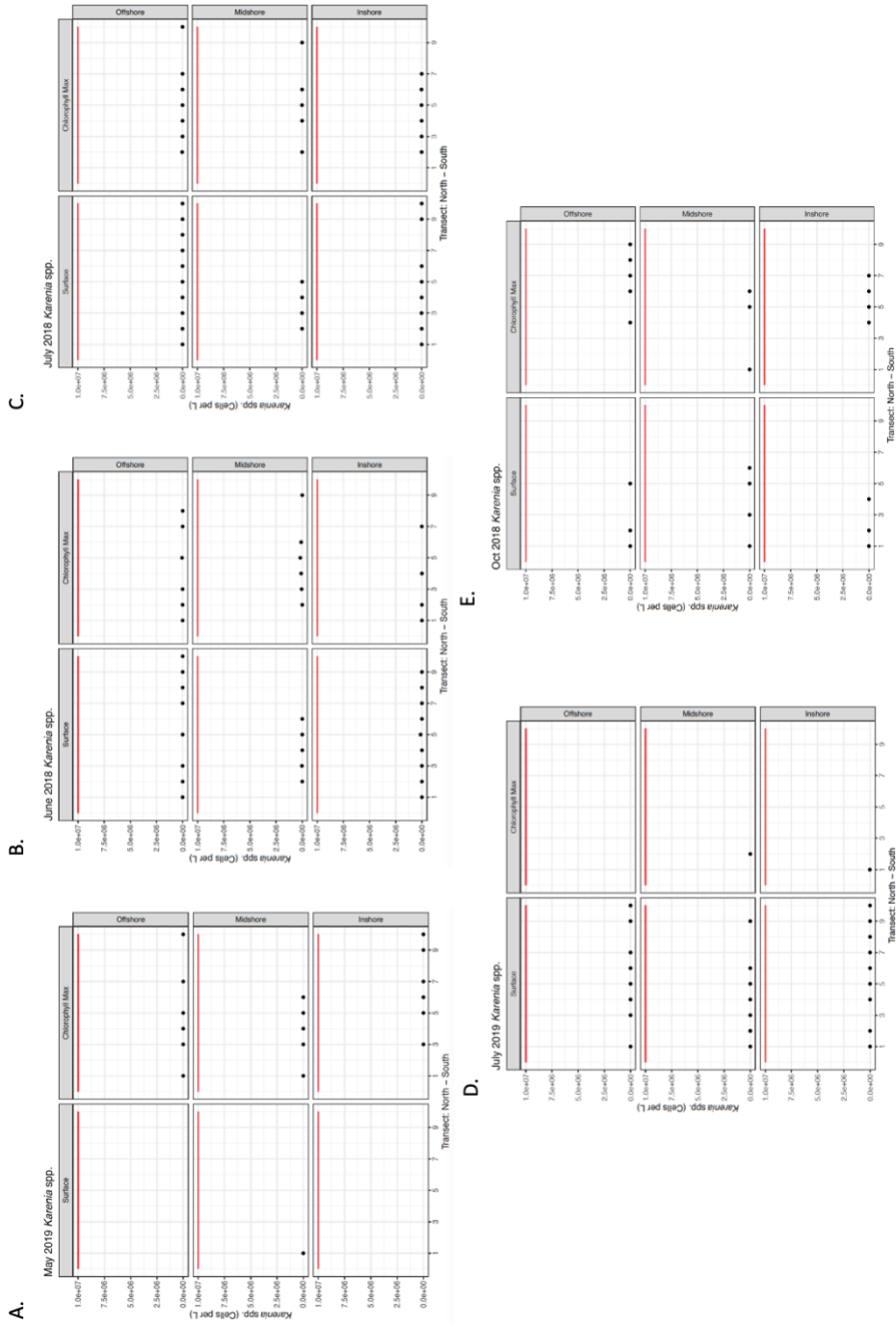


Figure 21: Matrix plots of raw data split into with two columns to categorize by depth (surface and chl a max) and three rows to categorize by proximity to shore. Each plot within the matrix has individual data points from transects 1-10 along the x-axis and concentration values of *Karenia* spp. (cells L⁻¹) on the y-axis. The red line indicates the MCB threshold of 10,000,000 cells L⁻¹. (A) May 2019, (B) June 2018, (C) July 2018, (D) July 2019, (E) October 2018.

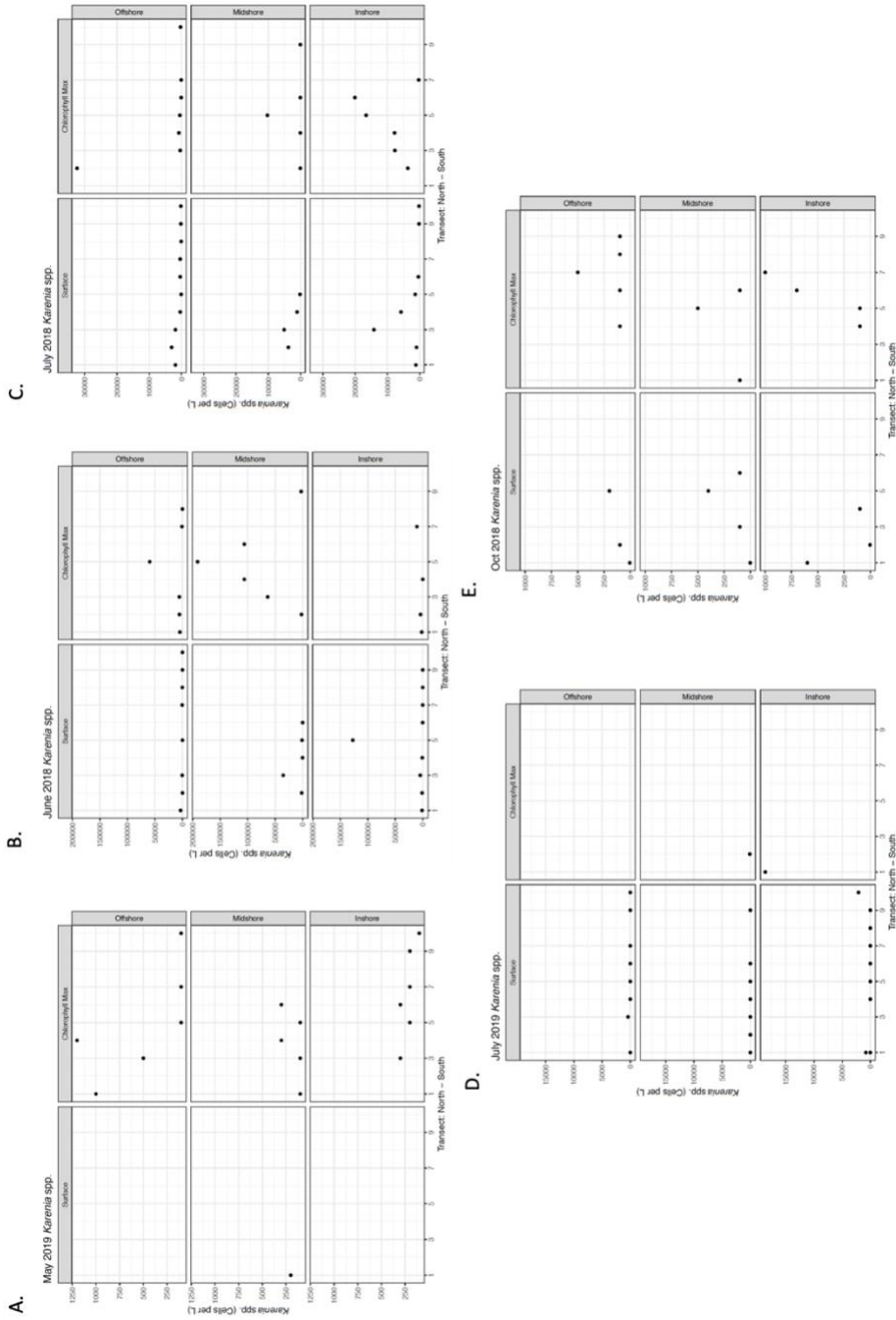


Figure 22: Matrix plots of raw data split into with two columns to categorize by depth (surface and chl *a* max) and three rows to categorize by proximity to shore. Each plot within the matrix has individual data points from transects 1-10 along the x-axis and concentration values of *Karenia* spp. (cells L⁻¹) on the y-axis. (A) May 2019, (B) June 2018, (C) July 2018, (D) July 2019, (E) October 2018.

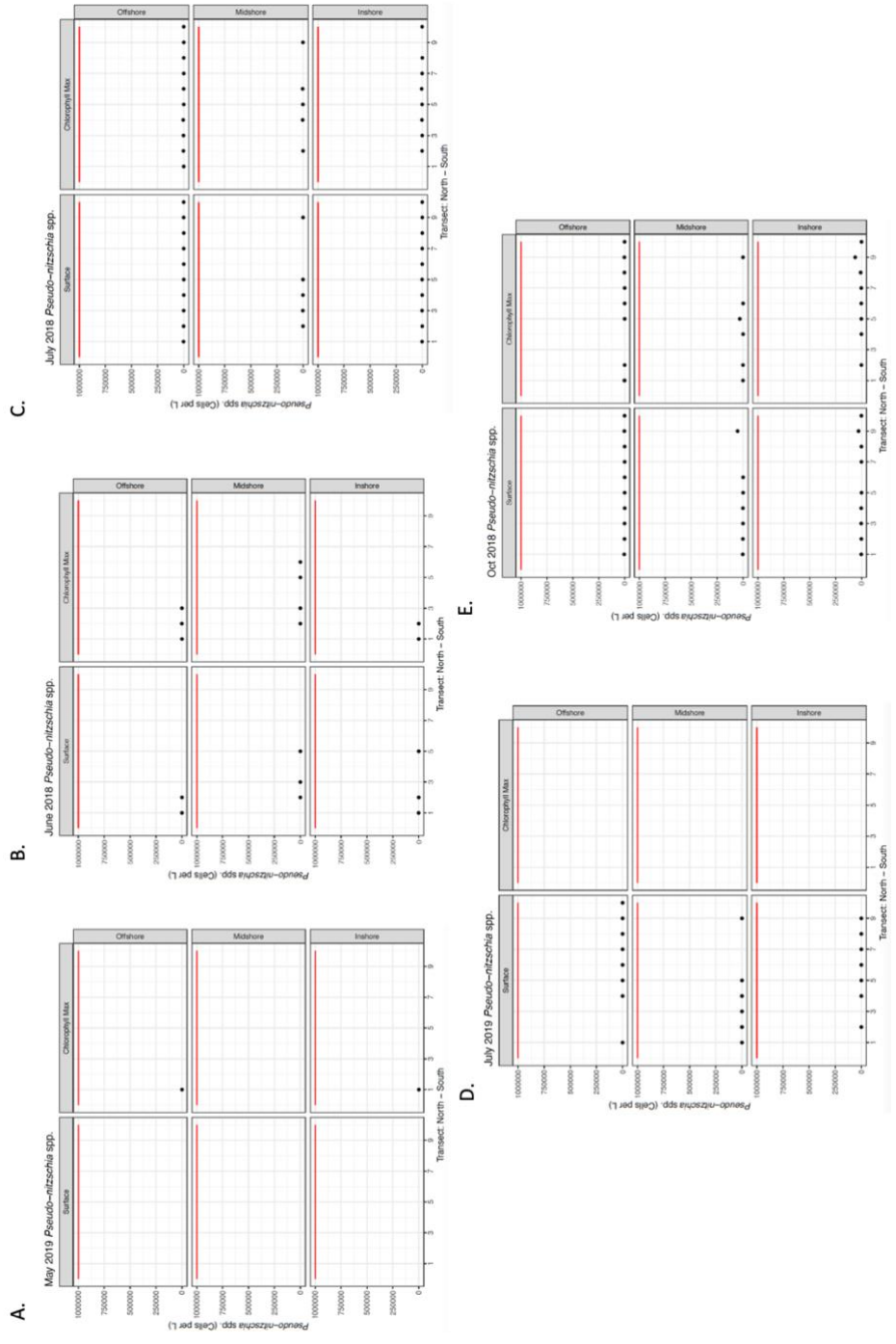


Figure 23: Matrix plots of raw data split into with two columns to categorize by depth (surface and chl *a* max) and three rows to categorize by proximity to shore. Each plot within the matrix has individual data points from transects 1-10 along the x-axis and concentration values of *Pseudo-nitzschia* spp. (cells L⁻¹) on the y-axis. The red line indicates the MCB threshold of 1,000,000 cells L⁻¹. (A) May 2019, (B) June 2018, (C) July 2018, (D) July 2019, (E) October 2018.

cells L⁻¹ (Figure 23c). In July 2019 there were concentrations of *Pseudo-nitzschia* spp. only in surface samples, but at inshore, midshore, and offshore sites along nearly every transect (Figure 23d). October 2018 had the highest concentrations as well as the most presence (Figure 23e). The highest concentrations reached up to ~52,000 cells L⁻¹ at the inshore and midshore sites along transect 9 (surface and chl *a* max). Nearly every sampling location and depth had some presence of the HAB species, but at concentrations less than 10,000 cells L⁻¹.

Bioassay Experiments

Chlorophyll *a*

Bioassay experiments had highest chl *a* concentrations in the N+P treatments in June and July, and NO_x in September (Figure 24a, 24b, 24c). The highest concentration from bioassay 1 was N+P treatment at 22.9 µg L⁻¹, followed closely by nitrate and ammonium treatments (Figure 24a). The highest concentration from the July bioassay was the N+P treatment with 18.2 µg chl *a* L⁻¹, followed closely by the NH₄⁺ treatment (Figure 24b). The September bioassay was slightly different than June and July, with the highest chl *a* concentrations in the NO_x treatment, followed by the N+P treatment, then the PO₄³⁻ treatment (Figure 24c). September bioassay results were different from the other experiments likely because the initial water samples were collected under a storm surge and hurricane warning, so the nutrient concentrations were probably much higher during the initial water collection. For all bioassay results, chl *a* concentrations remained low in the PO₄³⁻ treatment and control, even within replicates.

Harmful Algal Bloom species

Dinophysis spp. had the highest concentration in bioassay 1 with a peak of 600 cells L⁻¹ during day 1 from the control treatment (Figure 25a). *Karenia* spp. had concentrations up to 400 cells L⁻¹ during bioassays 1 and 3. Higher concentrations of *Karenia* spp. occurred in the control, N+P and NO₃⁻ treatments (Figure 25b). *Pseudo-nitzschia* spp. had the highest concentrations of all HAB species for every bioassay (up to 18,000 cells L⁻¹ in bioassay 3) (Figure 25c). The highest concentrations of *Pseudo-nitzschia* spp. occurred on days 2 and 3 in the N+P, and NH₄⁺ and PO₄³⁻ treatments.

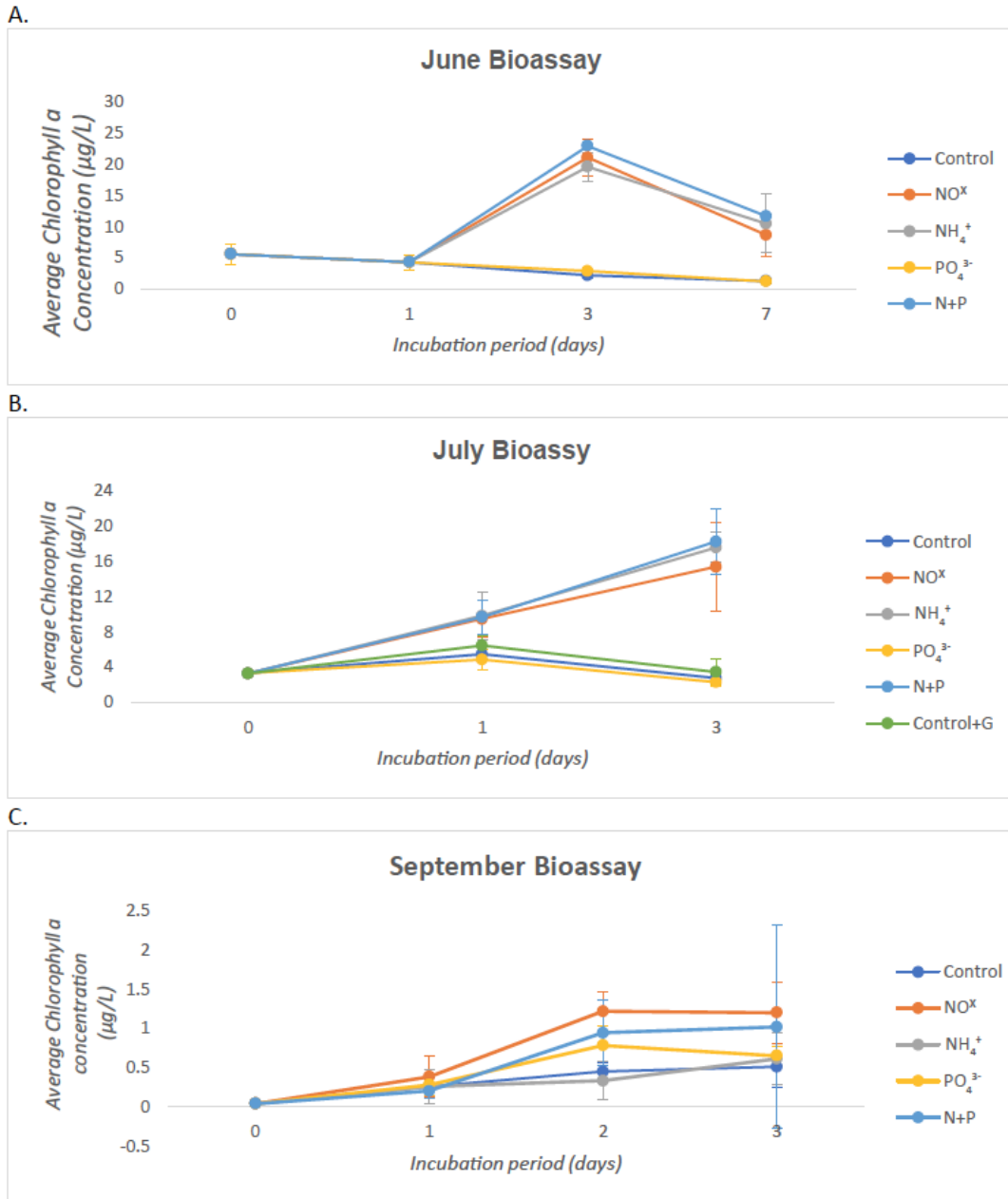


Figure 24: Average extracted chl *a* concentrations from bioassay experiments under nutrient treatments (Control, N+P, NH_4^+ , NO_x , PO_4^{3-}) from the Ocean City Inlet. (A) Bioassay 1 - June 2019, (B) Bioassay 2 - July 2019, (C) Bioassay 3 – September 2019.

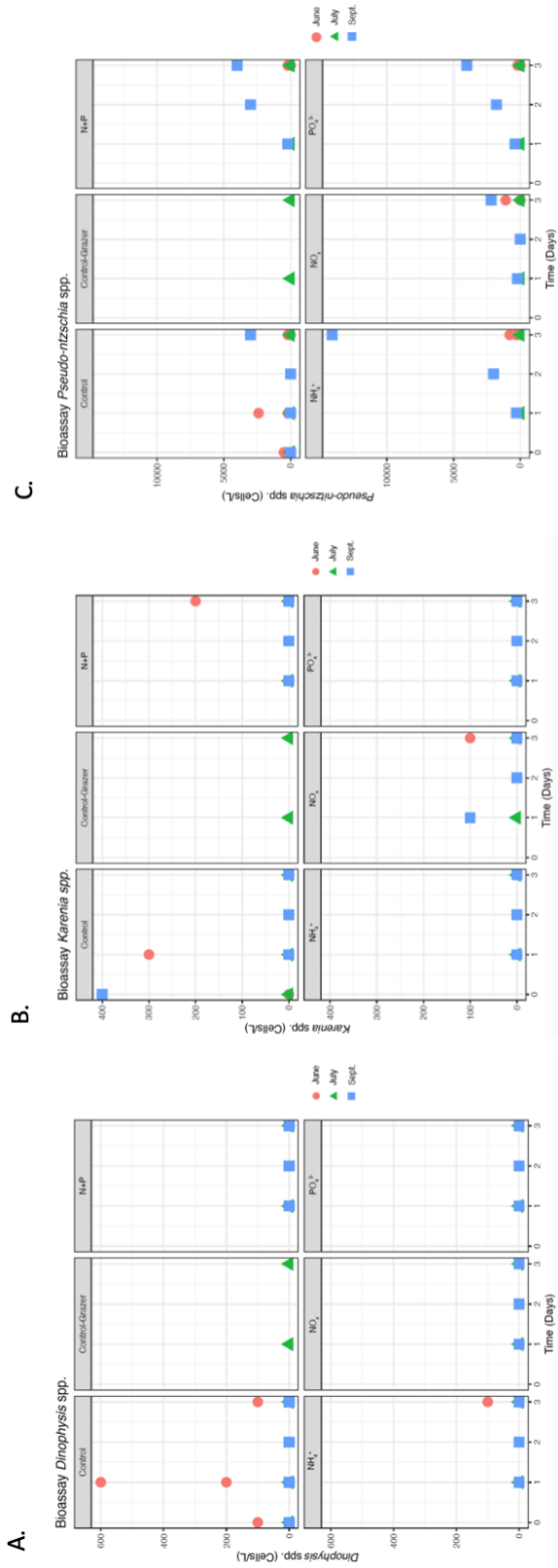


Figure 25: HAB species concentrations from bioassay experiments with nutrient treatments (Control, N+P, NH₄⁺, NO_x, PO₄³⁻). (A) *Dinophysis* spp., (B) *Karenia* spp., (C) *Pseudo-nitzschia* spp.

DISCUSSION

Physical factors

Physical factors are the dominant source of variation in the nutrient, chl *a*, and HAB concentrations in the coastal waters of the Mid-Atlantic Bight (MAB) but they are neither stable nor predictable (Cloern and Jassby 2008; Racault et al. 2012).

Statistical analyses and seasonal comparisons from the present study showed strong influence of physics including stratification, on the water column in MD's coastal ocean. Intra-annual temperature, salinity, and density changes in the water column affecting stratification in the region's coastal waters are influenced by estuarine and freshwater discharge as well as precipitation and storm frequency (Xu et al. 2011; Xu et al. 2020). Statistical significance testing of temperature and salinity identified temperature as a significant factor in the HAB concentration variations. The regional physical variables (wind direction, freshwater discharge) affect the water column stratification (including the presence of a sub-surface chl *a* max layer) and the seasonal phytoplankton bloom dynamics (Li et al. 2015). Wind forcing and upwelling are also important factors in shorter term water column stratification and chl *a* concentrations (Glenn et al. 2004a; Kang et al. 2017). In the MCBs in particular, wind forcing and tidal exchange of saltwater into the embayments are both important for nutrient, chl *a*, and salt flux, but tides become less important when there are higher stronger winds that align with the shape of the bays (southwest) (Kang et al. 2017).

The North Atlantic coastal waters are influenced by the Gulf Stream moving north, offshore near the edge of the continental shelf. Anti-cyclonic eddies can spin

off from the Gulf Stream and transport cold, nutrient rich waters into the coastal environment. Cyclonic eddies, which tend to last longer and have higher energy, can also propagate westward towards the coastal United States transporting nutrients (Kang and Curchitser 2013). Labrador Slope Water from the Labrador Sea and Warm Slope Water from the Central North Atlantic can be carried southwest to the MAB during years with low North Atlantic Oscillation (NAO) indices (Townsend et al. 2004). The Labrador Slope Water is low in inorganic nutrients (such as NO_x), whereas Warm Slope Water has NO_x concentrations averaging $17 \mu\text{M}$ (Townsend 1998). The influence of these water masses impacts the primary production and phytoplankton community structure of the North Atlantic coastal waters.

Summertime upwelling events are common on the New Jersey shelf (north of MD coastal waters) and are often associated with strong southwesterly winds (Glenn et al. 2004a). Similarly, in the present study, July and October observations provided evidence of upwelling conditions with colder, saltier, and nutrient-rich waters at the bottom near Chincoteague Inlet. Weather events, such as tropical storms and hurricanes, are common in late summer and early autumn in this region and create a well-mixed water column (from wind/storm-surges) which re-suspend nutrients and phytoplankton and enhances benthic-pelagic coupling (Griffiths et al. 2017; Friedrichs et al. 2019).

When combining all the data collected over 5 cruises, strong seasonal patterns emerged for both dissolved nutrients and chl *a* concentrations (Figure 26). Across all sampling times, dissolved nutrients were highest at the bottom sampling depths and NH_4^+ had the highest concentration of all dissolved nutrients, with varying

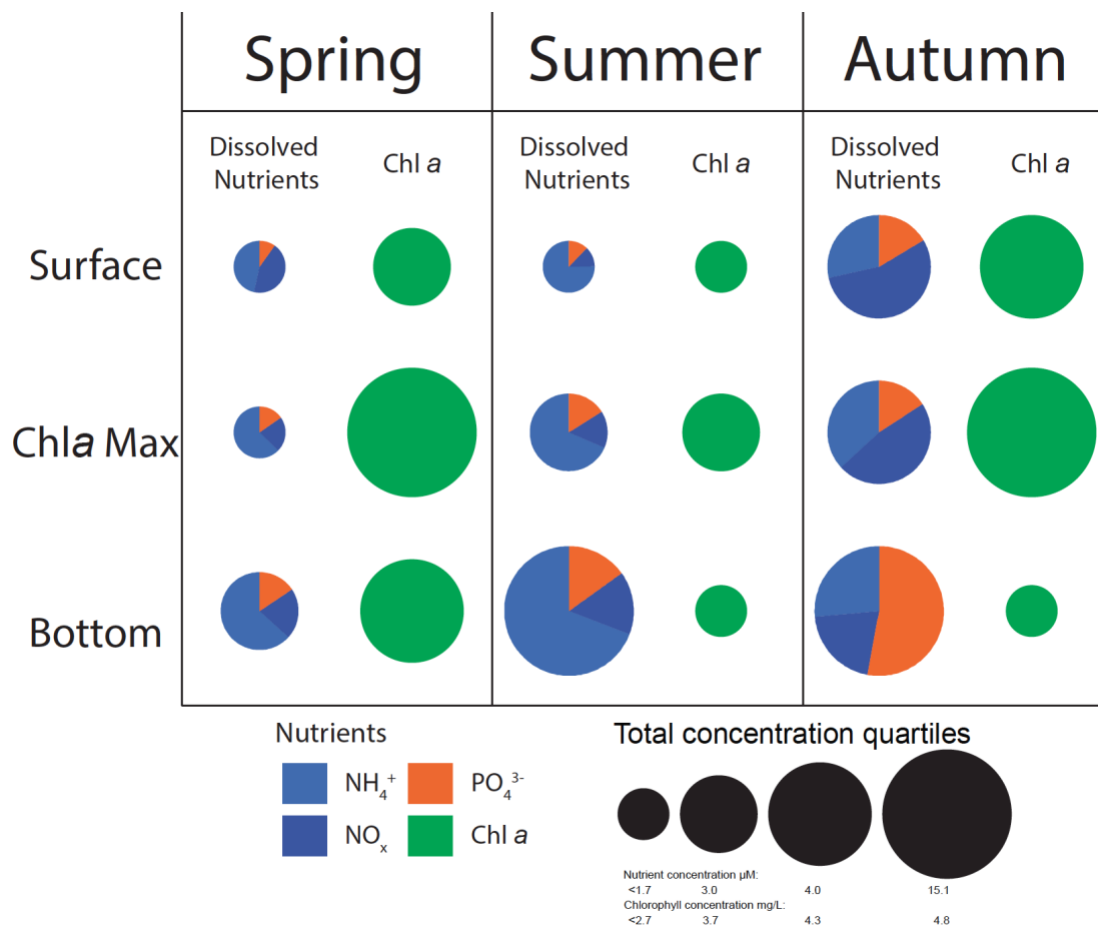


Figure 26: Seasonal diagram summarizing the chl *a* and dissolved nutrient (NH₄⁺, NO_x, PO₄³⁻) concentration patterns by depth and season. The size of each pie chart is determined by the quartile value of the combined dataset—<2.7-4.8 μg L⁻¹ for chl *a* and <1.7-15.1 μM for nutrients. Individual nutrients are distinguished by color and represent their portion of the total average concentration across the entire sampling grid. Columns are separated by season and rows are separated by depth. Spring consists of May 2019 and June 2018 sampling times; summer is July 2018 and July 2019, and Autumn is October 2018.

proportions of PO_4^{3-} and NO_x . In the spring, combined dissolved nutrient concentrations were lower than in the summer and autumn (with elevated NO_x concentrations at the surface) but chl *a* concentrations overall, were the highest. Summer samples were slightly elevated for dissolved nutrients, but much lower for chl *a*. However, because there is a stark difference between the 2018 (record rainfall) and 2019 (less rainfall) summer samples (Ocean City Municipality Airport, Surface from the University of Utah MesoWest Surface Weather Maps), it is important to note that dissolved nutrients were much higher in both the surface and chl *a* max in summer 2019 (Figure 27) (cf. Sedwick et al. 2018). This difference was perhaps due to a lag effect of record rains of late 2018 into the following season of 2019, caused by freshwater storage in soils that was slowly released through groundwater (Brookfield et al. 2021). Based on PCA analysis, summer months had less overlap of data categorized by depth, which indicates stronger depth stratification—particularly in July 2019. The relationship between NH_4^+ and depth was negative in July 2019, unlike any other sampling time. Additionally, 2019 chl *a* concentrations were lower at the surface samples compared to 2018. After strong physical mixing events and increased precipitation, October 2018 observations had the highest dissolved nutrient concentrations (with elevated NO_x and PO_4^{3-}) compared to other sampling times.

The highest chl *a* concentrations occurred at the bottom sampling depths, potentially as a result of nutrient upwelling and benthic pelagic coupling (Nixon 1981). NH_4^+ was the primary dissolved nutrient during the spring and summer months, but higher concentrations of PO_4^{3-} and NO_x occurred in the autumn, likely due to mixing events (such as hurricanes and other storm events). Episodic small

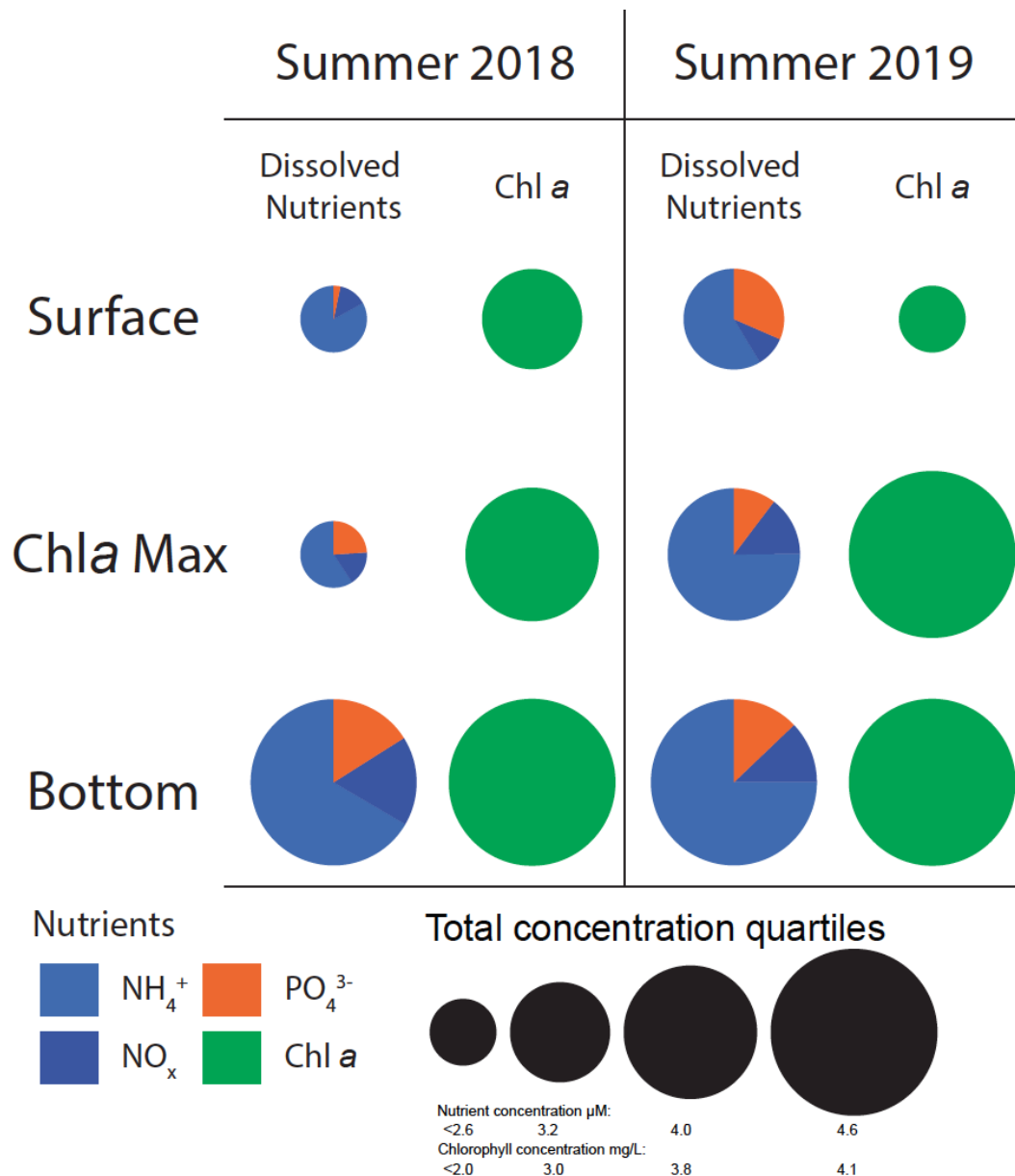


Figure 27: Diagram summarizing the chl *a* and dissolved nutrient (NH₄⁺, NO_x, PO₄³⁻) concentration patterns by depth for July 2018 and July 2019. The size of each pie chart is determined by the quartile value of the combined dataset—<2.6-4.6 μg L⁻¹ for chl *a* and <2.0-4.1 μM for nutrients. Individual nutrients are distinguished by color and represent their portion of the total average concentration across the entire sampling grid. Columns are separated by season and rows are separated by depth.

upwelling events are a common phenomenon north of this sampling grid, in New Jersey (especially during the late summer, early autumn months) (Glenn et al. 2004b). More details of the physical oceanographic features of the Delmarva region of the Mid-Atlantic coast would help discern some of the causes of these features.

Spatial Comparison

The coastal waters of the Mid Atlantic Bight (MAB) consist of North Atlantic waters on the eastern US continental shelf. The water depth in this region ranges from 14 – 98 m and varies in surface salinity from 30-35.3 psu (Balthius et al. 2009). DIN and DIP are typically higher in the bottom waters, with average concentrations ~ 3 $\mu\text{M-N}$ and ~ 1.3 $\mu\text{M-P}$ (Balthius et al. 2009). Chl *a* concentrations of the shelf waters have an average of 0.23 $\mu\text{g chl } a \text{ L}^{-1}$ in surface waters and 0.3 $\mu\text{g chl } a \text{ L}^{-1}$ in bottom waters (Balthius et al. 2009). In the New York Harbor region, TN concentrations range from 28.6 – 85.7 $\mu\text{M-N}$, TP concentrations range from 1.0 – 4.1 $\mu\text{M-P}$, and chl *a* concentrations range from 5 - 20 $\mu\text{g chl } a \text{ L}^{-1}$ (Taillie et al. 2020). The MCB thresholds are 46 $\mu\text{M-N}$ (0.65 mg L^{-1}) for TN, 1.2 $\mu\text{M-P}$ (0.037 mg L^{-1}) for TP, and 15 $\mu\text{g L}^{-1}$ for chl *a* (Table 1) (Dennison et al. 2009). Regional chl *a* ranges are also broad, with average concentrations of 10.3 $\mu\text{g chl } a \text{ L}^{-1}$ in the lower Chesapeake Bay, 4.4 $\mu\text{g chl } a \text{ L}^{-1}$ in the inshore MAB, and 0.36 $\mu\text{g chl } a \text{ L}^{-1}$ in the offshore MAB (Harding et al. 2005). Additionally, an EPA technical report in 2001, established Chesapeake Bay polyhaline chl *a* ranges; 3 – 7 $\mu\text{g chl } a \text{ L}^{-1}$ in the spring, 4 – 9 $\mu\text{g chl } a \text{ L}^{-1}$ in the summer (EPA 2001).

Average chl *a* concentrations from MD coastal waters data in 2018 and 2019 (Table 9) had ranges from 2.7 – 5.0 $\mu\text{g chl } a \text{ L}^{-1}$, which aligns well with the inshore

Table 9: Average (+ standard deviation) concentrations from each sampling period of nutrient and environmental variables: DO, temperature, salinity, chl *a*, TN, TP, NH₄⁺, NO_x, PO₄³⁻ from all sampling depths and locations.

Date	Dissolved Oxygen ± SD	Temperature ± SD	Salinity ± SD	Chlorophyll <i>a</i> ± SD	NH ₄ ± SD	NO _x ± SD	TN ± SD	PO ₄ ± SD	TP ± SD
May 2019	5.9 ± 0.4	14.4 ± 1.8	30.5 ± 0.5	5.0 ± 1.8	1.1 ± 0.4	0.3 ± 0.1	10.7 ± 2.5	0.2 ± 0.1	0.9 ± 0.2
June 2018	6.3 ± 1.1	19.8 ± 2.2	30.0 ± 0.4	3.5 ± 1.4	0.6 ± 0.3	0.4 ± 0.3	10.3 ± 4.7	0.2 ± 0.1	0.8 ± 0.2
July 2018	7.3 ± 0.3	21.8 ± 2.5	31.1 ± 0.4	2.7 ± 1.2	1.7 ± 1.2	0.4 ± 0.4	11.1 ± 5.8	0.6 ± 0.2	1.1 ± 0.4
July 2019	5.7 ± 1.4	21.2 ± 4.3	30.4 ± 0.5	2.9 ± 1.8	2.4 ± 1.8	0.5 ± 0.3	11.3 ± 3.2	0.3 ± 0.2	1.1 ± 0.5
October 2018	7.1 ± 0.1	23.9 ± 0.3	30.3 ± 0.5	4.0 ± 2.3	2.0 ± 1.4	2.3 ± 2.0	17.4 ± 4.0	0.7 ± 0.2	1.4 ± 0.3

MAB, but is higher (in many cases) than the EPA ranges, and lower than the New York Harbor region, MCBs and Chesapeake Bay. Average 2018 – 2019 TN concentrations in MD's coastal waters are about half of the New York Harbor and MCB concentrations, with a range of 10.3 – 17.4 $\mu\text{M-N}$. TP concentrations are only slightly lower in MD's coastal waters (0.8 – 1.4 $\mu\text{M-P}$) than in the New York Harbor region, but often exceed the MCB threshold.

Nutrient limitation

Nitrogen limitation is a key factor in coastal eutrophication and algal growth, and elevated nitrogen sources in coastal waters are often caused by human waste (Ryther and Dunstan 1971). The DIN:DIP ratio for the MAB region suggests nitrogen limitation (which is indicative of typical ocean water in the North Atlantic region) with an average ratio of 4.5 in bottom waters and 7.0 in surface waters (Balthius et al. 2009). The typical molar ratio associated with ocean ecosystems for nitrogen and phosphorus is 16:1 (Redfield 1934), with ratios less than 16:1 indicative of nitrogen limitation.

Excess nitrogen is a potential cause for the elevated HAB concentrations that coincided with sampling locations in proximity to areas with higher population densities on Fenwick Island during densely populated summer months (Figure 28). Based on statistical analyses, NO_x and NH_4^+ were the most determinant factors in the variation of nutrient, HAB and environmental variables in the sampling region. Additionally, bioassay experiment results and N:P ratios were consistent with nitrogen limitation. Nutrient input into the coastal ocean is multi-faceted and has numerous sources—submarine groundwater discharge, riverine input, oceanic

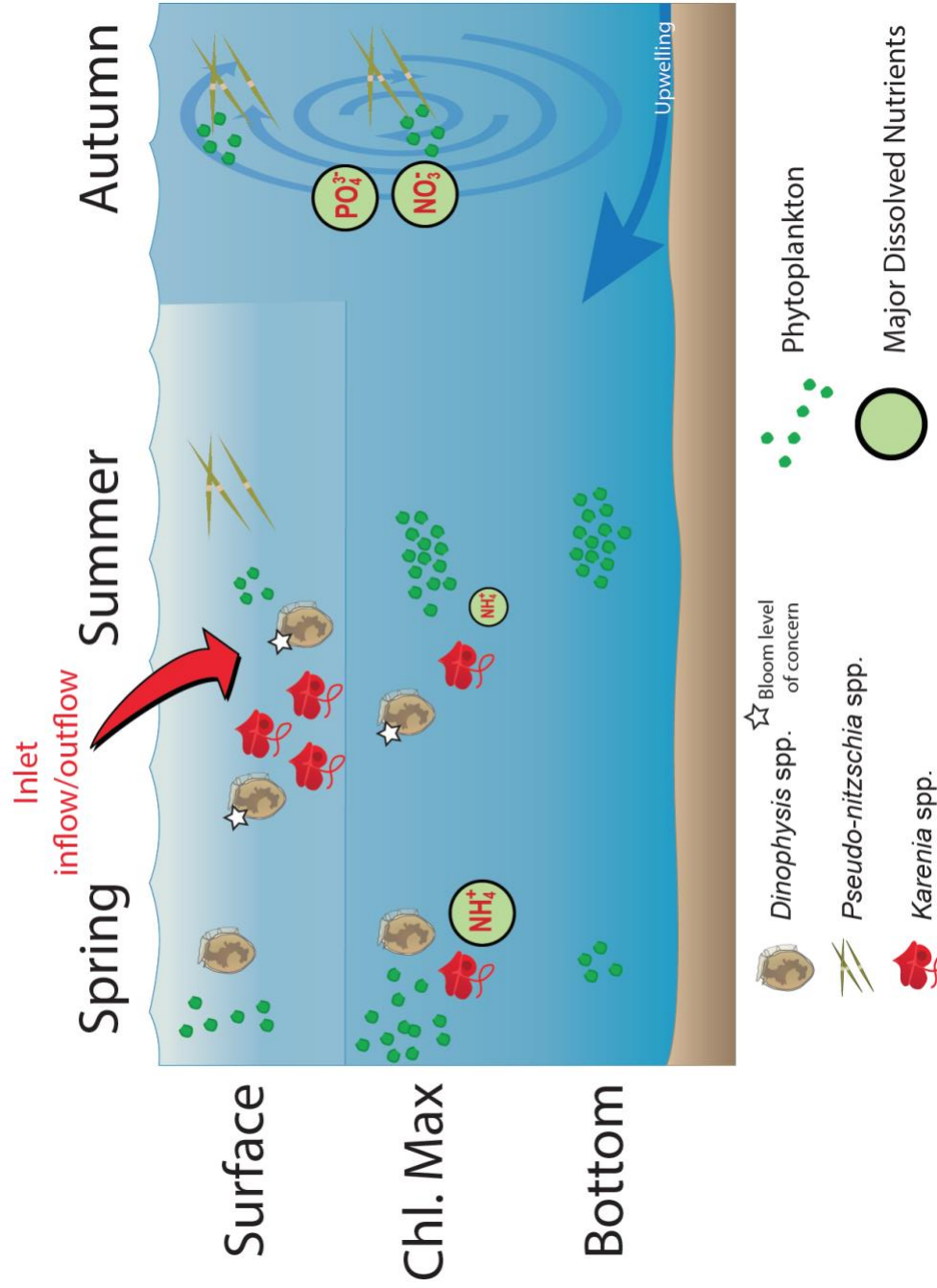


Figure 28: Conceptual diagram outlining the various chemical, biological, and physical processes that occur within the study region. Three columns are categorized by season, three rows categorized by depth (Integration and Application Network ian.umces.edu/media-library).

circulation, and atmospheric deposition of nitrogen can all impact the regional nutrient budget and cause major changes in algal growth ability (Fisher et al. 1992; Paerl et al. 2002; Sedwick et al. 2018; Brookfield et al. 2021).

Karenia spp.

Karenia spp. are more commonly associated with sub-tropical conditions, but the spatial variability has been increasing over time (Heisler et al. 2008; Townhill et al. 2018; X. Li et al. 2019; Anderson et al. 2021). *Karenia mikimotoi* is commonly found in New England, and has been found in bloom concentrations as far north as Maine in 2019 (Townhill et al. 2018; X. Li et al. 2019). While *Karenia* spp. has some mixotrophic ability; taking up dissolved organic nitrogen and phosphorus from *Trichodesmium* (Mulholland et al. 2004; Sipler et al. 2013) and preying on picoplankton (Glibert et al. 2009; Procise 2012), there are still a lot of unknowns regarding species details, bloom triggers, and toxicity (Burkholder et al. 2008; Heil et al. 2014a; Glibert et al. 2016; Stoecker et al. 2017). *Karenia* spp. are most prominent in Florida's Gulf Coast, and typically associated with increased terrestrially sourced nitrogen during summer months (Heil et al. 2007; Heil et al. 2014a; Heil. et al. 2014b; Medina et al. 2020).

While the MD coastal data from 2018 and 2019 had evidence of several toxin producing *Karenia* spp. in low concentrations, there are questions over the regulatory threshold values in the region, given the mixed species assemblage, and the fact that most research has revolved around *K. brevis* in the Gulf of Mexico. The National Shellfish Sanitation Program (NSSP) has set the *Karenia brevis* cell concentration threshold at 5,000 cells L⁻¹—due to the prevalence of NSP in that regions and the

potential human health impacts. Due to difficulties in distinguishing species of *Karenia*, this threshold is often used nationally to increased monitoring and test for toxins (*National Shellfish Sanitation Program (NSSP) Guide for the Control of Molluscan Shellfish* 2015). However, given that *K. brevis* has not been the dominant species of *Karenia* sampled in MD waters, and the questions about toxicity of the more prominent species in this region, *K. papilionacea* and *K. mikimotoi*, the threshold of concern in MD is currently 10,000,000 cells L⁻¹ (Table 1) (Allen et al. 2014; Heil and Steidinger 2009). None of the 2018 – 2019 MD coastal water data exceeded the MD DNR threshold, but there were concentrations up to 300,000 cells L⁻¹ in June 2018, 30,000 cells L⁻¹ in July 2018, and 22,000 cells L⁻¹ in July 2019, which did exceed the NSSP threshold and, in June 2018, the human respiratory health impact threshold (Heil and Steidinger 2009; *National Shellfish Sanitation Program (NSSP) Guide for the Control of Molluscan Shellfish* 2015). Additional research regarding the toxicity of other *Karenia* spp. is urgently needed to establish appropriate monitoring thresholds.

Dinophysis spp.

Dinophysis spp. is found all around the world because it is adaptable to a wide range of water quality conditions (De Gruyter et al. 2012; Tong et al. 2015).

However, high concentrations of toxin producing *Dinophysis* spp. are typically found in areas with stable water columns (Tong et al. 2015; Anderson et al. 2021).

Dinophysis spp. is known to be strongly mixotrophic and specifically reliant on grazing, particularly on *Myrionecta rubra*, and has employs chloro-kleptoplasticity, retaining acquired plastids from prey, which allows *Dinophysis* to survive in a broad

range of geographic regions (Kim et al. 2008, Pappas pers comms). Indeed, toxin production in *Dinophysis* spp. is associated with high reliance on grazing (Tong et al. 2011). Increased rates of DIN and DIP do not directly affect *Dinophysis* spp. toxin production but increase prey biomass as a food source (Kozlowsky-Suzuki et al. 2006; Tong et al. 2015). *Dinophysis* spp. is also preyed upon by numerous copepods, including *Acartia biflosa*, *Temora longicornis*, and *Centropages typicus*, which do not appear to be affected by the toxicity (Kozlowsky-Suzuki et al. 2006).

In MD's coastal waters, *Dinophysis* spp. had higher concentrations associated with lower ambient dissolved nutrients in the present study. This is likely due to better suitability to physical conditions that are known to be exploited by HAB species, such as temperature, light availability, and prey rapidly taking up dissolved nutrients, and its strong mixotrophic capacity. *Dinophysis* spp. exceeded MD bloom level of concern thresholds at both the surface and chl *a* max 0.03% of the time in July 2018. In June 2018, samples of *Dinophysis* spp. exceeded MD threshold values 0.1% of the time at the surface; and 0.03% of the time at the chl *a* max. These exceedances all occurred at inshore sites adjacent to MCB inlets/sewage outflow areas (transects 1, 2, 8, 9). Due to increased eutrophication associated with global climate, *Dinophysis* spp. toxicity, bloom concentration frequency and intensity, as well as spatial distribution is increasing (Heisler et al. 2008). Thus, close future monitoring of *Dinophysis* spp. is warranted.

Pseudo-nitzschia spp.

Pseudo-nitzschia spp. is one of the dominant phytoplankton in the MAB (De Gruyter et al. 2012). Toxigenic *Pseudo-nitzschia* spp. have high competitive fitness

and are able to survive in unfavorable conditions (Olson et al. 2008; Trainer et al. 2012). In the Chesapeake Bay region in particular, *Pseudo-nitzschia* spp. is known to occur in low temperature, high light fluctuation events (upwelling conditions) and some species are found primarily in upwelling zones (Thessen and Stoecker 2007). . These areas are generally higher in NO_x, which diatoms such as *Pseudo-nitzschia* generally uptake better than other phytoplankton (Glibert et al. 2016). Additionally, *Pseudo-nitzschia* spp. abundance is important to toxin bioaccumulation in the food web because its predators, which include copepods such as *Calanus* spp. *Acartia* spp., and dinoflagellates such as *Protoperidinium* spp., do not appear to be affected by the toxin (Olson et al. 2006; Trainer et al. 2012; Miesner et al. 2021).

In MD coastal waters from 2018 – 2019, *Pseudo-nitzschia* spp. occurred in higher concentrations in October 2018, which is consistent with being re-suspended by mixing events partially because they lack flagella and are unable to move up and down in the water column (Trainer et al. 2012), as well as the increase in NO_x during this time period which is also consistent with other studies (Glibert et al 2016). It is also possible that the increased PO₄³⁻ concentrations present in the water column created more suitable nutrient conditions (Lema et al. 2017). There are, however, significant knowledge gaps in the dissolved nutrient and grazing effects on *Pseudo-nitzschia* spp. as well as toxin production, in MD's coastal waters.

Management Implications

The MCBs water quality has been routinely monitored for over a decade, with nutrient and chl *a* thresholds in place to monitor ecosystem changes (Table 1). There have been significant management measures implemented to improve the health of

the MCBs, and an annual report card is published by the University of Maryland Center for Environmental Science- Integration and Application Network (UMCES- IAN) in association with the MD DNR and the MCBs Program (MCBP) among others (Dennison et al. 2009; *2018 Coastal Bays Report Card*).

In 2009, scientists and managers established the following water quality nutrient threshold concentrations; $46\mu\text{M}$ (0.65 mg L^{-1}) for TN, $1.2\ \mu\text{M}$ (0.037 mg L^{-1}) for TP, and $15\ \mu\text{g chl a L}^{-1}$ (Table 1) (Dennison et al. 2009). These threshold values were determined from data collected between 2004-2006 and are used to indicate the ecosystem health conditions of the MCBs. The annual Coastal Bays Report Card ranks the condition of the coastal bays in regard to the threshold values previously established (*2018 Coastal Bays Report Card*). In 2018, the overall health of the MCBs was ranked “good” scoring 71/100. TN concentrations were “good”, Total Chl *a* concentrations were “very good” , and TP concentrations were “moderate” (*2018 Coastal Bays Report Card*). While the health of the MCB system is important, it is not a closed system. Influences from the connected waterways impact the water quality of the MCBs as well, and vice versa. There are two inlets connecting the Atlantic Ocean into the MCBs: Ocean City Inlet, and Chincoteague Inlet in VA to the south (Figure 1). Tides and currents create an exchange of the water from rivers flowing into the MCBs with the Atlantic Ocean water (Kang et al. 2017). This water can carry nutrients and phytoplankton which ultimately affect the health of the coastal ocean ecosystem.

On the east coast, it is unusual to have an undeveloped coastal National Park region that is protected and preserved, such as ASIS (Carruthers et al. 2013), which

makes this region particularly unique. The NPS has the responsibility of monitoring all natural resources that influence ASIS, as well as “protect water and the people, and environment that rely on the availability of clean water,” (National Parks Service 1916). Data from the present study in 2018 and 2019, showed the highest concentrations of nutrients, chl *a*, and HABs all occurred in areas in proximity to estuarine inlets and/or sewage outflow areas. The most northern sites were impacted more intensely by anthropogenic influences and have larger inlet inflow and outflow through DE sewage outflow to the north of the sampling grid, the OC sewage outflow and the OC inlet. In the summertime when there are more people visiting the region for vacation, recreation, fishing, etc., there is compounding influence of high nutrients, chl *a*, and HAB concentrations in the northern transects, especially in surface samples. While there is substantial nutrient, HAB and chl *a* monitoring inside MD’s coastal lagoons, coastal ocean waters are not given the same attention. There is a significant need to monitor the sewage outflows in the region in order to understand the baseline nutrient and chl *a* concentrations that are being released into offshore ocean waters in order to protect the integrity of ASIS as a unique area as well as the coastal MD communities.

Additionally, there are current and future development projects that will significantly impact ASIS, the MCBs, Fenwick Island and the coastal inland region of MD. Fenwick Island is regularly stabilized by pumping offshore sand onto the beaches, and an artificial jetty was built in 1934 to preserve the Ocean City inlet. The artificial inlet and stabilization has disrupted the natural sand cycling that is still occurring on ASIS (Dennison et al. 2009). Additionally, Ocean City has proposed a

controversial offshore windfarm development project that could increase boat traffic in the area during construction, and create irreversible changes to the ocean ecosystem (Soper 2021; Town of Ocean City Maryland 2021). Without regular monitoring of the current ocean ecosystem, it will not be possible to understand the full extent to which these construction projects alter the landscape.

FUTURE RESEARCH

The statistically significant differences in HAB species concentrations between the surface and chl *a* max sampling depths suggest that further routine monitoring is needed in the area. Currently, only monthly surface samples are taken by the Maryland Department of the Environment (MDE) in conjunction with MD DNR analyses for emergent HAB species presence. Surface samples alone do not provide enough information about the potential for bloom events. Additionally, the threshold values used by the MCBs are not adequate for the coastal ocean. New threshold values for chl *a*, HABs, total nutrients, and dissolved nutrients should be formulated for the coastal ocean because the physical, chemical, and biological processes that occur and the potential impacts in coastal waters are very different to those of estuarine waters such as the MCBs.

There is still much more information that can be synthesized from the dataset that was generated as part of this project, including the impact of temperature and precipitation over time with regards to nutrients and HABs. Additionally, identifying the physical dynamics of the coastal region, as well as potential nutrient sources using stable isotope (δN^{15}) techniques will help determine the causes of nutrient and HAB fluctuations. Tidal inlet exchange, upwelling and other physical models can help paint a more complete picture of MD's coastal ocean. Precipitation and temperature studies are underway to compliment this dataset as well.

References

2018 Coastal Bays Report Card.

Aighewi, I. T., O. K. Nosakhare, and A. B. Ishaque. 2013. Land Use–Land Cover Changes and Sewage Loading in the Lower Eastern Shore Watersheds and Coastal Bays of Maryland: Implications for Surface Water Quality. *Journal of Coastal Research* 290: 1073–1082. <https://doi.org/10.2112/jcoastres-d-11-00195.1>.

Allen, M., J. Brainard, J. Clark, and F. Moser. 2014. *Remote Sensing Harmful Algal Bloom Workshop Chesapeake and Coastal Bays Region Workshop Report Edited by A Maryland Sea Grant Publication.*

American Community Survey. 2021. 2019: ACS Demographic and Housing Estimates Data Profiles. *2019: ACS 5-year Estimates.* <https://data.census.gov/cedsci/table?g=1600000US2458225&tid=ACSDP5Y2019.DP05&hidePreview=false>. Accessed March 30.

Anderson, D. M., E. Fensin, C. J. Gobler, A. E. Hoeglund, K. A. Hubbard, D. M. Kulis, J. H. Landsberg, et al. 2021. Marine harmful algal blooms (HABs) in the United States: History, current status and future trends. *Harmful Algae* 102. Elsevier B.V.: 101975. <https://doi.org/10.1016/j.hal.2021.101975>.

Arar, E. J., and G. B. Collins. 2021. *Method 445.0 - In Vitro Determination of Chlorophyll a and Pheophytin a in Marine and Freshwater Algae by Fluorescence.* [http://flrules.elaws.us/gateway/refpdf/62/D62/Ref-02922/m445_0\[1\].pdf](http://flrules.elaws.us/gateway/refpdf/62/D62/Ref-02922/m445_0[1].pdf). Accessed March 24.

Baden, D. G., and T. J. Mende. 1982. Toxicity of two toxins from the Florida red tide

- marine dinoflagellate, *Ptychodiscus brevis*. *Toxicon* 20. *Toxicon*: 457–461.
[https://doi.org/10.1016/0041-0101\(82\)90009-5](https://doi.org/10.1016/0041-0101(82)90009-5).
- Balthius, W. L. , J. L. Hyland, M. H. Fulton, E. F. Wirth, J. A. Kiddon, and J. Macauley. 2009. *Ecological Condition of Coastal Ocean Waters Along the U. S . Mid-Atlantic Bight : 2006. NOAA Technical Memorandum NOS NCCOS 109*.
- Basti, L., H. Hegaret, and S. E. Shumway. 2018. Harmful Algal Blooms and Shellfish. In *Harmful Algal Blooms: A Compendium Desk Reference*, ed. S. E. Shumway, J.M. Burkholder, and S.L. Morton, First, 135–190. John Wiley & Sons, Ltd.
- Beaulac, M. N., and K. H. Reckhow. 1982. An Examination of Land Use - Nutrient Export Relationships. *JAWRA Journal of the American Water Resources Association* 18. John Wiley & Sons, Ltd: 1013–1024.
<https://doi.org/10.1111/j.1752-1688.1982.tb00109.x>.
- Beckert, K. A., T. R. Fisher, J. M. O’Neil, and R. V. Jesien. 2011. Characterization and comparison of stream nutrients, land use, and loading patterns in Maryland coastal bay watersheds. *Water, Air, and Soil Pollution* 221: 255–273.
<https://doi.org/10.1007/s11270-011-0788-7>.
- Boynton, W. R. , L .Murray, W. M. Kemp, J. D. Hagy, C. Stokes. 1993. Maryland’s Coastal Bays: An Assessment of Aquatic Ecosystems.
- Brand, L. E., L. Campbell, and E. Bresnan. 2012. *Karenia*: The biology and ecology of a toxic genus. *Harmful Algae* 14. Elsevier: 156–178.
<https://doi.org/10.1016/j.hal.2011.10.020>.
- Brookfield, A. E., A.T. Hansen, P. L. Sullivan, J. A. Czuba, M. F. Kirk, L. Li, M. E.

- Newcomer, and G. Wilkinson. 2021. Predicting algal blooms: Are we overlooking groundwater? *Science of the Total Environment* 769. <https://doi.org/10.1016/j.scitotenv.2020.144442>.
- Burkholder, J. M., P. M. Glibert, and H. M. Skelton. 2008. Mixotrophy, a major mode of nutrition for harmful algal species in eutrophic waters. *Harmful Algae* 8. Elsevier: 77–93. <https://doi.org/10.1016/j.hal.2008.08.010>.
- Carruthers, T., K. Beckert, C. Schupp, T. Saxby, J. Kumer, J. Thomas, B. Sturgis, W, Dennison, M. Williams, T. Fisher and C. Zimmerman. 2013. Improving management of a mid-Atlantic coastal barrier island through assessment of habitat condition. *Estuarine, Coastal and Shelf Science* 116: 74–86. <https://doi.org/10.1016/j.ecss.2012.08.012>.
- Chambers, J. M. 1992. Linear Models. In *Statistical Models in S*, ed. J. M. Chambers and T. J. Hastie. Wadsworth & Brooks/Cole.
- Chincoteague: About Our Island. *The Town of Chincoteague Virginia*. *City of Rehoboth Beach Ocean Outfall Project Town Hall Q&A Workshop*. 2017.
- Clesceri, L.S., A.E. Greenberg, and R.R. Trussell. 1998. *Standard Methods for the Examination of Water and Waste Water*. APHA-AWWA-WPCF.
- Cloern, J. E., and A. D. Jassby. 2008. Complex seasonal patterns of primary producers at the land-sea interface. *Ecology Letters* 11. John Wiley & Sons, Ltd: 1294–1303. <https://doi.org/10.1111/j.1461-0248.2008.01244.x>.
- D’Elia, C. F., P. A. Steudler, and N. Corwin. 1977. Determination of total nitrogen in aqueous samples using persulfate digestion¹. *Limnology and Oceanography* 22. John Wiley & Sons, Ltd: 760–764. <https://doi.org/10.4319/lo.1977.22.4.0760>.

- Dance, S. 2018. As Hurricane Florence targets Southeast, Gov. Hogan warns of possibly “historic” flooding in Maryland. *The Baltimore SUN*, September 11.
- Delaware Department of Natural Resources and Environmental Control. 2020. *Delaware Statewide Assessments of Wastewater Facilities and Current Status and Future Needs 2020-2025*.
- Dennison, W. C., J. E. Thomas, C. J. Cain, T. J.B. Carruthers, M. R. Hall, R. V. Jesien, C. E. Wazniak, and D. E. Wilson. 2009. *Shifting Sands: Environmental and cultural change in Maryland’s Coastal Bays*. IAN PRESS. Cambridge, MD: UMCES- IAN Press.
- Dillow, J. J. A., and E. A. Greene. 1999. *Ground-water discharge and nitrate loadings to the coastal bays of Maryland*.
- Dodge, J. D. 1982. *Marine Dinoflagellates of the British Isles*. London: HM Stationary Office.
- EPA. 2001. *Technical Guidance Manual For Estuarine and Coastal Marine Waters*. EPA-822-B-01-003.
- Errera, R. M., and L. Campbell. 2011. Osmotic stress triggers toxin production by the dinoflagellate *Karenia brevis*. *Proceedings of the National Academy of Sciences of the United States of America* 108. National Academy of Sciences: 10597–10601. <https://doi.org/10.1073/pnas.1104247108>.
- Fisher, T. R., E. R. Peele, J. W. Ammerman, and L. W. Harding. 1992. Nutrient limitation of phytoplankton in Chesapeake Bay. *Marine Ecology Progress Series* 82. Inter-Research: 51–63. <https://doi.org/10.3354/meps082051>.
- Fowler, N., C. Tomas, D. Baden, L. Campbell, and A. Bourdelais. 2020. Chemical

- analysis of *Karenia papilionacea*. <https://doi.org/10.1016/j.toxicon.2015.05.007>.
- Friedrichs, M. A. M., P. St-Laurent, Y. Xiao, E. Hofmann, K. Hyde, A. Mannino, R. G. Najjar, et al. 2019. Ocean Circulation Causes Strong Variability in the Mid-Atlantic Bight Nitrogen Budget. *Journal of Geophysical Research: Oceans* 124: 113–134. <https://doi.org/10.1029/2018JC014424>.
- Glenn, S., R. Arnone, T. Bergmann, W. Paul Bissett, M. Crowley, J. Cullen, J. Gryzmski, et al. 2004a. Biogeochemical impact of summertime coastal upwelling on the New Jersey Shelf. *Journal of Geophysical Research C: Oceans* 109: 1–15. <https://doi.org/10.1029/2003JC002265>.
- Glenn, S., R. Arnone, T. Bergmann, W. P. Bissett, M. Crowley, J. Cullen, J. Gryzmski, et al. 2004b. Biogeochemical impact of summertime coastal upwelling on the New Jersey Shelf. *J. Geophys. Res* 109: 12–14. <https://doi.org/10.1029/2003JC002265>.
- Glibert, P. M., J. M. Burkholder, T. M. Kana, J. Alexander, H. Skelton, and C. Shilling. 2009. Grazing by *Karenia brevis* on *Synechococcus* enhances its growth rate and may help to sustain blooms. *Aquatic Microbial Ecology* 55: 17–30. <https://doi.org/10.3354/ame01279>.
- Glibert, P. M., F. P. Wilkerson, R. C. Dugdale, J. A. Raven, C. L. Dupont, P. R. Leavitt, A. E. Parker, J. M. Burkholder, and T. M. Kana. 2016. Pluses and minuses of ammonium and nitrate uptake and assimilation by phytoplankton and implications for productivity and community composition, with emphasis on nitrogen-enriched conditions. *Limnology and Oceanography* 61: 165–197. <https://doi.org/10.1002/lno.10203>.

- Griffiths, J. R., M. Kadin, F. J.A. Nascimento, T. Tamelander, A. Törnroos, S. Bonaglia, E. Bonsdorff, et al. 2017. The importance of benthic–pelagic coupling for marine ecosystem functioning in a changing world. *Global Change Biology* 23: 2179–2196. <https://doi.org/10.1111/gcb.13642>.
- De Gruyter, W., C. P Makinen, and T. A H Moisan. 2012. Phytoplankton assemblage patterns in the southern Mid-Atlantic Bight. *Botanica Marina* 55: 445–457. <https://doi.org/10.1515/bot-2012-0110>.
- Harding, L. W., A. Magnuson, and M. E. Mallonee. 2005. SeaWiFS retrievals of chlorophyll in Chesapeake Bay and the mid-Atlantic bight. *Estuarine, Coastal and Shelf Science* 62. Academic Press: 75–94. <https://doi.org/10.1016/j.ecss.2004.08.011>.
- Harmful algal bloom management in the Chesapeake and Coastal Bays. 2014.
- Hayward, L. 2007. *Assateague Island National Seashore: A Resource Assessment*.
- Heil, C. A., and K. A. Steidinger. 2009. Monitoring, management, and mitigation of *Karenia* blooms in the eastern Gulf of Mexico. *Harmful Algae* 8: 611–617. <https://doi.org/10.1016/j.hal.2008.11.006>.
- Heil, C.A., D. A. Bronk, K. Dixon, G. L. Hitchcock, G. J. Kirkpatrick, M. R. Mulholland, J. M. O’Neil, J. J. Walsh, R. Weisberg, and M. Garrett. 2014a. *The gulf of mexico ECOHAB: Karenia program 2006-2012. Harmful Algae*. Vol. 38. Elsevier. <https://doi.org/10.1016/j.hal.2014.07.015>.
- Heil, C. A., K. Dixon, E. Hall, M. Garrett, J. M. Lenos, J. M. O’Neil, B. M. Walsh, et al. 2014b. Blooms of *Karenia brevis* (Davis) G. Hansen & Ø. Moestrup on the West Florida Shelf: Nutrient sources and potential management strategies based

- on a multi-year regional study. *Harmful Algae* 38. Elsevier: 127–140.
<https://doi.org/10.1016/j.hal.2014.07.016>.
- Heil, C. A., M. Revilla, and P. M. Glibert. 2007. Nutrient quality drives differential phytoplankton community composition on the southwest Florida shelf. *Limnology and Oceanography* 52: 1067–1078.
- Heisler, J., P. M. Glibert, J. M. Burkholder, D. M. Anderson, W. Cochlan, W. C. Dennison, Q. Dortch, et al. 2008. Eutrophication and harmful algal blooms: A scientific consensus. *Harmful Algae* 8. Elsevier: 3–13.
<https://doi.org/10.1016/j.hal.2008.08.006>.
- Kang, D., and E. N. Curchitser. 2013. Gulf Stream eddy characteristics in a high-resolution ocean model. *Journal of Geophysical Research: Oceans* 118. Blackwell Publishing Ltd: 4474–4487. <https://doi.org/10.1002/jgrc.20318>.
- Kang, X., M. Xia, J. S. Pitula, and P. Chigbu. 2017. Dynamics of water and salt exchange at Maryland Coastal Bays. *Estuarine, Coastal and Shelf Science* 189. Elsevier Ltd: 1–16. <https://doi.org/10.1016/j.ecss.2017.03.002>.
- Kaplan, M. R., and A. P. Wolfe. 2006. Spatial and temporal variability of Holocene temperature in the North Atlantic region.
<https://doi.org/10.1016/j.yqres.2005.08.020>.
- Kim, S., Y. G. Kang, H. S. Kim, W. Yih, D. W. Coats, and M. G. Park. 2008. Growth and grazing responses of the mixotrophic dinoflagellate *Dinophysis acuminata* as functions of light intensity and prey concentration. *Aquatic Microbial Ecology* 51: 301–310.
- Kozlowsky-Suzuki, B., P. Carlsson, A. Rühl, and E. Granéli. 2006. Food selectivity

- and grazing impact on toxic *Dinophysis* spp. by copepods feeding on natural plankton assemblages. *Harmful Algae* 5. Elsevier: 57–68.
<https://doi.org/10.1016/j.hal.2005.05.002>.
- Lema, K. A., M. Latimier, É. Nézan, J. Fauchot, and M. Le Gac. 2017. Inter and intra-specific growth and domoic acid production in relation to nutrient ratios and concentrations in *Pseudo-nitzschia*: phosphate an important factor. *Harmful Algae* 64. Elsevier B.V.: 11–19. <https://doi.org/10.1016/j.hal.2017.03.001>.
- Li, Xi., T. Yan, R. Yu, and M. Zhou. 2019. A review of *Karenia mikimotoi*: Bloom events, physiology, toxicity and toxic mechanism. *Harmful Algae*. Elsevier B.V. <https://doi.org/10.1016/j.hal.2019.101702>.
- Li, Y., P. S Fratantoni, C. Chen, J. A Hare, Y. Sun, R. C Beardsley, and R. Ji. 2015. Spatio-temporal patterns of stratification on the Northwest Atlantic shelf. *Progress in Oceanography* 134: 123–137.
<https://doi.org/10.1016/j.pocean.2015.01.003>.
- Maier Brown, A. F., Q. Dortch, F. M. Van Dolah, T. A. Leighfield, W. Morrison, A. E. Thessen, K. Steidinger, B. Richardson, C. A. Moncreiff, and J. R. Pennock. 2006. Effect of salinity on the distribution, growth, and toxicity of *Karenia* spp. *Harmful Algae* 5. Elsevier: 199–212. <https://doi.org/10.1016/j.hal.2005.07.004>.
- Mao, M., and M. Xia. 2018. Wave–current dynamics and interactions near the two inlets of a shallow lagoon–inlet–coastal ocean system under hurricane conditions. *Ocean Modelling* 129. Elsevier: 124–144.
<https://doi.org/10.1016/j.ocemod.2018.08.002>.
- Martin, N., and H. Maes. 2008. *Multivariate Analysis*.

- Maryland Coastal Bays. 1999. *Today's Treasures for Tomorrow: Towards a Brighter Future: The Comprehensive Conservation and Management Plan for Maryland's Coastal Bays*.
- Maryland Parks Service. 2020. Assateague State Park. *Maryland Department of Natural Resources*.
- Medina, M., R. Huffaker, J. W. Jawitz, and R. Muñoz-Carpena. 2020. Seasonal dynamics of terrestrially sourced nitrogen influenced *Karenia brevis* blooms off Florida's southern Gulf Coast. *Harmful Algae* 98. Elsevier: 101900.
<https://doi.org/10.1016/j.hal.2020.101900>.
- Miesner, Anna K, Nina Lundholm, Bernd Krock, And Torkel, Gissel Nielsen, and Germany Bremerhaven. 2021. The effect of *Pseudo-nitzschia seriata* on grazing and fecundity of *Calanus finmarchicus* and *Calanus glacialis*.
<https://academic.oup.com/plankt/article/38/3/564/2223995>. Accessed April 21.
- Miles, C. O, A. L. Wilkins, D. J. Stirling, and A. L. Mackenzie. 2003. Gymnodimine C, an Isomer of Gymnodimine B, from *Karenia selliformis*.
<https://doi.org/10.1021/jf030101r>.
- Morton, S. L., D. L. Roelke, S. R. Manning, A. D. Cembella, Urban Tillman, Christopher J. Gobler, Carmelo R. Tomas, et al. 2018. Harmful Algal Species Fact Sheets. In *Harmful Algal Blooms: A Compendium Desk Reference*, ed. Sa.E. Shumway, J. M. Burkholder, and S.L. Morton, 597–598. Wiley-Blackwell.
- Mulholland, M. R., C. A. Heil, D. A. Bronk, J. M. O'Neil, and P. Bernhardt. 2004. Does nitrogen regeneration from the N₂ fixing cyanobacteria *Trichodesmium* spp. fuel *Karenia brevis* blooms in the Gulf of Mexico? *Harmful Algae* 2002

2001: 47–49.

National Parks Service. 1916. *America's National Park System: The Critical*

Documents. Edited by Lary M. Dilsaver.

National Parks Service. 2018. Assateague Island National Seashore History and Culture.

National Shellfish Sanitation Program (NSSP) Guide for the Control of Molluscan Shellfish. 2015.

NewGen Strategies and Solutions. 2020. *Water and Sewer Rate Study*. Ocean City, Maryland.

Nixon, S. W. 1981. Remineralization and Nutrient Cycling in Coastal Marine

Ecosystems. In *Estuaries and Nutrients*, 111–138. Humana Press.

https://doi.org/10.1007/978-1-4612-5826-1_6.

Nosakhare, O.K., I. T. Aighewi, A. Y. Chi, A B. Ishaque, and G. Mbamalu. 2012.

Land Use–Land Cover Changes in the Lower Eastern Shore Watersheds and

Coastal Bays of Maryland: 1986–2006. *Journal of Coastal Research* 278: 54–62.

<https://doi.org/10.2112/jcoastres-d-09-00074.1>.

Ocean City Chamber of Commerce. Ocean City History. *The Greater Ocean City,*

Maryland Chamber of Commerce.

Olson, M. B., E.J. Lessard, W. P. Cochlan, and V. L. Trainer. 2008. Intrinsic growth

and microzooplankton grazing on toxigenic *Pseudo-nitzschia* spp. diatoms from

the coastal northeast Pacific. *Limnology and Oceanography* 53: 1352–1368.

Paerl, H. W., R. L. Dennis, and D. R. Whitall. 2002. Atmospheric deposition of

nitrogen: Implications for nutrient over-enrichment of coastal waters. *Estuaries*

25. Springer: 677–693. <https://doi.org/10.1007/BF02804899>.
- Papadopoulos, S., M. Tolbert, S. Chesson, T. Clark, and K Conklin. 2013.
Wastewater Management Plan - Chincoteague Island, VA. Chincoteague Island.
- Parson, T. R., Y. Maita, and C. M. Lalli. 1984. *A manual of chemical & biological methods for seawater analysis*. Toronto: Pergamon Press.
[https://doi.org/10.1016/0025-326x\(84\)90262-5](https://doi.org/10.1016/0025-326x(84)90262-5).
- Procise, L. A. 2012. Grazing on *Synechococcus* spp. by the Red-Tide Dinoflagellate *Karenia brevis*: Implications for Bloom Dynamics in the Gulf of Mexico. *OEAS Theses and Dissertations*. <https://doi.org/10.25777/jy09-7349>.
- Racault, M., C. Le Quéré, E. Buitenhuis, S. Sathyendranath, and T. Platt. 2012.
Phytoplankton phenology in the global ocean. *Ecological Indicators* 14: 152–163. <https://doi.org/10.1016/j.ecolind.2011.07.010>.
- Redfield, A. C. 1934. On the proportions of organic derivatives in sea water and their relation to the composition of phytoplankton.
- Reguera, B., and J. Blanco. 2019. Dinophysis toxins: Distribution, fate in shellfish and impacts. *Toxins*. MDPI AG. <https://doi.org/10.3390/toxins11070413>.
- Rountree, H. C., and T. E. Davidson. 1997. Eastern Shore Indians of Virginia and Maryland.
- Ryther, J. H., and W. M. Dunstan. 1971. Nitrogen, phosphorus, and eutrophication in the coastal marine environment 1008-1013. *Science* 171. American Association for the Advancement of Science: 1008–1013.
<https://doi.org/10.1126/science.171.3975.1008>.
- Satake, M., M. Shoji, Y. Oshima, H. Naoki, T. Fujita, and T. Yasumoto. 2002.

- Gymnocin-A, a cytotoxic polyether from the notorious red tide dinoflagellate, *Gymnodinium mikimotoi*. *Tetrahedron Letters* 43. Pergamon: 5829–5832.
[https://doi.org/10.1016/S0040-4039\(02\)01171-1](https://doi.org/10.1016/S0040-4039(02)01171-1).
- Sedwick, P. N., P. W. Bernhardt, M. R. Mulholland, R. G. Najjar, L. M. Blumen, B. M. Sohst, C. Sookhdeo, and B. Widner. 2018. Assessing Phytoplankton Nutritional Status and Potential Impact of Wet Deposition in Seasonally Oligotrophic Waters of the Mid-Atlantic Bight. *Geophysical Research Letters* 45: 3203–3211. <https://doi.org/10.1002/2017GL075361>.
- Seki, T., M. Satake, L. Mackenzie, H. F. Kaspar, and T. Yasumoto. 1995. Gymnodimine, a new marine toxin of unprecedented structure isolated from New Zealand oysters and the dinoflagellate, *Gymnodinium* sp. *Tetrahedron Letters* 36. Pergamon: 7093–7096. [https://doi.org/10.1016/0040-4039\(95\)01434-J](https://doi.org/10.1016/0040-4039(95)01434-J).
- Sipler, R. E., D. A. Bronk, S. P. Seitzinger, R. J. Lauck, L. R. McGuinness, G. J. Kirkpatrick, C. A. Heil, L. J. Kerkhof, and O. M. Schofield. 2013. Trichodesmium-derived dissolved organic matter is a source of nitrogen capable of supporting the growth of toxic red tide *Karenia brevis*. *Marine Ecology Progress Series* 483: 31–45. <https://doi.org/10.3354/meps10258>.
- Smayda, T. J. 1997. What is a bloom? A commentary. *Limnology and Oceanography* 42. Wiley-Blackwell: 1132–1136.
https://doi.org/10.4319/lo.1997.42.5_part_2.1132.
- Solórzano, L., and J. H. Sharp. 1980a. Determination of total dissolved nitrogen in natural waters. *Limnology and Oceanography*.

- <https://doi.org/10.4319/lo.1980.25.4.0751>.
- Solórzano, L., and J. H. Sharp. 1980b. Determination of total dissolved phosphorus and particulate phosphorus in natural waters. *Limnology and Oceanography*. <https://doi.org/10.4319/lo.1980.25.4.0754>.
- Soper, S. 2021. Offshore Wind Turbine Location Concerns Resurface. *Maryland Coast Dispatch*, February 18.
- Steidinger, K.A., J. L. Wolny, and A. J. Haywood. 1997. *Identification of Kareniaceae (Dinophyceae) in the Gulf of Mexico*. Academic Press. Nova Hedwigia: Academic Press.
- Stoecker, D. K., P. J. Hansen, D. A. Caron, and A. Mitra. 2017. Mixotrophy in the Marine Plankton. *Annual Review of Marine Science* 9. Annual Reviews Inc.: 311–335. <https://doi.org/10.1146/annurev-marine-010816-060617>.
- Taillie, D. M., J. M. O’Neil, and W. C. Dennison. 2020. Water quality gradients and trends in New York Harbor. *Regional Studies in Marine Science* 33. Elsevier B.V.: 100922. <https://doi.org/10.1016/j.rsma.2019.100922>.
- Tango, P., W. Butler, and C. Wazniak. 2004. *Analysis of phytoplankton populations in the Maryland Coastal Bays - Coastal Bays: An ecosystem health assessment 2004*.
- Thessen, A. E, and D. K. Stoecker. 2007. Taxonomy and Ecoyphysiology of *Pseudo-nitzschia* in the Chesapeake Bay.
- Timmons, M., M. Sweeney-Reeves, and S. L. Morton. 2018. Harmful Algal Bloom Education and Outreach. In *Harmful Algal Blooms: A Compendium Desk Reference*, ed. S.E. Shumway, J.M. Burkholder, and S. L. Morton, 419–433.

John Wiley & Sons, Ltd.

Tomas, C. R. 1997. *Identifying Marine Phytoplankton*. New York: Academic Press.

Tong, M., D. M. Kulis, E. Fux, J. L. Smith, P. Hess, Q. Zhou, and D. M. Anderson.

2011. The effects of growth phase and light intensity on toxin production by *Dinophysis acuminata* from the northeastern United States. *Harmful Algae* 10: 254–264. <https://doi.org/10.1016/j.hal.2010.10.005>.

Tong, M., J. L. Smith, D. M. Kulis, and D. M. Anderson. 2015. Role of dissolved nitrate and phosphate in isolates of *Mesodinium rubrum* and toxin-producing *Dinophysis acuminata*. *Aquatic Microbial Ecology* 75: 169–185.

<https://doi.org/10.3354/ame01757>.

Town of Chincoteague. 2015. *Town of Chincoteague | History. Eastern Shore of Virginia Hazard Mitigation Plan*.

Town of Ocean City Maryland. 2021. OC Supports Green & Unseen Wind Farms.

Townhill, B. L., J. Tinker, M. Jones, S. Pitois, V. Creach, S. D. Simpson, S. Dye, E.

Bear, and J. K. Pinnegar. 2018. Harmful algal blooms and climate change: exploring future distribution changes. Edited by Rubao Ji. *ICES Journal of Marine Science* 75. Oxford University Press (OUP): 1882–1893.

<https://doi.org/10.1093/icesjms/fsy113>.

Townsend, D. W. 1998. Sources and cycling of nitrogen in the Gulf of Maine.

Journal of Marine Systems 16: 283–295.

Townsend, D. W., A. C. Thomas, L. M. Mayer, M.A. Thomas, and J. A. Quinlan.

2004. Oceanography of the Northwest Atlantic Continental Shelf (1,W). In *The Sea: The Global Coastal Ocean: Interdisciplinary Regional Studies and*

- Syntheses*, 1–57. Harvard University Press.
- Trainer, V. L., S. S. Bates, N. Lundholm, A. E. Thessen, W. P. Cochlan, N.G. Adams, and C. G. Trick. 2012. *Pseudo-nitzschia* physiological ecology, phylogeny, toxicity, monitoring and impacts on ecosystem health. *Harmful Algae* 14: 271–300. <https://doi.org/10.1016/j.hal.2011.10.025>.
- US Census Bureau. 2018. QuickFacts: Ocean City town, Maryland.
- US Department of the Environment. 2020. Sec. 26.08.06.03. Phosphate Ban, Chapter 26.08.06. Cleaning Agents, Subtitle 08. Water Pollution Part 2., Title 26. *Code of Regulations*. <http://mdrules.elaws.us/comar/26.08.06.03>. Accessed May 27.
- US Fish and Wildlife Service. 2015. Chincoteague National Wildlife Refuge.
- Valderrama, J.C. 1981. The simultaneous analysis of total nitrogen and total phosphorus in natural waters. *Marine Chemistry* 10: 109–122.
- Vargo, G. A. 2009. A brief summary of the physiology and ecology of *Karenia brevis* Davis (G. Hansen and Moestrup comb. nov.) red tides on the West Florida Shelf and of hypotheses posed for their initiation, growth, maintenance, and termination. *Harmful Algae*. Elsevier. <https://doi.org/10.1016/j.hal.2008.11.002>.
- Venables, W. N., and B. D Ripley. 2002. *Modern Applied Statistics with S*. 4th ed. New York, NY: Springer-Verlag.
- Vilacoba, K. 2017. Mid-Atlantic residents see ocean health as major economic issue: 1–3.
- Wilkinson, G. N., and C. E. Rogers. 1973. Symbolic Description of Factorial Models for Analysis of Variance. *Applied Statistics* 22: 392. <https://doi.org/10.2307/2346786>.

Xu, Y., R. Chant, D. Gong, R. Castelao, S. Glenn, and O. Schofield. 2011. Seasonal variability of chlorophyll a in the Mid-Atlantic Bight. *Continental Shelf*

Research 31: 1640–1650. <https://doi.org/10.1016/j.csr.2011.05.019>.

Xu, Y., T. Miles, and O. Schofield. 2020. Physical processes controlling chlorophyll-a variability on the Mid-Atlantic Bight along northeast United States. *Journal of*

Marine Systems 212. <https://doi.org/10.1016/j.jmarsys.2020.103433>.